W. Wagner[1]

J. R. Cooper[2]

A. Dittmann[3]

J. Kijima[4]

H.-J. Kretzschmar[5]

A. Kruse[6]

R. Mareš[7]

K. Oguchi[4]

H. Sato[8]

I. Stöcker[5]

O. Šifner[9]

Y. Takaishi[4]

I. Tanishita[4]

J. Trübenbach[3]

Th. Willkommen[3]

The IAPWS Industrial Formulation 1997 for the Thermodynamic Properties of Water and Steam

In 1997, the International Association for the Properties of Water and Steam (IAPWS) adopted a new formulation for the thermodynamic properties of water and steam for industrial use. This new formulation, called IAPWS Industrial Formulation 1997 for the Thermodynamic Properties of Water and Steam (IAPWS-IF97), replaces the previous industrial formulation, IFC-67, that had formed the basis for power-plant calculations and other applications in energy engineering since the late 1960's. IAPWS-IF97 improves significantly both the accuracy and the speed of the calculation of the thermodynamic properties compared with IFC-67. The differences between IAPWS-IF97 and IFC-67 will require many users, particularly boiler and turbine manufacturers, to modify design and application codes. This paper summarizes the need and the requirements for such a new industrial formulation and gives the entire numerical information about the individual equations of IAPWS-IF97. Moreover, the scientific basis for the development of the equations is summarized and the achieved quality of IAPWS-IF97 is presented regarding the three criterions accuracy, consistency along region boundaries, and computation speed. For comparison, corresponding results for the previous standard IFC-67 are also presented.

1 Introduction

In the 1960s an industrial formulation for the thermodynamic properties of water and steam was developed. This was called "The 1967 IFC Formulation for Industrial Use" (IFC-67) [1]. IFC-67 was formally recognized for the calculation of thermodynamic properties of water and steam for official use such as performance guarantee calculations of power cycles. In addition to this, IFC-67 was used for innumerable other industrial applications. However, compared with today's requirements IFC-67 contains a number of weaknesses. Moreover, because of the progress that has been achieved in mathematical methods to develop accurate equations of state, a number of reasons warranted the development of a new industrial formulation.

This newly developed formulation was adopted by the International Association for the Properties of Water and Steam (IAPWS) at its meeting in Erlangen (Germany), September 1997, under the name "IAPWS Industrial Formulation 1997 for the Thermodynamic Properties of Water and Steam" abbreviated to "IAPWS Industrial Formulation 1997" or even shorter IAPWS-IF97 [2]. Since this date IAPWS-IF97 has been officially valid. However, due to the need to modify design and application codes, IAPWS has recommended an introductory period, lasting until January 1, 1999, during which IAPWS-IF97 should not be used for contractual commitments.

This article contains details relevant to the development of IAPWS-IF97, the full numerical information on the individual equations needed for their use, details of their accuracy, consistency along region boundaries, and results of computing-time investigations in comparison with IFC-67.

[1] Ruhr-Universität Bochum, Lehrstuhl für Thermodynamik, D-44780 Bochum, Germany, corresponding author

[2] Queen Mary and Westfield College, Department of Engineering, London, United Kingdom

[3] Technische Universität Dresden, Institut für Thermodynamik und Technische Gebäudeausrüstung, Dresden, Germany

[4] Kanagawa Institute of Technology, Faculty of Engineering, Atsugi, Japan

[5] Hochschule Zittau/Görlitz (FH), Fachgebiet Technische Thermodynamik, Zittau, Germany

[6] Ruhr-Universität Bochum, Lehrstuhl für Thermodynamik, Bochum, Germany
Current address: Bayern Innovativ GmbH, Nürnberg, Germany

[7] University of West Bohemia, Department of Thermodynamics, Plzen, Czech Republic

[8] Keio University, Faculty of Science & Technology, Yokohama, Japan

[9] Academy of Sciences of Czech Republic, Institute of Thermomechanics, Prague, Czech Republic

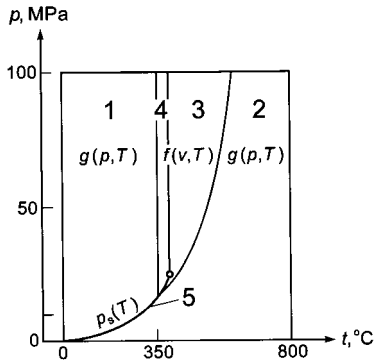

Fig. 1 Regions and equations of IFC-67. The boundary between regions 2 and 3 is described by the L-function

Those who are only interested in the numerical information needed to use the equations of IAPWS-IF97 can find this information in compact form in several steam tables, for example [3, 4, 4a], or in the release on IAPWS-IF97 [2].

2 Need for the Development of the New Industrial Formulation IAPWS-IF97

In order to demonstrate the need for a new industrial formulation, the characteristics of the industrial formulation IFC-67 are considered. As shown in Fig. 1, the entire range of validity ($0°C \leq t \leq 800°C$ for $p \leq 100$ MPa) was divided into five regions with separate equations. For each of the regions 1 (liquid) and 2 (vapor) there was an equation of the specific Gibbs free energy g as function of pressure p and temperature T, namely $g(p, T)$. Each of the regions 3 and 4 was covered by an equation of the specific Helmholtz free energy f as function of specific volume v and temperature T, namely $f(v, T)$. The fifth region was the saturation curve for which a saturation-pressure equation $p_s(T)$ was given.

Based on the equations for the industrially most important regions 1, 2, and 5, the following properties could be directly calculated with IFC-67 as a function of p and T: specific volume v, specific enthalpy h, specific entropy s and specific isobaric heat capacity c_p, and in addition the saturation pressure p_s as a function of T. If other combinations of variables were of interest, for example the combinations $v(p, h)$, $T(p, h)$, $s(p, h)$, $h(p, s)$, $T(p, s)$, and $T_s(p)$ for turbine-expansion calculations, these had to be determined via corresponding iterations. Due to these iterations in combination with a relatively complex structure of the equations, calculations for the complete power cycle with the whole set of the IFC-67 equations required relatively long computing times.

Nowadays, with modern mathematical tools to establish effective structures of such property formulations [5], the long process-calculation times with the IFC-67 equations became a real weakness of this formulation. Besides this main disadvantage of IFC-67 there were several other deficiencies which are summarized as follows:

1 For certain regions IFC-67 no longer met the present standard of accuracy.
2 For some properties there were considerable inconsistencies at region boundaries.
3 The technically important property speed of sound w was not incorporated in the set of the IFC-67 equations.
4 IFC-67 was not based on the current temperature scale ITS-90 [6].
5 IFC-67 was based on earlier data and was therefore not connected to the current scientific standard of IAPWS for the thermodynamic properties of ordinary water substance, the IAPWS-95 formulation [7, 8].

More details concerning the above mentioned items can be seen in the figures of Section 5.5.

3 Administrative Measures of IAPWS for the Development and Examination of IAPWS-IF97

Due to the weaknesses of the IFC-67 formulation listed in the previous section, at the IAPWS meeting in Buenos Aires in 1990 it was decided that a set of new fast equations should be developed for industrial calculations. This new industrial formulation, later called IAPWS-IF97, should then replace the industrial formulation IFC-67. In order to develop the entire equation package in an international collaboration, the Task Group "New Industrial Formulation" was established. It consisted of the following 12 members from seven countries: W. Wagner (Chairman, Germany), A. Alexandrov (Russia), J. R. Cooper (United Kingdom), A. Dittmann (Germany), J. Gallagher (USA), P. G. Hill (Canada), H.-J.

Nomenclature

a, b, c = adjustable parameters
c_p = specific isobaric heat capacity
c_v = specific isochoric heat capacity
d = adjustable parameter
f = specific Helmholtz free energy, $f = u - Ts$
g = specific Gibbs free energy, $g = h - Ts$
h = specific enthalpy
I = exponent
i = serial number
J = exponent
j = serial number
M = molar mass
n = coefficient
p = pressure
R = specific gas constant
R_m = molar gas constant
s = specific entropy
T = thermodynamic temperature[10]
t = Celsius temperature, $t = T - 273.15$ K
u = specific internal energy
v = specific volume
w = speed of sound
β = transformed pressure, Eqs. (27*a*) and (55*a*)
γ = dimensionless Gibbs free energy, $\gamma = g/(RT)$
Δ = difference in any quantity
δ = reduced density, $\delta = \rho/\rho^*$
η = reduced enthalpy, $\eta = h/h^*$
θ = reduced temperature, $\theta = T/T^*$
ϑ = transformed temperature, Eq. (27*b*)
π = reduced pressure, $\pi = p/p^*$
ρ = mass density
σ = reduced entropy, $\sigma = s/s^*$
τ = inverse reduced temperature, $\tau = T^*/T$
ϕ = dimensionless Helmholtz free energy, $\phi = f/(RT)$

Superscripts

o = ideal-gas part; ideal gas
r = residual part
$*$ = reducing quantity
$'$ = saturated liquid state
$''$ = saturated vapor state

Subscripts

b = normal boiling point
c = critical point
max = maximum value
s = saturation state
t = triple point
tol = tolerated

[10] All temperature values given in this article are temperatures according to the International Temperature Scale of 1990 (ITS-90)

Kretzschmar (Germany), R. Mareš (Czech Republic), K. Oguchi (Japan), H. Sato (Japan), O. Šifner (Czech Republic), and J. T. R. Watson (United Kingdom). This group was responsible for the development of IAPWS-IF97 with respect to organizational questions of scientific nature (structure of the formulation, selection of the individual equations, official report to IAPWS, etc.). The final form of IAPWS-IF97 is based on contributions and equations by the scientists who form the group of authors of this article.

The entire project was continuously supervised by the IAPWS Working Group "Industrial Calculations" of which many members are representatives of international companies involved in the power industry. This working group, chaired by B. Rukes (Germany), is the successor of the IAPWS "Subcommittee on Industrial Calculations." The progress of the development of IAPWS-IF97 was continuously discussed in joint sessions of this group with the IAPWS Working Group "Thermophysical Properties of Water and Steam" which was chaired by J. R. Cooper (United Kingdom).

Finally, at the IAPWS meeting in Paris in 1995 the Task Group "New Industrial Formulation-Evaluation" was founded. This group was responsible for the examination of IAPWS-IF97 and consisted of the following members: K. Miyagawa, (Chairman, previously Fuji Electric, Japan), H. W. Bradly (Bradly Associates, United Kingdom), R. B. McClintock (previously General Electric, USA), I. Kodl (Skoda, Czech Republic), W. T. Parry (General Electric, USA), C. Perstrup (Elsam Project, Denmark), B. Rukes (Siemens KWU, Germany), M. Scala (Ansaldo, Italy), P. F. Smith (GEC Alstom Power Generation, United Kingdom), and R. C. Spencer (previously General Electric, USA).

4 Requirements for IAPWS-IF97

The requirements for the industrial formulation IAPWS-IF97 are based on the proposal of the former "Subcommittee on Industrial Calculations," which was agreed with the Task Group "New Industrial Formulation." The main items are summarized in the following sections.

4.1 Range of Validity. The entire set of equations of IAPWS-IF97 should have the same range of validity as given for IFC-67, which is defined by the following temperature and pressure range:

$$0°C \le t \le 800°C \quad p \le 100 \text{ MPa}.$$

For high-temperature applications such as in gas turbines the following extension of the range of validity was requested:

$$800°C \le t \le 2000°C \quad p \le 10 \text{ MPa}.$$

4.2 Accuracy. For the properties specific volume v, specific enthalpy h, and saturation pressure p_s, IAPWS-IF97 should generally meet the corresponding values from the scientific standard, the "IAPWS Formulation 1995 for the Thermodynamic Properties of Ordinary Water Substance for General and Scientific Use" [7, 8], hereafter abbreviated to IAPWS-95, within the tolerances of the International Skeleton Tables IST-85 in its version of 1994 [9]. Roughly summarizing, the relevant IST-85 tolerances are, dependent on the state range, for v between ± 0.01 percent and ± 0.3 percent, for h between ± 0.1 percent and ± 0.3 percent, and for p_s $\pm$ 0.025 percent. Based on extremely accurate experimental data, in the liquid region for $p < 1$ MPa the IST-85 tolerances [9] for v and h and on the saturation curve for $t < 100°C$ the tolerances for p_s are extraordinarily small; here, the smallest tolerances are ± 0.001 percent in v, ± 0.03 percent in h, and ± 0.002 percent in p_s. However, in view of the technical demands in this range, the permitted tolerances to the IAPWS-95 values were increased to ± 0.01 percent in v, to ± 0.1 percent in h, and to ± 0.025 percent in p_s. For the specific isobaric heat capacity c_p and the speed of sound w, IAPWS-IF97 should represent the values from IAPWS-95 to within ± 1 percent except for the range very near the critical point where clearly larger deviations were allowed. By taking as reference the IAPWS-95 formulation [7, 8] the agreement between the industrial formulation and the scientific formulation of IAPWS is ensured.

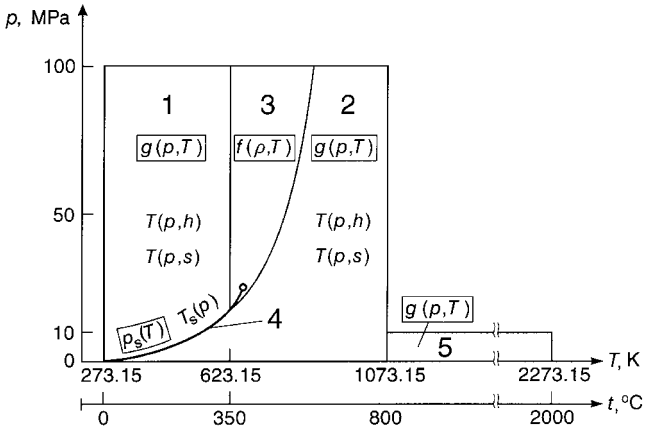

Fig. 2 Regions and equations of IAPWS-IF97. The boundary between regions 2 and 3 is described by the B23-equation, see section 5.3

Besides the representation of v, h, c_p, and w for the (stable) homogeneous regions including saturation, the specification included the requirement that the equations should also yield reasonable values for metastable states close to the stable regions.

4.3 Maximum Inconsistencies at Region Boundaries. With regard to the continuity at the region boundaries (see Fig. 2), reference is made to the so-called Prague values [10]. These Prague values, established for IFC-67, give permissible differences in the property values along the region boundaries when calculating these properties from all equations valid at the corresponding boundary. The continuity requirements are as follows:

(a) Single Phase.

Specific volume:	$\Delta v = \pm 0.05$ percent
Enthalpy:	$\Delta h = \pm 0.2$ kJ kg^{-1}
Heat capacity:	$\Delta c_p = \pm 1$ percent
Entropy:	$\Delta s = \pm 0.2$ J kg^{-1} K^{-1}
Gibbs free energy:	$\Delta g = \pm 0.2$ kJ kg^{-1}
Speed of sound:	$\Delta w = \pm 1$ percent

(b) Saturation.

Saturation pressure:	$\Delta p_s = \pm 0.05$ percent
Saturation temperature:	$\Delta T_s = \pm 0.02$ percent
Gibbs free energy:	$\Delta g = \pm 0.2$ kJ kg^{-1}

4.4 Increase of Computation Speed. This item was the most important demand for IAPWS-IF97. The main requirement regarding the computation speed was that the calculation of all property functions listed in Table 1 for regions 1, 2, and 4 should be altogether three times faster than with IFC-67; for the definition of the individual regions of IAPWS-IF97 see Fig. 2. Table 1 is based on a survey made by the "Subcommittee on Industrial Calculations" among the international power-cycle companies and related industries. In addition to the most important property functions for these regions the table also gives the average frequencies of use of the corresponding functions.

For regions 3 and 5 of IAPWS-IF97 the computation-speed requirements only related to a few functions (see Table 18), where these functions are not combined with frequency-of-use values. For region 3, corresponding to regions 3 and 4 of IFC-67, it was only necessary that IAPWS-IF97 was not slower than with IFC-67. For region 5, the computing-time requirements related only to 1073.15 K, the maximum temperature for which IFC-67 was valid. For this isotherm IAPWS-IF97 should be three times faster than with IFC-67.

Table 1 Most important property functions and their frequency of use

Region [a]	Function	Frequency of use [b] %	
1 (Liquid)	$v(p,T)$	2.9	
	$h(p,T)$	9.7	
	$\boxed{T(p,h)}$	3.5	3.5
	$\boxed{h(p,s)}$	1.2	1.2
2 (Vapor)	$v(p,T)$	6.1	
	$h(p,T)$	12.1	
	$s(p,T)$	1.4	
	$\boxed{T(p,h)}$	8.5	13.3
	$\boxed{v(p,h)}$	3.1	
	$\boxed{s(p,h)}$	1.7	
	$\boxed{T(p,s)}$	1.7	6.6
	$\boxed{h(p,s)}$	4.9	
4 (Saturation)	$p_s(T)$	8.0	
	$\boxed{T_s(p)}$	30.7	35.2
	$\boxed{h'(p)}$	2.25	
	$\boxed{h''(p)}$	2.25	
	Σ:	100.0	59.8

[a] For the definition of the regions see Fig. 2

[b] Functions with values less than 1 % have been neglected; these sum up to 8 %, the remaining values have been scaled up to 100 %

In order to perform all these computing-time investigations, special benchmark programs for a specified PC and compiler were developed. These programs took into account the frequencies of use (if any) of the corresponding property functions.

5 The IAPWS Industrial Formulation 1997

This section gives full information about the IAPWS Industrial Formulation 1997 (IAPWS-IF97) covering all numerical details needed for the use of the individual equations, statements on their development and details concerning accuracy, consistency along the region boundaries, and computation speed of IAPWS-IF97 compared with the previous industrial standard IFC-67.

5.1 Concept and Structure of IAPWS-IF97. The IAPWS Industrial Formulation 1997 consists of a set of equations for different regions which cover the following range of validity:

$$273.15\ \mathrm{K} \le T \le 1073.15\ \mathrm{K} \quad p \le 100\ \mathrm{MPa}$$

$$1073.15\ \mathrm{K} \le T \le 2273.15\ \mathrm{K} \quad p \le 10\ \mathrm{MPa}.$$

Figure 2 shows in which way the entire range of validity of IAPWS-IF97 is covered by its equations. The division into individual regions is very similar to IFC-67. One difference is that the middle density range is covered by only one region, namely by region 3. The other difference is that there is additionally a high-temperature region, region 5. Region 4 corresponds to the saturation curve. The boundaries of the regions can be directly taken from Fig. 2 except for the boundary between regions 2 and 3; this boundary is defined by the so-called B23-equation given in Section 5.3. Both regions 1 and 2 are individually covered by a fundamental equation for the specific Gibbs free energy $g(p, T)$, region 3 by a fundamental equation for the specific Helmholtz free energy $f(\rho, T)$, and the saturation curve, corresponding to region 4, by a saturation-pressure equation $p_s(T)$. The high-temperature region 5 is also covered by a $g(p, T)$ equation. These five equations, shown in rectangular boxes in Fig. 2, form the so-called *basic equations.*

In order to meet the main requirement of a short computing time, the entire set of the IAPWS-IF97 equations was developed based on the following two-step concept:

1 After finding convenient functional terms, the structure of the four basic equations for the homogeneous regions was optimized using the method by Setzmann and Wagner [5] in such a way that the requirements regarding accuracy and consistency along region boundaries were met with equation structures allowing short computing times. In this optimization process, the equations were fitted to input values calculated from the IAPWS-95 formulation [7, 8]. In this way IAPWS-IF97 was coupled with the current scientific standard IAPWS-95.

2 All those thermodynamic properties which are not direct functions of the independent variables of the basic equations are not found by iteration from the basic equations. Instead of this, so-called *backward equations* were developed, namely equations $T(p, h)$ and $T(p, s)$ for regions 1 and 2 and $T_s(p)$ for the saturation curve. With these backward equations, shown in Fig. 2 for the corresponding regions, all the functions shown in rectangular boxes in Table 1 can be calculated without any iteration. For example, if $h(p, s)$ is to be calculated in region 2, first the temperature T is calculated from the backward equation $T(p, s)$ and then $h(p, T)$ can be directly obtained from the corresponding basic equation $g(p, T)$.

However, this entire concept required that the numerical consistency between the backward and the basic equations was extremely good. Otherwise it would have caused numerical problems when "jumping" back and forth between the basic and the backward equations, for example, when calculating the turbine-expansion line of a power-cycle process. Based on test calculations with characteristic power cycles via iterations with IFC-67, the following numerical consistency requirements were finally set up:

(*a*) The temperature determined from the backward equation $T(p, h)$ for given values of p and h had to agree with the temperature value calculated for the same p and h from the corresponding basic equation $g(p, T)$ within a tolerated temperature difference ΔT_{tol}. This ΔT_{tol} value amounts to ± 25 mK for the entire region 1 and for region 2 at entropy values not greater than 5.85 kJ kg^{-1} K^{-1}. For region 2 at entropy values greater than 5.85 kJ kg^{-1} K^{-1}, the permissible ΔT_{tol} value amounts to ± 10 mK; the smaller ΔT_{tol} inconsistency value in this part of region 2 (turbine expansion) is particularly important for the power industry.

(*b*) The temperature determined from the backward equation $T(p, s)$ for given values of p and s had to agree with the temperature calculated for the same p and s from the corresponding basic equation $g(p, T)$ within a tolerated temperature difference ΔT_{tol}. For the tolerated ΔT_{tol} inconsistency values with regard to the $T(p, s)$ equation, the same statement held as given for the $T(p, h)$ equation under item (*a*).

(*c*) The saturation pressure calculated from the saturation-temperature equation $T_s(p)$ was not allowed to deviate by more than $\Delta p_s = \pm 0.003$ percent from the p_s value determined from the saturation-pressure equation $p_s(T)$.

The permissible numerical inconsistencies between the basic and backward equations, summarized under items (*a*) to (*c*), were extremely small, namely about one tenth of the uncertainties of the scientific standard IAPWS-95.

5.2 Reference Constants. This section summarizes all reference constants needed for evaluating the equations given in Section 5.5.

The specific gas constant of ordinary water,

$$R = 0.461\ 526\ \mathrm{kJ\,kg^{-1}\,K^{-1}}, \tag{1}$$

results from the recommended values of the molar gas constant [11],

$$R_m = 8.314\ 51\ \mathrm{J\,mol^{-1}\,K^{-1}}, \tag{2}$$

and from the molar mass of ordinary water,

$$M = 18.015\ 257\ \mathrm{g\,mol^{-1}}. \tag{3}$$

The value of M results from the molar masses obtained from isotopic molar masses in [12] and representative isotopic compositions given in [13].

The values of the critical parameters

$$T_c = 647.096 \text{ K}, \tag{4}$$

$$p_c = 22.064 \text{ MPa}, \tag{5}$$

$$\rho_c = 322 \text{ kg m}^{-3} \tag{6}$$

are from the corresponding IAPWS release [14]. The triple-point temperature is

$$T_t = 273.16 \text{ K} \tag{7}$$

according to the International Temperature Scale of 1990 (ITS-90) [6] and the triple-point pressure

$$p_t = 611.657 \text{ Pa} \tag{8}$$

was determined by Guildner et al. [15]. According to the scientific standard of the thermodynamic properties of ordinary water, the IAPWS-95 formulation [7, 8], the temperature of the normal boiling point (at a pressure of 0.101 325 MPa (1 atm)) amounts to

$$T_b = 373.124\ 3 \text{ K}. \tag{9}$$

5.3 Auxiliary Equation for the Boundary between Regions 2 and 3. The boundary between regions 2 and 3 (see Fig. 2) is defined by the following simple quadratic pressure-temperature relation, the B23-equation

$$\pi = n_1 + n_2\theta + n_3\theta^2, \tag{10}$$

where $\pi = p/p^*$ and $\theta = T/T^*$ with $p^* = 1$ MPa and $T^* = 1$ K. The coefficients n_1 to n_3 of Eq. (10) are listed in Table A1 of the appendix. Equation (10) describes roughly an isentropic line; the entropy values along this boundary line are between $s = 5.047$ kJ kg^{-1} K^{-1} and $s = 5.261$ kJ kg^{-1} K^{-1}.

Alternatively Eq. (10) can be expressed explicitly in temperature as

$$\theta = n_4 + [(\pi - n_5)/n_3]^{0.5} \tag{11}$$

with θ and π as defined for Eq. (10) and the coefficients n_3 to n_5 listed in Table A1. Equations (10) and (11) cover the range from 623.15 K at 16.5292 MPa up to 863.15 K at 100 MPa.

5.4 Functional Forms Adopted for Short Computing Times. Wide-range equations of state in reference quality are nowadays explicit in the Helmholtz free energy as function of density and temperature [7, 8, 16, 17]. As functional forms for such equations pure polynomials in density and temperature and particularly such polynomials combined with exponential functions in density have proved very successful.

Since, however, for IAPWS-IF97 a short computing time was one of the most important criterions, the computing times of selected arithmetic operations were investigated [18]. Compared with the two most important basic operations addition and multiplication, all the other operations are slower by a factor of ten or more. After these tests it was clear that it was only possible to use polynomials in the form of series of additions and multiplications as basic functional forms for the new equations. Based on many tests for the general functional dependency

$$z = z(x, y), \tag{12}$$

where, for example, $z = f$, $x = \rho$, and $y = T$, the following general functional expression has proved most effective [18]:

$$z(x, y) = \sum_i n_i \left(\frac{x}{a} + b\right)^{I_i} \left(\frac{y}{c} + d\right)^{J_i}. \tag{13}$$

This general expression forms the basis for the majority of the equations of IAPWS-IF97.

The final form of all equations (except for the saturation curve, region 4) of IAPWS-IF97 was found by using the structure-optimization method of Setzmann and Wagner [5] or a modified version of Wagner's method [19]. These procedures require a so-called bank of terms from which the best combination of an optimum number of terms is determined. For the development of the backward equations, these procedures were combined with further optimization tools, see later.

5.5 The Basic Equations for Regions 1 to 5. For those homogeneous regions of IAPWS-IF97 for which it is thermodynamically reasonable the corresponding equations of state were established as function of the "technical" variables pressure p and temperature T; this is the case for regions 1, 2, and 5. For these regions, the equations are formulated explicit in the specific Gibbs free energy g which is, as a function of p and T, a fundamental equation. Since region 3 contains the critical point, this region cannot be reasonably covered by an equation with p and T as independent variables. However, it can be represented by an equation as a function of density ρ and temperature T. Thus, for region 3 an equation explicit in the specific Helmholtz free energy as a function of ρ and T is used which is a fundamental equation, also. One advantage of using fundamental equations (instead of equations of state in form of $p(v, T)$ and $v(p, T)$, respectively) is that all thermodynamic properties can be calculated from derivatives of the equations, no integrations with further information are needed. If the first and second derivatives of g with respect to p and T and of f with respect to ρ and T, respectively, are correctly represented, then any thermodynamic property, based on these derivatives (which is the case for the vast majority of properties), can be correctly calculated from such fundamental equations.

Proceeding from Eq. (13) with $z = g/(RT)$, $x = p$, $a = p^*$, $y = T^{-1}$, and $c = (T^*)^{-1}$ one obtains the following general form of a so-called combined polynomial for the $g(p, T)$ equations:

$$\frac{g}{RT} = \sum_i n_i \left(\frac{p}{p^*} + b\right)^{I_i} \left(\frac{T^*}{T} + d\right)^{J_i}, \tag{14}$$

where p^* and T^* are reducing parameters.

In the following sections first the final form of the corresponding basic equation is given including all numerical information for its use, then details of its development are summarized and finally its accuracy is discussed; all table numbers starting with an "A" are listed in the appendix.

5.5.1 The Gibbs Free Energy Equation for Region 1. The basic equation for this region is a fundamental equation for the specific Gibbs free energy g. This equation is expressed in dimensionless form, $\gamma = g/(RT)$, and reads

$$\frac{g(p, T)}{RT} = \gamma(\pi, \tau) = \sum_{i=1}^{34} n_i (7.1 - \pi)^{I_i} (\tau - 1.222)^{J_i}, \tag{15}$$

where $\pi = p/p^*$ and $\tau = T^*/T$ with $p^* = 16.53$ MPa and $T^* = 1386$ K; R is given by Eq. (1). The coefficients n_i and exponents I_i and J_i of Eq. (15) are listed in Table A2.

All thermodynamic properties can be derived from Eq. (15) by using the appropriate combinations of the dimensionless Gibbs free energy γ and its derivatives. The relations of the relevant thermodynamic properties to γ and its derivatives are summarized in Table 2. All required derivatives of the dimensionless Gibbs free energy γ, Eq. (15), are explicitly given in Table 3.

Since the 5th International Conference on the Properties of Steam in London in 1956, the specific internal energy and the specific entropy of the saturated liquid at the triple point have been set equal to zero, as follows:

$$u'_t = 0; \quad s'_t = 0. \tag{16}$$

Table 2 Relations of thermodynamic properties to the dimensionless Gibbs free energy γ and its derivatives when using Eq. (15)[a]

Property	Relation
Specific volume $v=(\partial g/\partial p)_T$	$v(\pi,\tau)\frac{p}{RT}=\pi\gamma_\pi$
Specific internal energy $u=g-T(\partial g/\partial T)_p-p(\partial g/\partial p)_T$	$\frac{u(\pi,\tau)}{RT}=\tau\gamma_\tau-\pi\gamma_\pi$
Specific entropy $s=-(\partial g/\partial T)_p$	$\frac{s(\pi,\tau)}{R}=\tau\gamma_\tau-\gamma$
Specific enthalpy $h=g-T(\partial g/\partial T)_p$	$\frac{h(\pi,\tau)}{RT}=\tau\gamma_\tau$
Specific isobaric heat capacity $c_p=(\partial h/\partial T)_p$	$\frac{c_p(\pi,\tau)}{R}=-\tau^2\gamma_{\tau\tau}$
Specific isochoric heat capacity $c_v=(\partial u/\partial T)_v$	$\frac{c_v(\pi,\tau)}{R}=-\tau^2\gamma_{\tau\tau}+\frac{(\gamma_\pi-\tau\gamma_{\pi\tau})^2}{\gamma_{\pi\pi}}$
Speed of sound $w=v\left[-(\partial p/\partial v)_s\right]^{0.5}$	$\frac{w^2(\pi,\tau)}{RT}=\frac{\gamma_\pi^2}{\frac{(\gamma_\pi-\tau\gamma_{\pi\tau})^2}{\tau^2\gamma_{\tau\tau}}-\gamma_{\pi\pi}}$

$\gamma_\pi=\left(\frac{\partial\gamma}{\partial\pi}\right)_\tau,\ \gamma_{\pi\pi}=\left(\frac{\partial^2\gamma}{\partial\pi^2}\right)_\tau,\ \gamma_\tau=\left(\frac{\partial\gamma}{\partial\tau}\right)_\pi,\ \gamma_{\tau\tau}=\left(\frac{\partial^2\gamma}{\partial\tau^2}\right)_\pi,\ \gamma_{\pi\tau}=\left(\frac{\partial^2\gamma}{\partial\pi\partial\tau}\right)$

[a] A general procedure how to obtain the relation of any property and any differential quotient to γ and its derivatives when using Eq. (15) can be found in [19a]

In order to meet this condition at the temperature and pressure of the triple point, see Eqs. (7) and (8), the coefficients n_3 and n_4 in Eq. (15) have been adjusted accordingly. As a consequence, Eq. (15) yields for the specific enthalpy of the saturated liquid at the triple point

$$h'_t = 0.611\ 783\ \mathrm{J\,kg^{-1}}. \tag{17}$$

Equation (15) covers region 1 of IAPWS-IF97 defined by the following range of temperature and pressure (see Fig. 2):

$$273.15\ \mathrm{K} \le T \le 623.15\ \mathrm{K} \quad p_s(T) \le p \le 100\ \mathrm{MPa}.$$

In addition to the properties in the stable single-phase liquid region, Eq. (15) also yields reasonable values in the metastable superheated-liquid region close to the saturated liquid line. For temperatures between 273.15 K and 273.16 K at pressures below the melting pressure [20] (metastable subcooled liquid) all values are calculated by extrapolation from Eqs. (15) and (28).

To assist the user in computer-program verification of Eq. (15), Table A3 contains test values of the most relevant properties.

5.5.1.1 Development of Eq. (15). Based on test calculations with Eq. (14) regarding the maximum ranges of the exponents I_i and J_i, the values for the reducing parameters p^* and T^* and the shifting parameters b and d, the following general functional expression of 911 terms (bank of terms) was used as a starting point for the development of the equation for the dimensionless Gibbs free energy for region 1 [18]:

$$\gamma = \sum_{i=0}^{8}\sum_{j=-18}^{18} n_{ij}(7.1-\pi)^i(\tau-1.222)^j + \sum_{i=16}^{32}\sum_{j=-43}^{-10} n_{ij}(7.1-\pi)^i(\tau-1.222)^j, \tag{18}$$

Table 3 The dimensionless Gibbs free energy γ, Eq. (15), and its derivatives

$\gamma = \sum_{i=1}^{34} n_i(7.1-\pi)^{I_i}(\tau-1.222)^{J_i}$	$\gamma_\tau = \sum_{i=1}^{34} n_i(7.1-\pi)^{I_i} J_i(\tau-1.222)^{J_i-1}$
$\gamma_\pi = \sum_{i=1}^{34} -n_i I_i(7.1-\pi)^{I_i-1}(\tau-1.222)^{J_i}$	$\gamma_{\tau\tau} = \sum_{i=1}^{34} n_i(7.1-\pi)^{I_i} J_i(J_i-1)(\tau-1.222)^{J_i-2}$
$\gamma_{\pi\pi} = \sum_{i=1}^{34} n_i I_i(I_i-1)(7.1-\pi)^{I_i-2}(\tau-1.222)^{J_i}$	$\gamma_{\pi\tau} = \sum_{i=1}^{34} -n_i I_i(7.1-\pi)^{I_i-1} J_i(\tau-1.222)^{J_i-1}$

$\gamma_\pi=\left(\frac{\partial\gamma}{\partial\pi}\right)_\tau,\ \gamma_{\pi\pi}=\left(\frac{\partial^2\gamma}{\partial\pi^2}\right)_\tau,\ \gamma_\tau=\left(\frac{\partial\gamma}{\partial\tau}\right)_\pi,\ \gamma_{\tau\tau}=\left(\frac{\partial^2\gamma}{\partial\tau^2}\right)_\pi,\ \gamma_{\pi\tau}=\left(\frac{\partial^2\gamma}{\partial\pi\partial\tau}\right)$

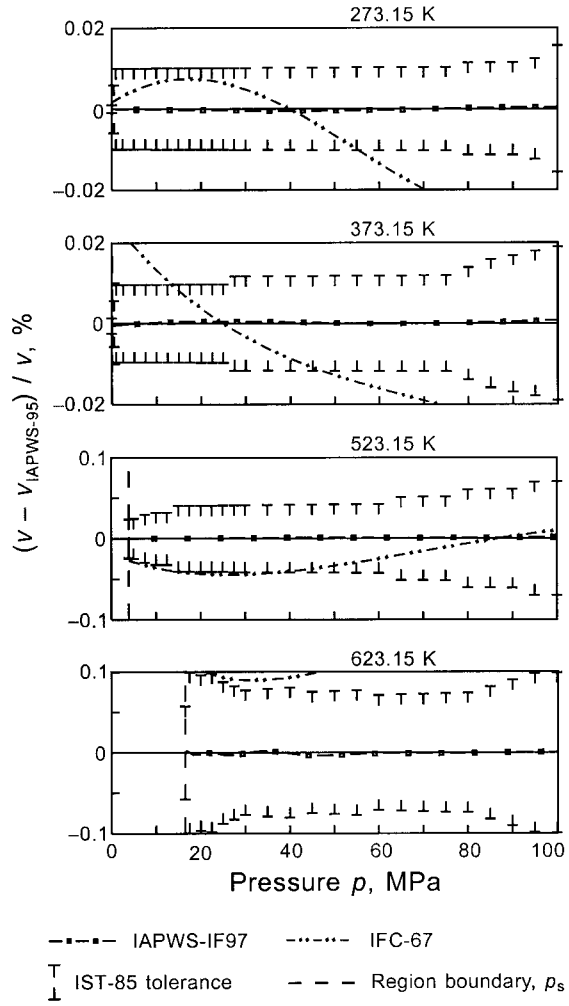

Fig. 3(*a*) Percentage deviations of the specific volumes v calculated from Eq. (15) and IFC-67, respectively, from values $v_{\mathrm{IAPWS\text{-}95}}$ calculated from IAPWS-95 [7, 8]

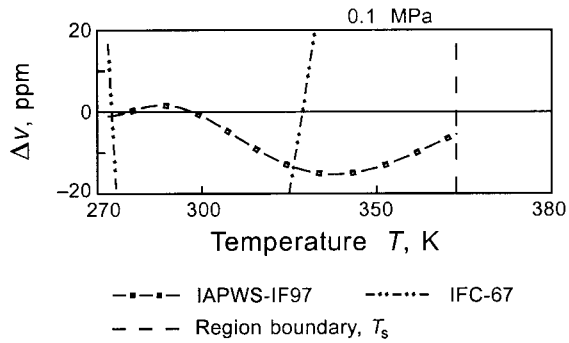

Fig. 3(*b*) Relative deviations in ppm of the specific volumes v calculated from Eq. (15) and IFC-67, respectively, from values $v_{\mathrm{IAPWS\text{-}95}}$ calculated from IAPWS-95 [7, 8]; $\Delta v = (v - v_{\mathrm{IAPWS\text{-}95}})/v$.

where $\pi = p/p^*$ and $\tau = T^*/T$ with $p^* = 16.53$ MPa and $T^* = 1386$ K. Equation (15), obtained from Eq. (18) by the method of Setzmann and Wagner [5] for optimizing the functional structure of the final γ equation, was fitted to values of the properties v, h, c_p, s, and the two partial derivatives $(\partial v/\partial p)_T$ and $(\partial v/\partial T)_p$. All these values were calculated from IAPWS-95 [7, 8] for given values of p and T distributed as selected grid points over region 1. Details of this fitting process (formulation of the sums of squares based on the relations given in Table 2, weighting factors, etc.) are given by Kruse and Wagner [18]. The inclusion of the partial

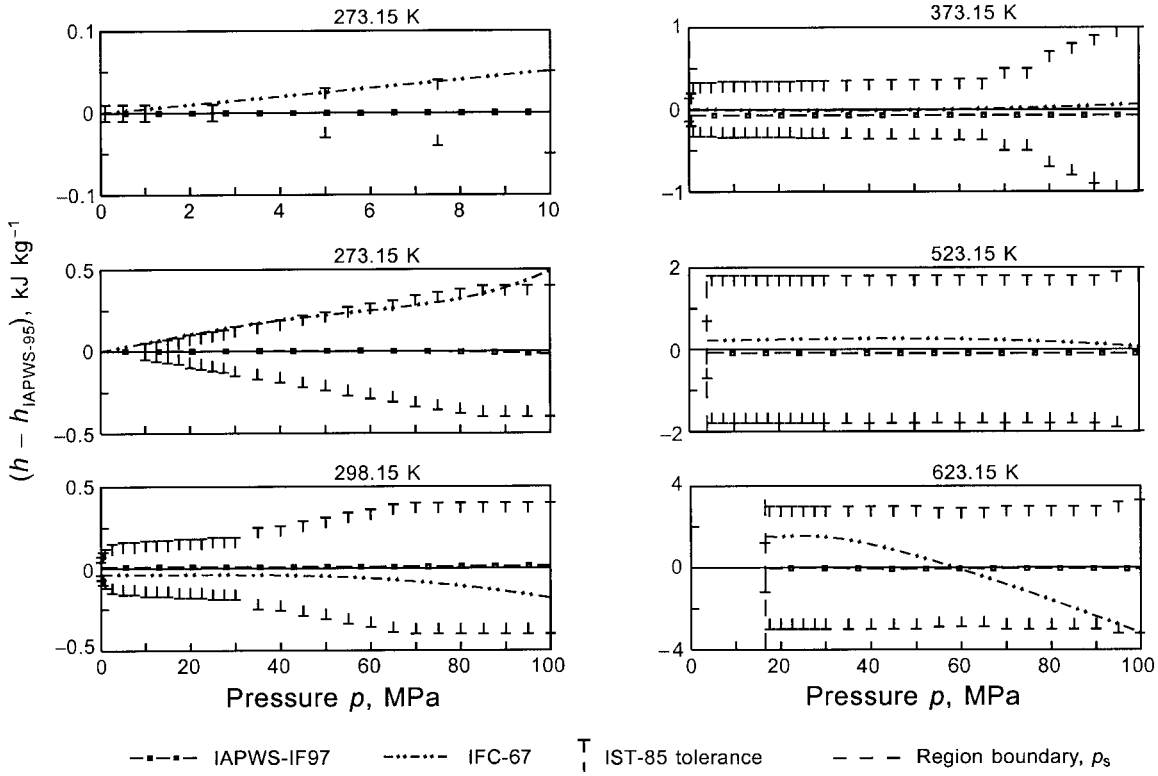

Fig. 4 Absolute deviations of the specific enthalpies h calculated from Eq. (15) and IFC-67, respectively, from values $h_{IAPWS-95}$ calculated from IAPWS-95 [7, 8]; see the spread pressure scale up to p = 10 MPa in the first deviation diagram for 273.15 K.

derivatives of v with respect to p and T made it unnecessary to fit the equations to the corresponding values of c_v and w which would have led to a nonlinear system of normal equations when minimizing the sum of squares. Such a nonlinear fitting process could not have been combined with the procedure of optimizing the structure of the equations because this procedure can only cope with sums of squares which are linear in the coefficients n_{ij}. Moreover, fitting Eq. (15) to the properties mentioned above ensures that Eq. (15) yields reasonable values for any property based on the first and second derivatives of g, see also the general statement at the beginning of Section 5.5.

5.5.1.2 Accuracy of Eq. (15). Equation (15) clearly meets the accuracy requirements listed in Section 4.2. However, this statement on the formal fulfillment of the requirements gives an insufficient impression of the accuracy of Eq. (15). Therefore, the quality of representing the IAPWS-95 values [7, 8] by Eq. (15) is illustrated by Figs. 3(*a*) to 6 for the relevant properties v, h, c_p, and w along four isotherms considered to be characteristic for the entire region 1. All the diagrams show the deviations of the values calculated from Eq. (15) from the corresponding IAPWS-95 values. In the deviation diagrams for v and h, Figs. 3(*a*) to 4, the IST-85 tolerances [9] are plotted related to the IAPWS-95 values at the p-T values of the Skeleton Tables IST-85 [9]. For comparison, the figures also contain the corresponding lines generated from IFC-67. Figure 3(*a*) shows that Eq. (15) represents the values of the specific volume from IAPWS-95 so well that the v line from Eq. (15) is nearly identical with the zero line. Even for $T \leq 398.15$ K and $p \leq 0.5$ MPa, where the IST-85 tolerances are clearly smaller than the requirements (see Section 4.2), the IAPWS-95 values are represented to within the original tolerances; the only exception is the v value at 323.15 K and 0.1 MPa where the deviation is just outside the IST-85 tolerance. For the greatest part of region 1 the deviations are less than 10 ppm and the maximum deviation amounts to 44 ppm at about 16 MPa and 621 K. In larger ranges of region 1 IFC-67 does not meet the present requirements. Figure 3(*b*) illustrates the accuracy of Eq. (15) along the 0.1 MPa isobar which might be of interest for calibration purposes. The maximum deviation from the IAPWS-95 values, of which the uncertainty in v for this isobar is ± 1 ppm [7, 8], is less than 15 ppm and for $T \leq 300$ K even less than 2 ppm.

Figure 4 gives an impression of how Eq. (15) represents the specific enthalpy values from IAPWS-95 [7, 8]. It can be seen that Eq. (15) meets all enthalpy values from IAPWS-95 within the original IST-85 tolerances. This is also the case for pressures below 1 MPa where two to three times larger enthalpy deviations would have been allowed (see Section 4.2). For temperatures up to 423.15 K the absolute deviations from the IAPWS-95 values remain within ± 0.1 kJ kg^{-1} and for higher temperatures they are in most cases less than ± 0.2 kJ kg^{-1} which is 10 to 20 times smaller than the IST-85 tolerances; considering the entire region 1, the maximum deviation occurs at 569 K very close to the phase boundary and amounts to 0.24 kJ kg^{-1}. The enthalpy is the only property for which the IFC-67 values remain everywhere in this region within the tolerances. However, it should be pointed out that a good representation of the absolute enthalpy values is not the decisive criterion for practical applications, whereas a reasonable representation of enthalpy differences is the most important point. If one is interested in estimating the maximum uncertainties in isobaric enthalpy differences, one has to look at the uncertainties in the isobaric heat capacity.

Figure 5 illustrates the representation of the isobaric heat capacity by Eq. (15). In the entire region 1, the deviations from c_p values from IAPWS-95 are clearly smaller than the permitted tolerances of ± 1 percent, in most cases they are even smaller than ± 0.1 percent; the maximum deviation amounts to 0.15 percent at about 15 MPa and 618 K. A very high accuracy along the 623.15 K isotherm, the boundary to region 3, was the decisive precondition for meeting the consistency requirement along this region boundary.

Figure 6 gives an impression of the behavior of Eq. (15) regarding the speed of sound. This property was the most difficult one to

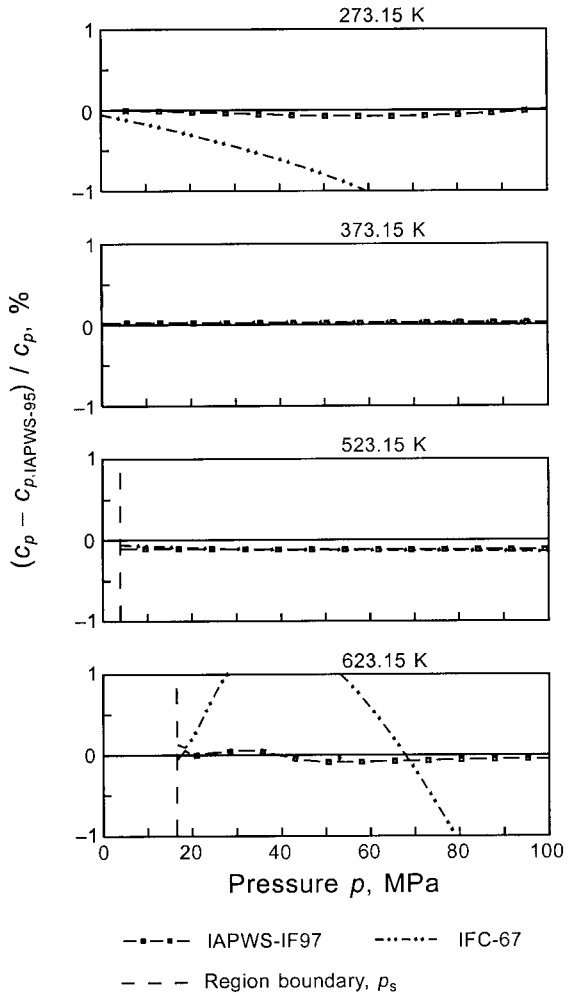

Fig. 5 Percentage deviations of the specific isobaric heat capacities c_p calculated from Eq. (15) and IFC-67, respectively, from values $c_{p,\text{IAPWS-95}}$ calculated from IAPWS-95 [7, 8]

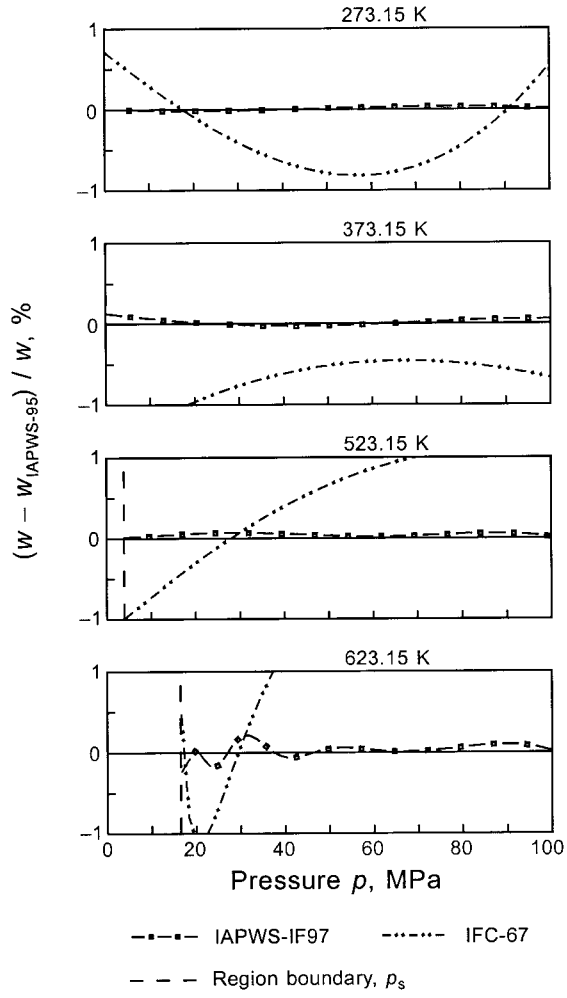

Fig. 6 Percentage deviations of the speeds of sound w calculated from Eq. (15) and IFC-67, respectively, from values $w_{\text{IAPWS-95}}$ calculated from IAPWS-95 [7, 8]

be represented in this region. Nevertheless, in most cases the deviations are less than ± 0.1 percent. The maximum deviation from the IAPWS-95 values occurs at 619 K near the phase boundary and amounts to -0.5 percent. Based on the wish to keep the deviations regarding the speed of sound everywhere below ± 0.5 percent and to keep the maximum inconsistency with respect to this property at the region boundaries definitely below ± 0.5 percent, it was not possible to have less than 34 terms for Eq. (15).

Metastable states. In addition to the properties in the stable single-phase liquid region, Eq. (15) also yields reasonable values in the metastable superheated-liquid region close to the saturated liquid line. Investigations yielded that for temperatures up to 573.15 K and pressures down to zero the deviations from the IAPWS-95 values remain practically the same as they are at the saturation curve (region 4). For 623.15 K, Eq. (15) can be extrapolated into the superheated-liquid region for pressures $|p - p_s| \leq 1.5$ MPa without showing deviations from IAPWS-95 greater than 0.1 percent in v.

5.5.2 The Gibbs Free Energy Equation for Region 2. The basic equation for this region is probably the most important equation of the entire package of IAPWS-IF97 because in actual plant the important processes, e.g., the expansions in steam turbines, occur in this region.

The auxiliary equation for defining the boundary between regions 2 and 3 is given as Eqs. (10) and (11) in Section 5.3.

The basic equation for this region is a fundamental equation for the specific Gibbs free energy g. This equation is expressed in dimensionless form, $\gamma = g/(RT)$, and is separated into two parts, an ideal-gas part γ^o and a residual part γ^r, so that

$$\frac{g(p, T)}{RT} = \gamma(\pi, \tau) = \gamma^o(\pi, \tau) + \gamma^r(\pi, \tau), \tag{19}$$

where $\pi = p/p^*$ and $\tau = T^*/T$ with R given by Eq. (1).

The equation for the ideal-gas part γ^o of the dimensionless Gibbs free energy reads

$$\gamma^o = \ln \pi + \sum_{i=1}^{9} n_i^o \tau^{J_i^o}, \tag{20}$$

where $\pi = p/p^*$ and $\tau = T^*/T$ with $p^* = 1$ MPa and $T^* = 540$ K. The coefficients n_1^o and n_2^o were adjusted in such a way that the values for the specific internal energy and specific entropy, calculated from Eq. (19), relate to Eq. (16). Table A4 contains the coefficients n_i^o and exponents J_i^o of Eq. (20).

The form of the residual part γ^r of the dimensionless Gibbs free energy is as follows:

$$\gamma^r = \sum_{i=1}^{43} n_i \pi^{I_i} (\tau - 0.5)^{J_i}, \tag{21}$$

Table 4 Relations of thermodynamic properties to the ideal-gas part γ^o and the residual part γ^r of the dimensionless Gibbs free energy and their derivatives when using Eqs. (19), (23), and (29)[a]

Property	Relation
Specific volume $v = (\partial g/\partial p)_T$	$v(\pi,\tau)\frac{p}{RT} = \pi\left(\gamma^o_\pi + \gamma^r_\pi\right)$
Specific internal energy $u = g - T(\partial g/\partial T)_p - p(\partial g/\partial p)_T$	$\frac{u(\pi,\tau)}{RT} = \tau\left(\gamma^o_\tau + \gamma^r_\tau\right) - \pi\left(\gamma^o_\pi + \gamma^r_\pi\right)$
Specific entropy $s = -(\partial g/\partial T)_p$	$\frac{s(\pi,\tau)}{R} = \tau\left(\gamma^o_\tau + \gamma^r_\tau\right) - \left(\gamma^o + \gamma^r\right)$
Specific enthalpy $h = g - T(\partial g/\partial T)_p$	$\frac{h(\pi,\tau)}{RT} = \tau\left(\gamma^o_\tau + \gamma^r_\tau\right)$
Specific isobaric heat capacity $c_p = (\partial h/\partial T)_p$	$\frac{c_p(\pi,\tau)}{R} = -\tau^2\left(\gamma^o_{\tau\tau} + \gamma^r_{\tau\tau}\right)$
Specific isochoric heat capacity $c_v = (\partial u/\partial T)_v$	$\frac{c_v(\pi,\tau)}{R} = -\tau^2\left(\gamma^o_{\tau\tau} + \gamma^r_{\tau\tau}\right) - \frac{(1+\pi\gamma^r_\pi - \tau\pi\gamma^r_{\pi\tau})^2}{1-\pi^2\gamma^r_{\pi\pi}}$
Speed of sound $w = v\left[-(\partial p/\partial v)_s\right]^{0.5}$	$\frac{w^2(\pi,\tau)}{RT} = \frac{1+2\pi\gamma^r_\pi + \pi^2\gamma^{r\,2}_\pi}{\left(1-\pi^2\gamma^r_{\pi\pi}\right) + \frac{\left(1+\pi\gamma^r_\pi - \tau\pi\gamma^r_{\pi\tau}\right)^2}{\tau^2\left(\gamma^o_{\tau\tau} + \gamma^r_{\tau\tau}\right)}}$

$\gamma^r_\pi = \left(\frac{\partial\gamma^r}{\partial\pi}\right)_\tau, \gamma^r_{\pi\pi} = \left(\frac{\partial^2\gamma^r}{\partial\pi^2}\right)_\tau, \gamma^r_\tau = \left(\frac{\partial\gamma^r}{\partial\tau}\right)_\pi, \gamma^r_{\tau\tau} = \left(\frac{\partial^2\gamma^r}{\partial\tau^2}\right)_\pi, \gamma^r_{\pi\tau} = \left(\frac{\partial^2\gamma^r}{\partial\pi\partial\tau}\right), \gamma^o_\tau = \left(\frac{\partial\gamma^o}{\partial\tau}\right)_\pi, \gamma^o_{\tau\tau} = \left(\frac{\partial^2\gamma^o}{\partial\tau^2}\right)_\pi$

[a] A general procedure how to obtain the relation of any property and any differential quotient to γ^o and γ^r and their derivatives when using Eqs. (19), (23), and (29) can be found in [19a]

where $\pi = p/p^*$ and $\tau = T^*/T$ with $p^* = 1$ MPa and $T^* = 540$ K. The coefficients n_i and exponents I_i and J_i of Eq. (21) are listed in Table A5.

All thermodynamic properties can be derived from Eq. (19) by using the appropriate combinations of the ideal-gas part γ^o, Eq. (20), and the residual part γ^r, Eq. (21), of the dimensionless Gibbs free energy and their derivatives. The relations of the relevant thermodynamic properties to γ^o and γ^r and their derivatives are summarized in Table 4. All required derivatives of the ideal-gas part and of the residual part of the dimensionless Gibbs free energy are explicitly given in Table 5 and Table 6, respectively.

Equation (19) covers region 2 of IAPWS-IF97 defined by the following range of temperature and pressure, see Fig. 2:

$$273.15\ \text{K} \le T \le 623.15\ \text{K} \quad 0 < p \le p_s(T)_{\text{Eq.(28)}}$$

$$623.15\ \text{K} < T \le 863.15\ \text{K} \quad 0 < p \le p(T)_{\text{Eq.(10)}}$$

$$863.15\ \text{K} < T \le 1073.15\ \text{K} \quad 0 < p \le 100\ \text{MPa}$$

Table 5 The ideal-gas part γ^o of the dimensionless Gibbs free energy, Eq. (20), and its derivatives

$\gamma^o = \ln\pi + \sum_{i=1}^{9} n_i^o \tau^{J_i^o}$	$\gamma^o_\tau = \sum_{i=1}^{9} n_i^o J_i^o \tau^{J_i^o - 1}$
$\gamma^o_\pi = \pi^{-1}$	$\gamma^o_{\tau\tau} = \sum_{i=1}^{9} n_i^o J_i^o \left(J_i^o - 1\right)\tau^{J_i^o - 2}$
$\gamma^o_{\pi\pi} = -\pi^{-2}$	$\gamma^o_{\pi\tau} = 0$

$\gamma^o_\pi = \left(\frac{\partial\gamma^o}{\partial\pi}\right)_\tau, \gamma^o_{\pi\pi} = \left(\frac{\partial^2\gamma^o}{\partial\pi^2}\right)_\tau, \gamma^o_\tau = \left(\frac{\partial\gamma^o}{\partial\tau}\right)_\pi, \gamma^o_{\tau\tau} = \left(\frac{\partial^2\gamma^o}{\partial\tau^2}\right)_\pi, \gamma^o_{\pi\tau} = \left(\frac{\partial^2\gamma^o}{\partial\pi\partial\tau}\right)$

Table 6 The residual part γ^r of the dimensionless Gibbs free energy, Eq. (21), and its derivatives

$\gamma^r = \sum_{i=1}^{43} n_i \pi^{I_i} (\tau - 0.5)^{J_i}$	$\gamma^r_\tau = \sum_{i=1}^{43} n_i \pi^{I_i} J_i (\tau - 0.5)^{J_i - 1}$
$\gamma^r_\pi = \sum_{i=1}^{43} n_i I_i \pi^{I_i - 1} (\tau - 0.5)^{J_i}$	$\gamma^r_{\tau\tau} = \sum_{i=1}^{43} n_i \pi^{I_i} J_i (J_i - 1)(\tau - 0.5)^{J_i - 2}$
$\gamma^r_{\pi\pi} = \sum_{i=1}^{43} n_i I_i (I_i - 1)\pi^{I_i - 2} (\tau - 0.5)^{J_i}$	$\gamma^r_{\pi\tau} = \sum_{i=1}^{43} n_i I_i \pi^{I_i - 1} J_i (\tau - 0.5)^{J_i - 1}$

$\gamma^r_\pi = \left(\frac{\partial\gamma^r}{\partial\pi}\right)_\tau, \gamma^r_{\pi\pi} = \left(\frac{\partial^2\gamma^r}{\partial\pi^2}\right)_\tau, \gamma^r_\tau = \left(\frac{\partial\gamma^r}{\partial\tau}\right)_\pi, \gamma^r_{\tau\tau} = \left(\frac{\partial^2\gamma^r}{\partial\tau^2}\right)_\pi, \gamma^r_{\pi\tau} = \left(\frac{\partial^2\gamma^r}{\partial\pi\partial\tau}\right)$

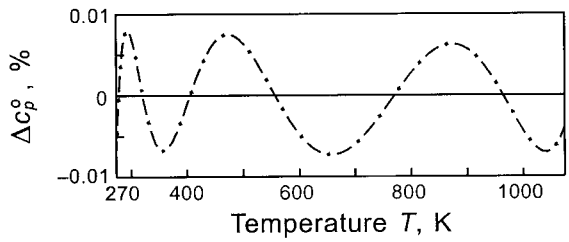

Fig. 7 Percentage deviations of the specific isobaric heat capacities in the ideal-gas state c_p^o calculated from Eq. (20) from values $c_{p,\text{IAPWS-95}}^o$ calculated from IAPWS-95 [7, 8]; $\Delta c_p^o = ((c_p^o/R) - (c_p^o/R)_{\text{IAPWS-95}})/(c_p^o/R)$.

In addition to the properties in the stable single-phase vapor region, Eq. (19) also yields reasonable values in the metastable-vapor region for pressures above 10 MPa. Equation (19) is not valid in the metastable-vapor region at pressures $p \le 10$ MPa; for this part of the metastable-vapor region see Section 5.5.2.3. For temperatures between 273.15 K and 273.16 K at pressures above the sublimation pressure [20] (metastable subcooled vapor) all values are calculated by extrapolation from Eqs. (19) and (28).

To assist the user in computer-program verification of Eq. (19), Table A6 contains test values of the most relevant properties.

5.5.2.1 Development of Eqs. (20) and (21). When developing an equation of state which should cover the typical gas-phase region starting from zero pressure, it is necessary to separate the part responsible for the behavior of the ideal gas from the rest of the equation. Thus, for region 2 the fundamental equation for the specific Gibbs free energy g in its dimensionless form, $\gamma = g/(RT)$, is separated into an ideal-gas part γ^o and a residual part γ^r according to Eq. (19). The relation for the ideal-gas part $\gamma^o(\pi, \tau)$, Eq. (20), consists of the pure pressure-dependent part $\gamma^o(\pi) = \ln\pi$ and of a pure temperature dependent part $\gamma^o(\tau)$. Keeping in mind a short computing time and the limited range of validity of Eq. (19), namely from 273.15 K to 1073.15 K, $\gamma^o(\tau)$ is expressed by a simple polynomial so that the entire equation for the ideal-gas part γ^o of the dimensionless Gibbs free energy has the form of Eq. (20). Its coefficients n_3 to n_9 were determined by fitting Eq. (20) to (c_p^o/R) values from IAPWS-95 [7, 8]; details of this fitting process, which was also combined with optimizing the structure of Eq. (20), can be found in reference [18]. The coefficients n_1^o and n_2^o were determined as described for Eq. (20).

Again, the development of the residual part γ^r of the dimensionless Gibbs free energy, Eq. (21), started with the formulation of the general functional expression based on the general form of the combined polynomial according to Eq. (14) and on similar considerations and test calculations as carried out for Eq. (18). Here, the shifting parameter b in Eq. (14) was set to zero to ensure a reasonable transition to the ideal gas. Thus, the final bank of terms consisted of 955 terms and had the following form [18]:

$$\gamma^r = \sum_{i=1}^{10}\sum_{j=0}^{33} n_{ij}\pi^i(\tau - 0.5)^j + \sum_{i=11}^{25}\sum_{j=20}^{60} n_{ij}\pi^i(\tau - 0.5)^j, \quad (22)$$

where $\pi = p/p^*$ and $\tau = T^*/T$ with $p^* = 1$ MPa and $T^* = 540$ K. Equation (21), obtained from Eq. (22) by the procedure of Setzmann and Wagner [5] for optimizing the functional structure of the final γ^r equation, was fitted as a part of Eq. (19) (i.e., in combination with Eq. (20)) to values of the properties v, h, c_p, s, $(\partial v/\partial p)_T$, and $(\partial v/\partial T)_p$. All these values were calculated from IAPWS-95 [7, 8] for given values of p and T distributed as selected grid points over region 2. The reasoning for including the partial derivatives of v in these properties is given for Eq. (18). Further details of the fitting process are given by Kruse and Wagner [18].

5.5.2.2 Accuracy of Eq. (19). Figure 7 shows that the γ^o equation, Eq. (20), represents the (c_p^o/R) values from IAPWS-95 [7, 8] with maximum deviations of ± 0.0081 percent. In order to

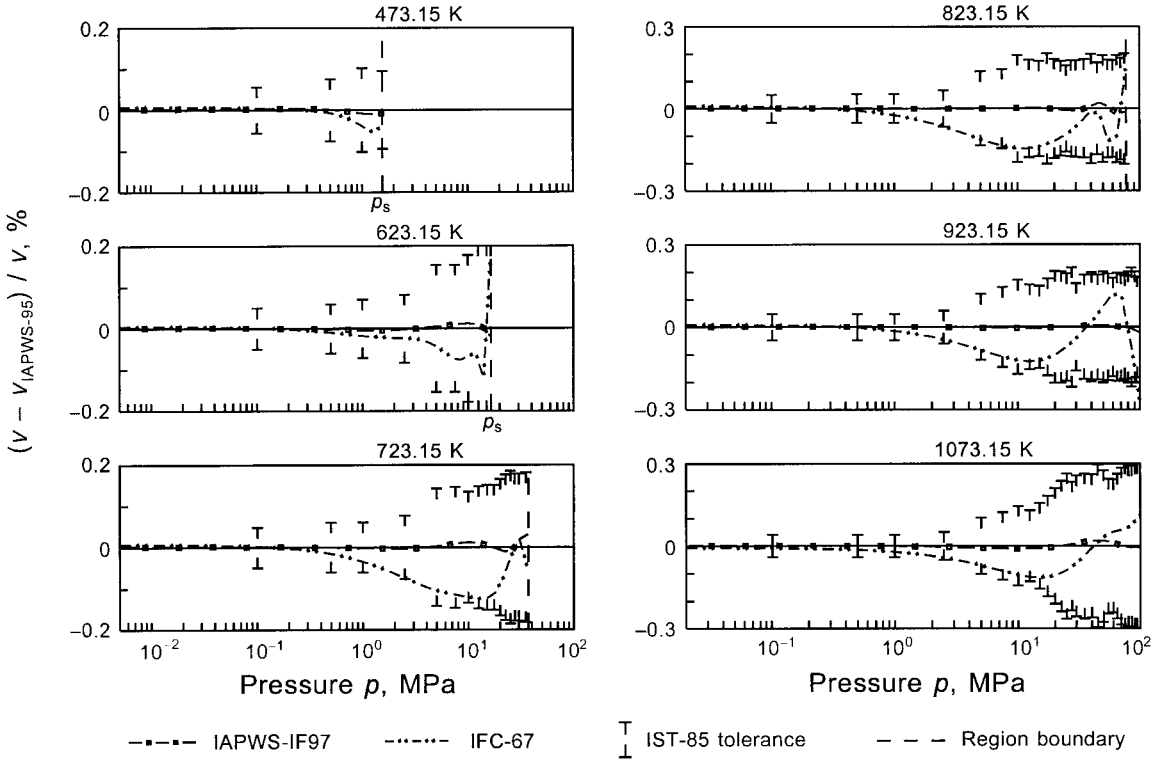

Fig. 8 Percentage deviations of the specific volumes v calculated from Eq. (19) and IFC-67, respectively, from values $v_{IAPWS-95}$ calculated from IAPWS-95 [7, 8]

obtain the difference in c_p^o itself between IAPWS-IF97 and IAPWS-95 a constant amount of +0.0017 percent has to be added to the deviations plotted in Fig. 7. This constant offset is caused by the older value of the gas constant used for IAPWS-95.

Equation (19) clearly meets the accuracy requirements listed in Section 4.2. The quality of representing the IAPWS-95 values [7, 8] by Eq. (19) is illustrated in Figs. 8 to 12 for the relevant properties v, h, c_p, and w. The figures show the deviations of the values calculated from Eq. (19) from the corresponding IAPWS-95 values along six isotherms and along the boundary between regions 2 and 3 described by the B23-equation corresponding to Eq. (10). These seven lines are considered to be characteristic examples for the behavior of Eq. (19) in the entire region 2. The corresponding values from IFC-67 are plotted for comparison.

Figure 8 provides information on the representation of the specific volumes by Eq. (19) which is better than the requirements by far; considering the entire region 2, the maximum deviation from the IAPWS-95 values amounts to 0.038 percent which occurs near 39 MPa and 750 K. In contrast to this, at higher temperatures IFC-67 makes full use of the tolerances reaching up to ±0.3 percent.

Figure 9 shows that the behavior of Eq. (19) regarding the representation of the specific enthalpies is very similar to that of the specific volumes. When considering the entire region, for $T \leq 750$ K the deviations from the IAPWS-95 values are less than ±0.2 kJ kg^{-1}, whereas for $T > 750$ K and $p > 10$ MPa the deviations increase up to about 0.4 kJ kg^{-1}; the maximum deviation occurs at 100 MPa near 900 K and amounts to 0.41 kJ kg^{-1}. Thus, for the largest part of region 2 the deviations are 20 to 40 times less than the IST-85 tolerances [9]. In contrast to this, the IFC-67 values show more systematic deviations from the values of IAPWS-95 which increase up to the IST-85 tolerances at the highest pressures of the corresponding isotherm.

Figure 10 illustrates the percentage difference between the isobaric heat capacities from IAPWS-95 and Eq. (19). In this region c_p was the property which gave the most problems. The most difficult problem was to keep the deviations along the boundary to region 3 within ±0.5 percent (see Fig. 12). This was the decisive precondition for meeting the consistency requirement along this region boundary. Nevertheless, apart from the boundaries to regions 3 and 4 the deviations are less than ±0.1 percent. However, when approaching the boundary to region 3 at higher temperatures, the deviations in c_p increase up to ±0.5 percent in a few cases; the maximum deviation amounts to 0.59 percent at about 56 MPa and 780 K. It can be seen that IFC-67, even for moderate pressures, does not meet the requirements set for IAPWS-IF97, although its enthalpy representation in this range does not seem to be too bad (see, however, the statement on this matter given in context with Fig. 4 in Section 5.5.1.2).

From Fig. 11 it can be seen that Eq. (19) does not have any difficulty in representing the speeds of sound. Along the entire boundary to region 4 (saturation curve) the deviations from the IAPWS-95 values remain within ±0.1 percent. When approaching the boundary to region 3, it is only at higher temperatures that the deviations increase to ±0.25 percent. Considering the entire region 2, the maximum deviation from the IAPWS-95 values amounts to 0.33 percent at 100 MPa near 900 K.

Figure 12 shows the deviations of the properties v, h, c_p, and w from the corresponding IAPWS-95 values along the boundary to region 3. It can be seen that Eq. (19) does not have any problems along this "difficult" boundary, neither for c_p nor for w. In contrast to this, the c_p values from IFC-67 deviate from IAPWS-95 by up to about 6 percent.

After looking at all these deviation diagrams and realizing that the accuracy requirements are clearly exceeded, it should be emphasized that the quality of Eq. (19) is absolutely necessary in order to meet for certain the requirements regarding the consistency along the boundary between region 2 and regions 3 and 4, respectively. The large differences in c_p at the equivalent boundaries were one of the greatest weaknesses of IFC-67.

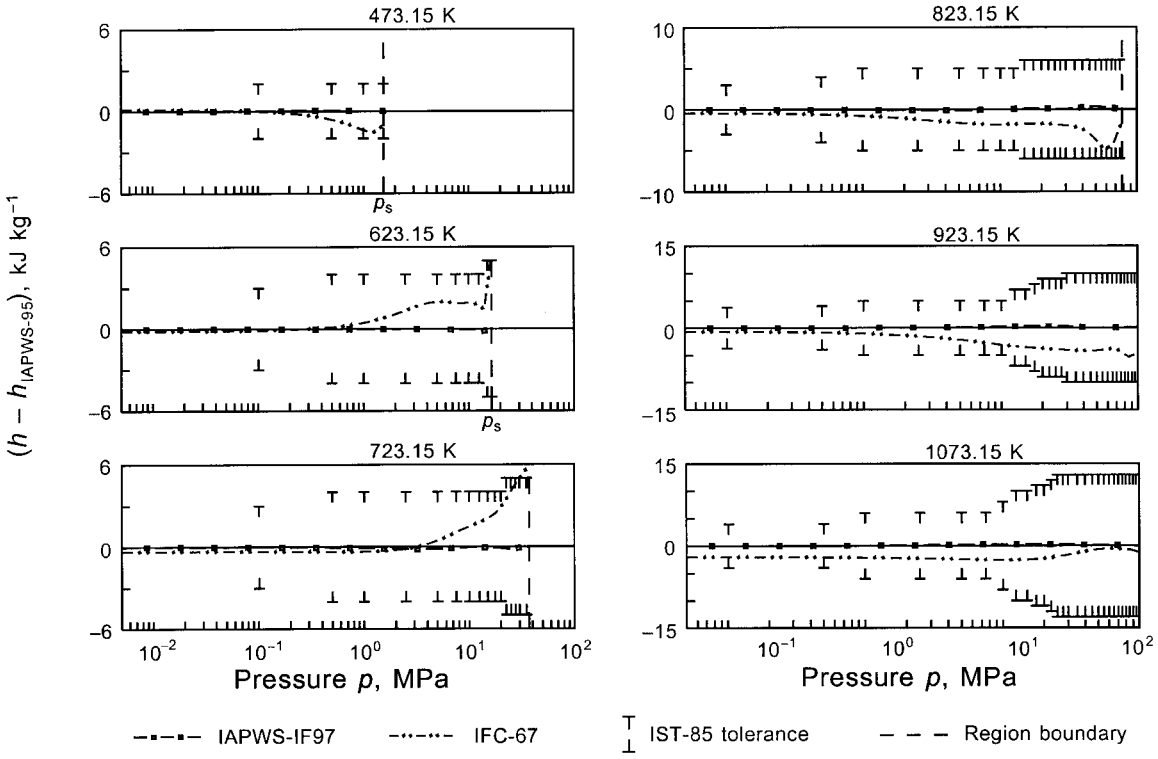

Fig. 9 Absolute deviations of the specific enthalpies h calculated from Eq. (19) and IFC-67, respectively, from values $h_{IAPWS-95}$ calculated from IAPWS-95 [7, 8]

5.5.2.3 Supplementary Equation for the Metastable-Vapor Region. As for the basic equation, Eq. (19), the supplementary equation for a part of the metastable-vapor region is given in the dimensionless form of the specific Gibbs free energy, $\gamma = g/(RT)$, consisting of an ideal-gas part γ^o and a residual part γ^r, so that

$$\frac{g(p, T)}{RT} = \gamma(\pi, \tau) = \gamma^o(\pi, \tau) + \gamma^r(\pi, \tau), \qquad (23)$$

where $\pi = p/p^*$ and $\tau = T^*/T$ with R given by Eq. (1).

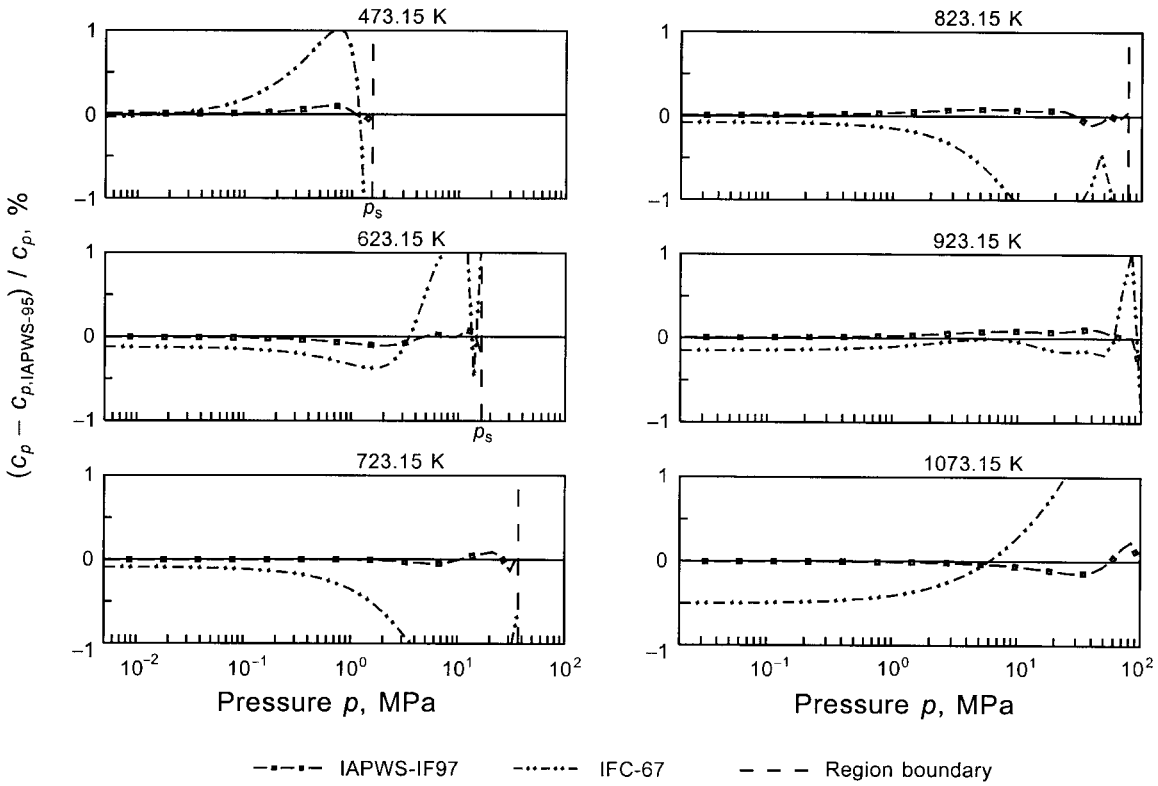

Fig. 10 Percentage deviations of the specific isobaric heat capacities c_p calculated from Eq. (19) and IFC-67, respectively, from values $c_{p,IAPWS-95}$ calculated from IAPWS-95 [7, 8]

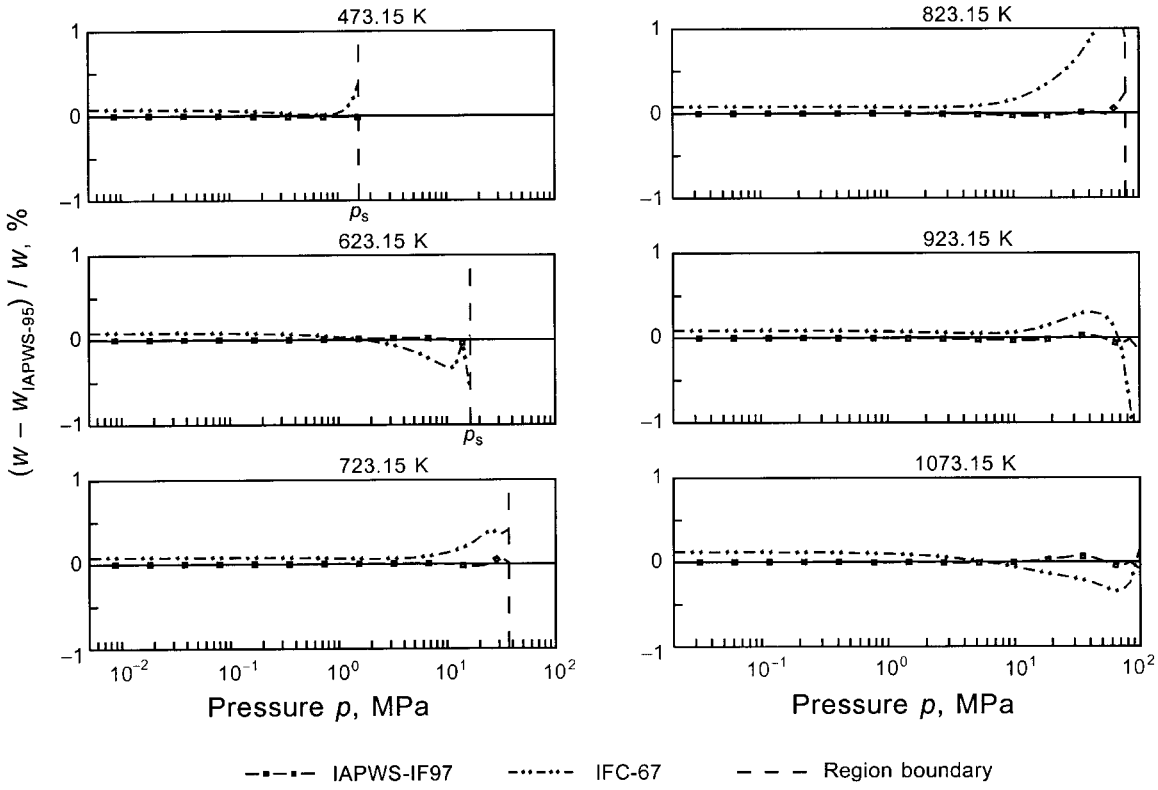

Fig. 11 Percentage deviations of the speeds of sound w calculated from Eq. (19) and IFC-67, respectively, from values $w_{IAPWS-95}$ calculated from IAPWS-95 [7, 8]

The equation for the ideal-gas part γ^o is identical with Eq. (20) except for the values of the two coefficients n_1^o and n_2^o, see Table A4. For the use of Eq. (20) as part of Eq. (23) the coefficients n_1^o and n_2^o were readjusted to meet the high consistency requirement between Eqs. (23) and (19) regarding the properties h and s along the saturated vapor line, see below.

The equation for the residual part γ^r reads

$$\gamma^r = \sum_{i=1}^{13} n_i \pi^{I_i} (\tau - 0.5)^{J_i}, \tag{24}$$

where $\pi = p/p^*$ and $\tau = T^*/T$ with $p^* = 1$ MPa and $T^* = 540$ K. The coefficients n_i and exponents I_i and J_i of Eq. (24) are listed in Table A7.

All thermodynamic properties can be derived from Eq. (23) by using the appropriate combinations of the ideal-gas part γ^o, Eq. (20), and the residual part γ^r, Eq. (24), of the dimensionless Gibbs free energy and their derivatives. The relations of the relevant thermodynamic properties to γ^o and γ^r and their derivatives are summarized in Table 4. All the required derivatives of the ideal-gas part and of the residual part of the dimensionless Gibbs free energy are explicitly given in Table 5 and Table 7, respectively.

Equation (23) is valid in the metastable-vapor region from the saturated vapor line to the 5 percent equilibrium moisture line at pressures from the triple-point pressure, see Eq. (8), up to 10 MPa. The 5 percent moisture line is determined from the equilibrium h' and h'' values where these enthalpy values at saturation belong to the pressure (not to the temperature) after the corresponding expansion.

To assist the user in computer-program verification of Eq. (23), Table A8 contains test values of the most relevant properties.

Reasons for Eq. (23). Initially the thermodynamic properties in the metastable-vapor region between the saturated vapor line and the 5 percent equilibrium moisture line were calculated from Eq. (19). Therefore, Eq. (19) was not only fitted to the properties of the stable part of region 2 calculated from IAPWS-95 [7, 8] but also to the corresponding properties in the metastable part adjacent to region 2. However, after the development of Eq. (19) it became clear that in the metastable region for pressures below 10 MPa Eq. (19) showed unexpected behavior [21]. In this range the vapor spinodal of IAPWS-95 is too close to the saturated vapor line [7, 8] and as a consequence Eq. (19) also displayed the same trend. Thus, it was decided to develop a supplementary equation for the metastable-vapor region for pressures up to 10 MPa. Since there are no experimental data in the metastable-vapor region to which such an equation could be fitted, the needed input values were determined by extrapolating a so-called gas equation into the metastable-vapor region for $p \leq 10$ MPa. This gas equation which provides a reliable representation of the thermodynamic properties of the gas region of H_2O at low densities ($\rho \leq 55$ kg m^{-3}) is described in reference [8]; it was used as an auxiliary equation for the development of IAPWS-95 [7, 8]. Besides fitting Eq. (23) to values of v, h, c_p, and s in the metastable-vapor region extrapolated from the gas equation, it was also fitted to corresponding values on the saturated vapor line calculated from Eq. (19).

Behavior of Eq. (23). Figure 13 shows in an h-s diagram the section of the metastable-vapor region which covers the temperature range from 300 K to 420 K corresponding to a pressure range from 0.0036 MPa to 0.44 MPa. The 5 percent moisture line is also shown which indicates approximately the lowest location of such Wilson lines which are considered to be the lower limit of the metastable region required for steam-turbine engineering. It can be seen that the paths of the isotherms calculated from the various equations considered are significantly different. Due to several thermodynamic reasons the IFC-67 isotherms seem to be too linear whereas the isotherms calculated from the basic equation of this region, Eq. (19), have a too strong curvature. The course of the isotherms calculated from the supplementary equation, Eq. (23), and the gas equation [8] to which Eq. (23) was fitted, are in very good agreement. Equation (23) is considered to yield reasonable

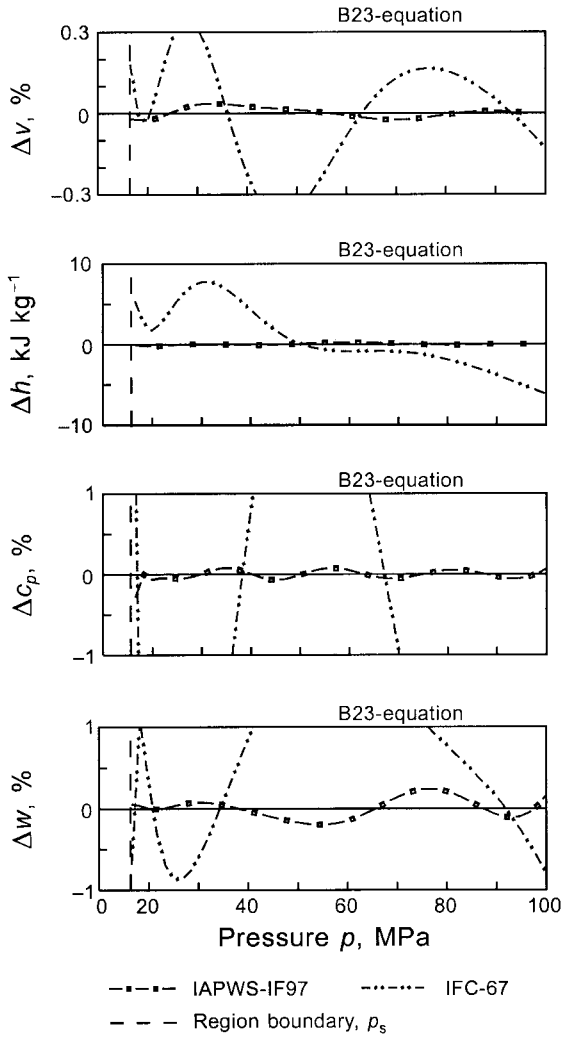

Fig. 12 Percentage deviations of the values of v, c_p, and w and absolute deviations of h values calculated from Eq. (19) and IFC-67, respectively, from the corresponding values calculated from IAPWS-95 [7, 8] along the boundary between regions 2 and 3 defined by the B23-equation: $\Delta v = (v - v_{\text{IAPWS-95}})/v$; $\Delta c_p = (c_p - c_{p,\text{IAPWS-95}})/c_p$; $\Delta h = h - h_{\text{IAPWS-95}}$; $\Delta w = (w - w_{\text{IAPWS-95}})/w$.

predictions for steam properties for industrial use in the metastable-vapor region.

The consistency of Eq. (23) with the basic equation, Eq. (19), along the saturated vapor line is characterized by the maximum and root-mean-square (RMS) inconsistencies regarding the properties v, h, c_p, s, g, and w; these values are listed in Table 8. The maximum inconsistencies are clearly smaller than the consistency requirements at the single-phase region boundaries corresponding to the so-called Prague values [10], which are given in Section 4.3.

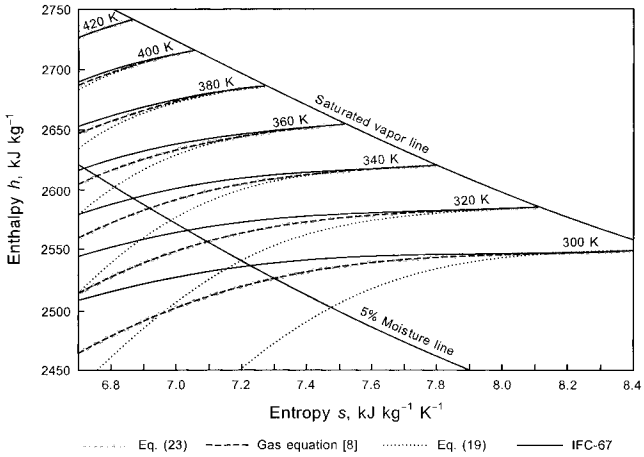

Fig. 13 Mollier *h-s* diagram for the metastable-vapor region with isotherms calculated from the equations given above

Along the 10 MPa isobar in the metastable-vapor region, the transition between Eqs. (23) and (19) is not smooth but for practical calculations unimportant.

5.5.3 The Helmholtz Free Energy Equation for Region 3. The basic equation for this region is a fundamental equation for the specific Helmholtz free energy f. This equation is expressed in dimensionless form, $\phi = f/(RT)$, and reads

$$\frac{f(\rho, T)}{RT} = \phi(\delta, \tau) = n_1 \ln \delta + \sum_{i=2}^{40} n_i \delta^{I_i} \tau^{J_i}, \qquad (25)$$

where $\delta = \rho/\rho^*$, $\tau = T^*/T$ with $\rho^* = \rho_c$, $T^* = T_c$, and R, T_c, and ρ_c given by Eqs. (1), (4), and (6). The coefficients n_i and exponents I_i and J_i of Eq. (25) are listed in Table A9.

Due to fitting Eq. (25) to the phase-equilibrium condition in the form of the Maxwell criterion for given values of T or p all properties along that part of the saturation curve belonging to region 3 can be calculated from Eq. (25) alone. Moreover, Eq. (25) reproduces exactly the critical parameters according to Eqs. (4) to (6) and yields zero for the first two pressure derivatives with respect to density at the critical point.

All thermodynamic properties can be derived from Eq. (25) by using the appropriate combinations of the dimensionless Helmholtz free energy ϕ and its derivatives. The relations of the relevant thermodynamic properties to ϕ and its derivatives are summarized in Table 9. All required derivatives of the dimensionless Helmholtz free energy are explicitly given in Table 10.

Equation (25) covers region 3 of IAPWS-IF97 defined by the following range of temperature and pressure, see Fig. 2:

$$623.15 \text{ K} \le T \le T(p)_{\text{Eq.(11)}} \quad p(T)_{\text{Eq.(10)}} \le p \le 100 \text{ MPa}.$$

Table 7 The residual part γ^r of the dimensionless Gibbs free energy, Eq. (24), and its derivatives

$\gamma^r = \sum_{i=1}^{13} n_i \pi^{I_i} (\tau - 0.5)^{J_i}$	$\gamma^r_\tau = \sum_{i=1}^{13} n_i \pi^{I_i} J_i (\tau - 0.5)^{J_i - 1}$
$\gamma^r_\pi = \sum_{i=1}^{13} n_i I_i \pi^{I_i - 1} (\tau - 0.5)^{J_i}$	$\gamma^r_{\tau\tau} = \sum_{i=1}^{13} n_i \pi^{I_i} J_i (J_i - 1)(\tau - 0.5)^{J_i - 2}$
$\gamma^r_{\pi\pi} = \sum_{i=1}^{13} n_i I_i (I_i - 1)\pi^{I_i - 2} (\tau - 0.5)^{J_i}$	$\gamma^r_{\pi\tau} = \sum_{i=1}^{13} n_i I_i \pi^{I_i - 1} J_i (\tau - 0.5)^{J_i - 1}$

$\gamma^r_\pi = \left(\frac{\partial \gamma^r}{\partial \pi}\right)_\tau$, $\gamma^r_{\pi\pi} = \left(\frac{\partial^2 \gamma^r}{\partial \pi^2}\right)_\tau$, $\gamma^r_\tau = \left(\frac{\partial \gamma^r}{\partial \tau}\right)_\pi$, $\gamma^r_{\tau\tau} = \left(\frac{\partial^2 \gamma^r}{\partial \tau^2}\right)_\pi$, $\gamma^r_{\pi\tau} = \left(\frac{\partial^2 \gamma^r}{\partial \pi \partial \tau}\right)$

Table 8 Inconsistencies between Eqs. (19) and (23) along the saturated vapor line given as maximum and root-mean square (RMS) values

Inconsistency	Prague value [10]	Maximum value[a]	RMS value
Δv, %	0.05	0.014	0.006
Δh, kJ kg^{-1}	0.2	0.043	0.020
Δc_p, %	1	0.78	0.357
Δs, J kg^{-1}K^{-1}	0.2	0.082	0.044
Δg, kJ kg^{-1}	0.2	0.023	0.009
Δw, %	1[b]	0.051	0.025

[a] Absolute value
[b] The permitted inconsistency value for w is not included in the Prague values

Table 9 Relations of thermodynamic properties to the dimensionless Helmholtz free energy ϕ and its derivatives when using Eq. (25)[a]

Property	Relation
Pressure $p = \rho^2(\partial f/\partial\rho)_T$	$\frac{p(\delta,\tau)}{\rho RT} = \delta\phi_\delta$
Specific internal energy $u = f - T(\partial f/\partial T)_\rho$	$\frac{u(\delta,\tau)}{RT} = \tau\phi_\tau$
Specific entropy $s = -(\partial f/\partial T)_\rho$	$\frac{s(\delta,\tau)}{R} = \tau\phi_\tau - \phi$
Specific enthalpy $h = f - T(\partial f/\partial T)_\rho + \rho(\partial f/\partial\rho)_T$	$\frac{h(\delta,\tau)}{RT} = \tau\phi_\tau + \delta\phi_\delta$
Specific isochoric heat capacity $c_v = (\partial u/\partial T)_\rho$	$\frac{c_v(\delta,\tau)}{R} = -\tau^2\phi_{\tau\tau}$
Specific isobaric heat capacity $c_p = (\partial h/\partial T)_p$	$\frac{c_p(\delta,\tau)}{R} = -\tau^2\phi_{\tau\tau} + \frac{(\delta\phi_\delta - \delta\tau\phi_{\delta\tau})^2}{2\delta\phi_\delta + \delta^2\phi_{\delta\delta}}$
Speed of sound $w = \left[(\partial p/\partial\rho)_s\right]^{0.5}$	$\frac{w^2(\delta,\tau)}{RT} = 2\delta\phi_\delta + \delta^2\phi_{\delta\delta} - \frac{(\delta\phi_\delta - \delta\tau\phi_{\delta\tau})^2}{\tau^2\phi_{\tau\tau}}$
Phase-equilibrium condition (Maxwell criterion)	$\frac{p_s}{RT\rho'} = \delta'\phi_\delta(\delta',\tau)$; $\frac{p_s}{RT\rho''} = \delta''\phi_\delta(\delta'',\tau)$
	$\frac{p_s}{RT}\left(\frac{1}{\rho''} - \frac{1}{\rho'}\right) = \phi(\delta',\tau) - \phi(\delta'',\tau)$

$\phi_\delta = \left(\frac{\partial\phi}{\partial\delta}\right)_\tau$, $\phi_{\delta\delta} = \left(\frac{\partial^2\phi}{\partial\delta^2}\right)_\tau$, $\phi_\tau = \left(\frac{\partial\phi}{\partial\tau}\right)_\delta$, $\phi_{\tau\tau} = \left(\frac{\partial^2\phi}{\partial\tau^2}\right)_\delta$, $\phi_{\delta\tau} = \left(\frac{\partial^2\phi}{\partial\delta\partial\tau}\right)$

[a] A general procedure how to obtain the relation of any property and any differential quotient to ϕ and its derivatives when using Eq. (25) can be found in [19a]

In addition to the properties in the stable single-phase region defined above, Eq. (25) also yields reasonable values in the metastable regions (superheated liquid and subcooled steam) close to the saturated liquid and saturated vapor line, see Section 5.5.3.2.

To assist the user in computer-program verification of Eq. (25), Table A10 contains test values of the most relevant properties.

5.5.3.1 Development of Eq. (25). In contrast to the fundamental equation of the Gibbs free energy g the fundamental equation of the Helmholtz free energy f chosen for region 3 of IAPWS-IF97 is suitable for the critical and supercritical region covered by region 3. The independent variables of such an f equation are the density ρ and the temperature T. When establishing an equation of state in the form of the fundamental equation of the Helmholtz free energy, the expression is usually separated into a part for the ideal gas and a residual part [8, 16, 17]. However, such a separation is not necessary for the special application only to the critical and supercritical region. Comprehensive test calculations yielded that there was no need to use the shifting parameters b and d as given in Eq. (14) for the general functional form of the $g(p, T)$ equations but to use the critical parameters ρ_c and T_c as reducing parameters ρ^* and T^*. Moreover, in addition to the pure polynomial in δ and τ the incorporation of $(\ln\delta)\tau^j$ terms proved favorable. As a result of all these considerations and test calculations the following general functional expression of 362 terms was used for the subsequent optimization process [18]:

$$\phi = \sum_{j=0}^{10} n_j(\ln\delta)\tau^j + \sum_{i=0}^{12}\sum_{j=0}^{26} n_{ij}\delta^i\tau^j, \qquad (26)$$

Table 10 The dimensionless Helmholtz free energy ϕ, Eq. (25), and its derivatives

$\phi = n_1\ln\delta + \sum_{i=2}^{40} n_i\,\delta^{I_i}\,\tau^{J_i}$	$\phi_\tau = \sum_{i=2}^{40} n_i\,\delta^{I_i}\,J_i\,\tau^{J_i-1}$
$\phi_\delta = n_1\delta^{-1} + \sum_{i=2}^{40} n_i\,I_i\,\delta^{I_i-1}\,\tau^{J_i}$	$\phi_{\tau\tau} = \sum_{i=2}^{40} n_i\,\delta^{I_i}\,J_i(J_i-1)\,\tau^{J_i-2}$
$\phi_{\delta\delta} = -n_1\delta^{-2} + \sum_{i=2}^{40} n_i\,I_i(I_i-1)\,\delta^{I_i-2}\,\tau^{J_i}$	$\phi_{\delta\tau} = \sum_{i=2}^{40} n_i\,I_i\,\delta^{I_i-1}\,J_i\,\tau^{J_i-1}$

$\phi_\delta = \left(\frac{\partial\phi}{\partial\delta}\right)_\tau$, $\phi_{\delta\delta} = \left(\frac{\partial^2\phi}{\partial\delta^2}\right)_\tau$, $\phi_\tau = \left(\frac{\partial\phi}{\partial\tau}\right)_\delta$, $\phi_{\tau\tau} = \left(\frac{\partial^2\phi}{\partial\tau^2}\right)_\delta$, $\phi_{\delta\tau} = \left(\frac{\partial^2\phi}{\partial\delta\partial\tau}\right)$

where $\delta = \rho/\rho^*$, $\tau = T^*/T$ with $\rho^* = \rho_c$, $T^* = T_c$ and T_c and ρ_c given by Eqs. (4) and (6). The incorporation of the ln δ term (which looks similar to an ideal gas term but is not) proved so effective that it was used in spite of its clearly slower computation speed; this is, however, not so bad because for region 3 the requirements regarding the computing time were clearly weaker than for regions 1, 2, and 4 (see Section 4.4).

Equation (25), obtained from Eq. (26) by the method of Setzmann and Wagner [5] for optimizing the functional structure of the final ϕ equation, was fitted to values of the properties p, h, c_v, s, and the two partial derivatives $(\partial p/\partial\rho)_T$ and $(\partial p/\partial T)_\rho$. These values were calculated from IAPWS-95 [7, 8] for given values of ρ and T distributed as selected grid points over region 3. The inclusion of the partial derivatives of p with respect to ρ and T made it unnecessary to fit the equations to the corresponding values of c_p and w which would have led to a nonlinear system of normal equations when minimizing the sum of squares. Such a nonlinear fitting process could not have been combined with the structure-optimization procedure [5] because this procedure can only cope with sums of squares which are linear in the coefficients n_j and n_{ij}, respectively. Moreover, fitting Eq. (25) just to the properties mentioned above ensures that Eq. (25) yields reasonable values for any property based on the first and second derivatives of ϕ, see also the general statement at the beginning of Section 5.5. In addition to the properties calculated from IAPWS-95 within region 3 the equations were also fitted to the corresponding properties calculated from the g equation of region 1, Eq. (15), along the boundary between regions 1 and 3 and from the g equation for region 2, Eq. (19), along the boundary between regions 2 and 3. In this way, Eq. (25) was fitted with good numerical consistency with the g equations of regions 1 and 2.

Moreover, for temperatures from 623.15 K to T_c = 647.096 K (see Eq. (4)) the equations were fitted to the phase-equilibrium condition $g'(T, p) = g''(T, p)$ in form of the Maxwell criterion (see Table 9). Simultaneously to this fitting process, the equations were also constrained to the conditions at the critical point, see the corresponding statement on Eq. (25). Details of this entire fitting process are given by Kruse and Wagner [18].

5.5.3.2 Accuracy of Eq. (25). Equation (25) meets clearly the accuracy requirements listed in Section 4.2. The quality of representing the IAPWS-95 values [7, 8] by Eq. (25) is illustrated in Figs. 14(*a*) to 17 for the relevant properties v, h, c_p, and w. The figures show the deviations of the values calculated from Eq. (25) from the corresponding IAPWS-95 values along five isotherms and along the boundary between regions 2 and 3 described by the B23-equation corresponding to Eq. (10). Since the 623.15 K isotherm is included in these isotherms, the behavior of Eq. (25) along the boundaries to the two adjacent regions 1 and 2 is recognizable. These six lines are considered to be characteristic examples for the behavior of Eq. (25) in the entire region 3. Where necessary, special deviation diagrams for the behavior of Eq. (25) in the critical region are given. Figure 14(*a*) illustrates how well Eq. (25) represents the specific volumes from IAPWS-95. For the largest part of region 3 including the "difficult" range along the boundary to region 2, the deviations from the IAPWS-95 values remain within ±0.03 percent whereas the IST-85 tolerances [9] are mostly between ±0.1 percent and ±0.2 percent. Even in the critical and enlarged critical region the deviations were kept within the tolerances, see Fig. 14(*b*). As a matter of course, the largest deviations from IAPWS-95 occur in the immediate vicinity of the critical point, but Fig. 14(*b*) shows that even for T = 648.15 K (T_c = 647.096 K) at about p = 22.3 MPa (p_c = 22.064 MPa) the deviation from IAPWS-95 only increases up to about 3 percent. Figure 14(*a*) also shows that over the entire region IFC-67 does not meet the present requirements.

As can be seen from Fig. 15 there is practically no difference between the specific enthalpies from Eq. (25) and from IAPWS-95. With very few exceptions along the critical isochore, Eq. (25) represents the IAPWS-95 values to within ±0.25 kJ kg^{-1}; the

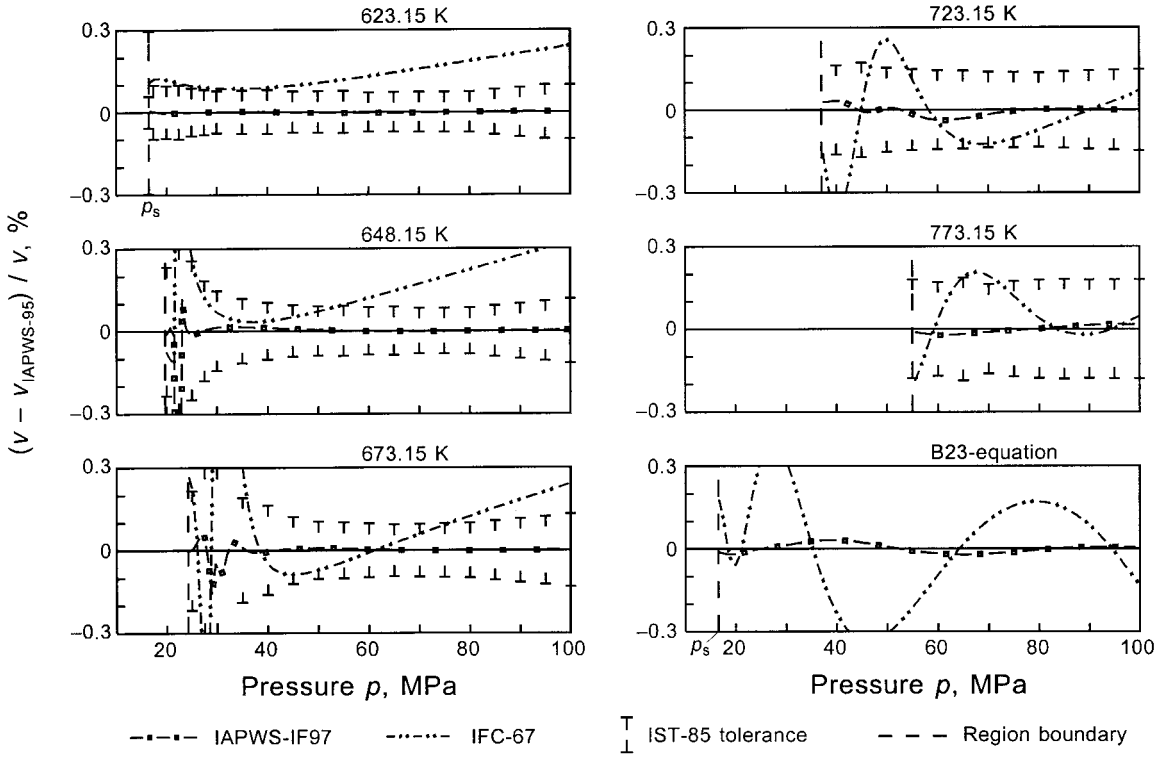

Fig. 14(*a*) Percentage deviations of the specific volumes *v* calculated from Eq. (25) and IFC-67, respectively, from values $v_{IAPWS-95}$ calculated from IAPWS-95 [7, 8]

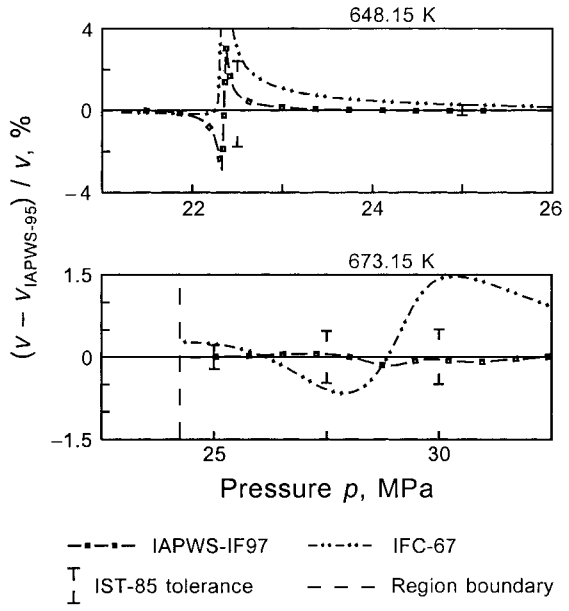

Fig. 14(*b*) Percentage deviations of the specific volumes *v* calculated from Eq. (25) and IFC-67, respectively, from values $v_{IAPWS-95}$ calculated from IAPWS-95 [7, 8]; spread pressure scale for the enlarged critical region.

maximum deviation is less than 0.6 kJ kg^{-1} occurring near 24 MPa and 650 K.

Figures 16(*a*) and 16(*b*) summarize the behavior of Eq. (25) with regard to the representation of the isobaric heat capacities which gave the most problems in region 3. Except for the critical region, Eq. (25) represents the values from IAPWS-95 to within ±0.5 percent, in wide ranges even to within ±0.1 percent. In contrast to this, the c_p values from IFC-67 deviate over large parts of this region by more than ±2 percent from the IAPWS-95 values. When approaching the critical point the values of c_p increase drastically and directly at the critical point c_p is infinite. Thus, it is not surprising, but one should be aware, that in the critical range c_p values calculated from different equations of state deviate considerably from each other. This fact is illustrated in Fig. 16(*b*) where the systematic deviations in this region are shown in more detail. For 648.15 K (T_c = 647.096 K) it can be seen that in a small pressure range slightly above the critical pressure (p_c = 22.064 MPa) the c_p values from Eq. (25) deviate considerably from the IAPWS-95 values, where the maximum deviation reaches up to −53 percent. The diagram also shows that the pressure range in which such significant deviations from IAPWS-95 occur is much wider for IFC-67 than for Eq. (25); the maximum deviation of the IFC-67 values amounts to −62 percent. For all these considerations it should not be forgotten that the uncertainty of IAPWS-95 in c_p in the immediate vicinity of the critical point is also relatively large. The lower diagram of Fig. 16(*b*) shows that at the border of the critical region, e.g., at 673.15 K, the c_p values from Eq. (25) deviate from the IAPWS-95 values by at most 1.7 percent.

In order to check whether these extraordinarily large deviations of c_p from Eq. (25) from those from IAPWS-95 in the near-critical region have consequences for practical calculations, isobaric enthalpy differences according to a temperature difference of 10 K were calculated from Eq. (25) and from IAPWS-95 in this region. These investigations covered a pressure range from 22.1 MPa to 24 MPa, where the isobaric enthalpy differences were calculated for the temperature difference between 652 K and 642 K for pressures up to 23 MPa and between 662 K and 652 K for 23.5 MPa and 24 MPa. For 22.1 MPa, 22.2 MPa, 22.3 MPa, 22.5 MPa, and 24 MPa the differences between the Δh values from IAPWS-95 and from Eq. (25) remained below 0.1 percent whereas for 22.7 MPa, 23 MPa, and 23.5 MPa the corresponding $\Delta(\Delta h)$ values increased to 0.23 percent, 0.85 percent, and 1.62 percent, respectively. These test calculations show that the very large c_p deviations hardly affect Δh values over temperature intervals of 10 K.

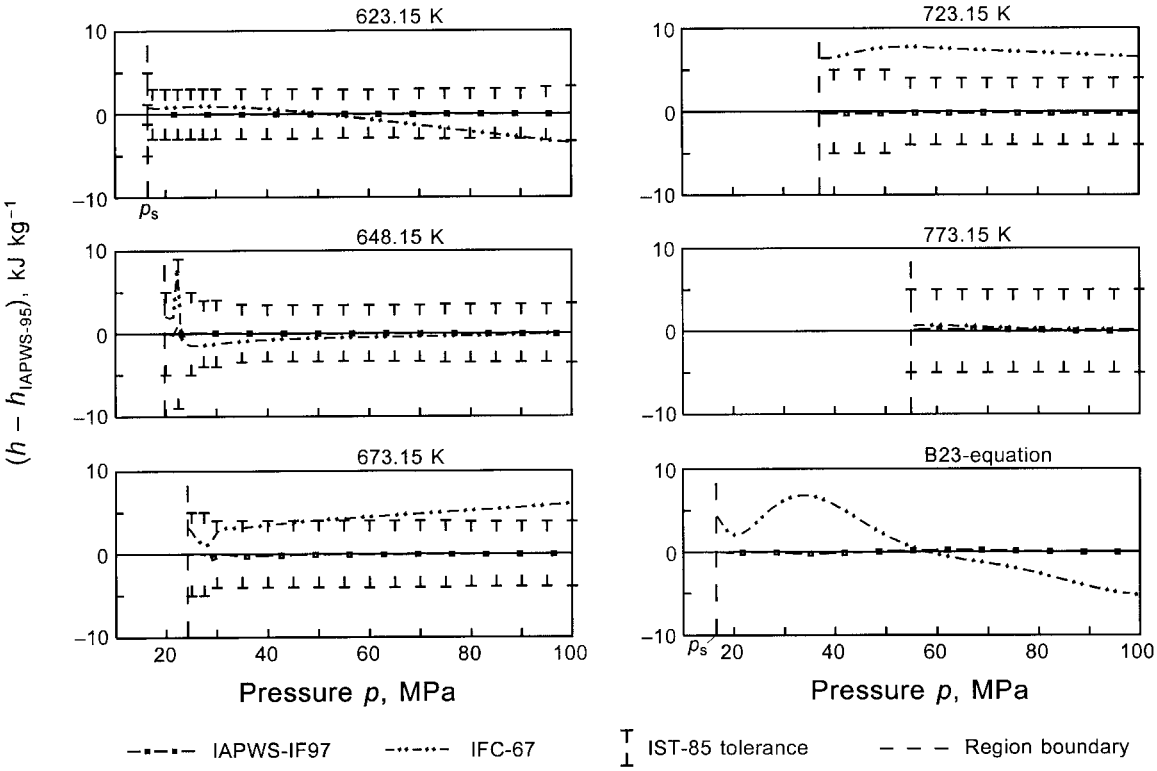

Fig. 15 Absolute deviations of the specific enthalpies h calculated from Eq. (25) and IFC-67, respectively, from values $h_{IAPWS-95}$ calculated from IAPWS-95 [7, 8]

From Fig. 17 it can be seen that the quality of Eq. (25) in representing the speeds of sound w from IAPWS-95 is very similar to that of c_p discussed above. Apart from the critical region, the deviations of the w values from Eq. (25) from those of IAPWS-95 remain within ± 0.3 percent whereas in the critical region the deviations increase, as expected, to values greater than ± 1 percent. It can also be seen that IFC-67 is not able to meet the present requirements of ± 1 percent regarding the representation of the speed of sound.

Metastable States. Figure 18 illustrates the behavior of Eq. (25) within the two-phase region along representative isotherms for the temperature range 623.15 K $\leq T \leq$ 647.096 K $= T_c$ and in addition along the 648.15 K isotherm in the single-phase region. All isotherms in the two-phase region have only one minimum and one maximum which are points of the spinodals meeting in the critical point. There are no further extrema and the two inflection points (instead of one) on the lower isotherms do not have any physical or practical meaning because they are within the unstable region. Thus, Eq. (25) predicts reasonable values in the metastable vapor and liquid region of region 3.

5.5.4 The Saturation-Pressure Equation for Region 4. For several reasons (see section 5.5.4.1) instead of a saturation-pressure equation, an implicit equation was developed describing the saturation curve. This equation can be solved directly for either saturation pressure p_s or saturation temperature T_s.

The equation for describing the saturation curve is an implicit bi-quadratic equation which reads

$$\beta^2\vartheta^2 + n_1\beta^2\vartheta + n_2\beta^2 + n_3\beta\vartheta^2 + n_4\beta\vartheta + n_5\beta + n_6\vartheta^2 + n_7\vartheta + n_8 = 0, \quad (27)$$

where

$$\beta = (p_s/p^*)^{0.25} \quad (27a)$$

and

$$\vartheta = \frac{T_s}{T^*} + \frac{n_9}{(T_s/T^*) - n_{10}} \quad (27b)$$

with $p^* = 1$ MPa and $T^* = 1$ K; for the coefficients n_1 to n_{10} see Table A11.

The explicit form of the saturation-pressure equation (basic equation) is obtained from the solution of Eq. (27) with respect to p_s as follows[11]:

$$\frac{p_s}{p^*} = \left[\frac{2C}{-B + (B^2 - 4AC)^{0.5}}\right]^4, \quad (28)$$

where $p^* = 1$ MPa and

$$A = \vartheta^2 + n_1\vartheta + n_2$$

$$B = n_3\vartheta^2 + n_4\vartheta + n_5$$

$$C = n_6\vartheta^2 + n_7\vartheta + n_8$$

with ϑ according to Eq. (27*b*). The coefficients n_i of Eq. (28) are listed in Table A11.

Equations (27) and (28) reproduce exactly the p-T values at the triple point according to Eqs. (7) and (8), at the normal boiling point according to Eq. (9) and at the critical point according to Eqs. (4) and (5). Due to the special fitting process of Eq. (27) with respect to Eq. (25), the specific volumes of the saturated liquid and vapor, v' and v'', can be simply calculated directly up to the critical point from the intersection of the saturation pressure from Eq. (28) with the pressure from the Helmholtz free energy equation, Eq. (25), for the temperature considered. Therefore, it is not necessary to calculate v' and v'' by solving Eq. (25) using the Maxwell criterion which is a complex iteration process.

[11] This solution is not quite simple, for details see [22]. The saturation-temperature equation (backward equation) which follows from Eq. (27) by solving it with respect to T_s is given in Section 5.6.4.

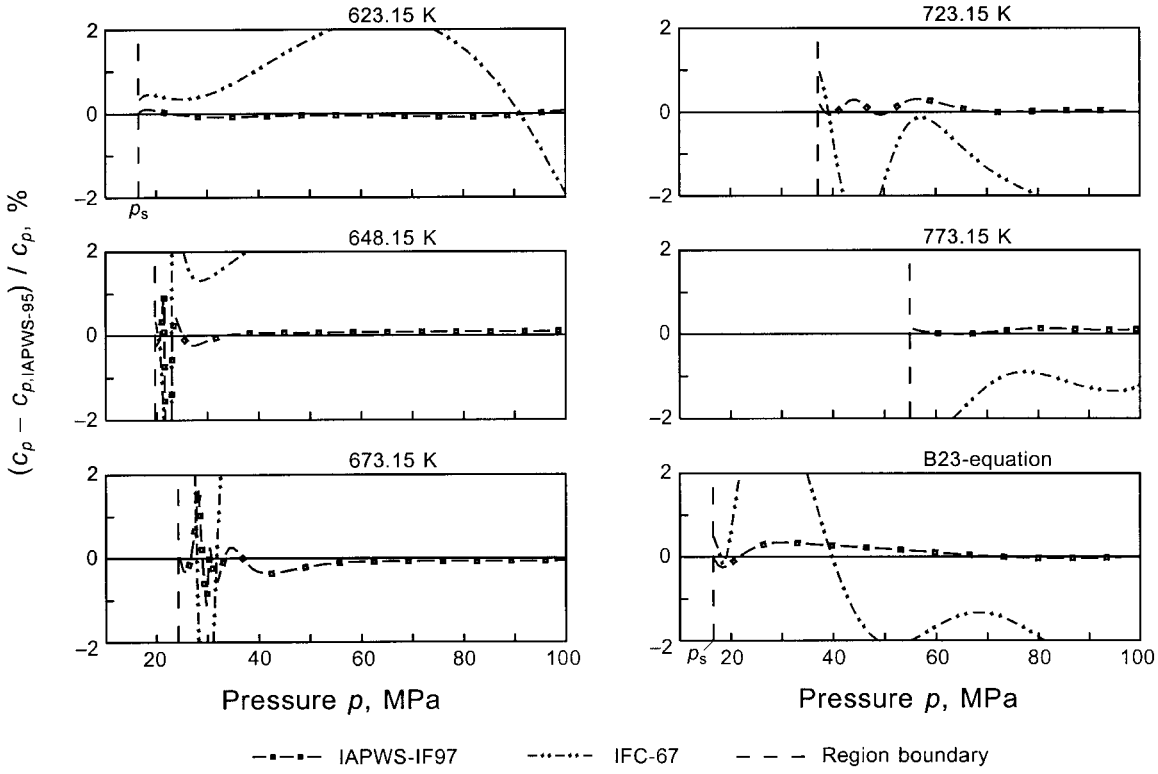

Fig. 16(*a*) Percentage deviations of the specific isobaric heat capacities c_p calculated from Eq. (25) and IFC-67, respectively, from values $c_{p,\text{IAPWS-95}}$ calculated from IAPWS-95 [7, 8]

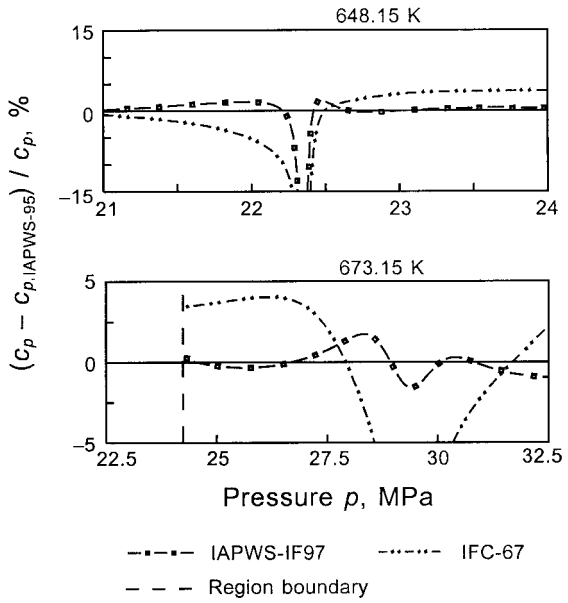

Fig. 16(*b*) Percentage deviations of the specific isobaric heat capacities c_p calculated from Eq. (25) and IFC-67, respectively, from values $c_{p,\text{IAPWS-95}}$ calculated from IAPWS-95 [7, 8]; spread pressure scale for the enlarged critical region.

Equation (28) is valid along the entire vapor-liquid saturation curve from the triple-point temperature T_t to the critical temperature T_c and can be simply extrapolated to 273.15 K so that it covers the temperature range

$$273.15\ \text{K} \le T \le 647.096\ \text{K}.$$

To assist the user in computer-program verification of Eq. (28), Table A12 contains corresponding test values.

5.5.4.1 Development of Eq. (27). In the course of the development of the basic and backward equation for the saturation curve three alternatives were pursued, namely a "fast" polynomial equation pair with integer exponents, a pair of so-called short polynomial equations with fractional exponents, and implicit equations which are directly solvable with regard to both $p_s(T)$ and $T_s(p)$, for details of these developments see Kretzschmar et al. [22]. After checking these equations and considering carefully their pros and cons, an implicit saturation equation, which provides complete numerical consistency between the $p_s(T)$ form and $T_s(p)$ form, was finally chosen as saturation equation for region 4 of IAPWS-IF97; this equation corresponds to Eq. (27).

Equation (27) was fitted to p_s values calculated from IAPWS-95 [7, 8] and was constrained to the p-T values at the triple point, normal boiling point and critical point given by Eqs. (7) to (9), (4), and (5). In addition, Eq. (27) was also fitted to the p_s values from the Helmholtz free energy equation of region 3, Eq. (25), so that Eq. (28) yields vapor pressures which are, even very close to the critical temperature, between the pressures of the vapor and liquid spinodals of Eq. (25); the reasoning of this special fitting process is given by the corresponding statement in connection with Eq. (28). The entire fitting procedure is based on the approximation algorithm developed by Willkommen et al. [23] which includes the simultaneous steady approximation of Zschunke et al. [24].

5.5.4.2 Accuracy of Eq. (28). Figure 19 shows that the saturation-pressure equation, Eq. (28), represents the saturation pressures calculated from IAPWS-95 for the entire range from the triple-point temperature T_t to the critical temperature T_c to within the IST-85 tolerances [9]. Even for temperatures below the temperature T_b of the normal boiling point, the p_s values from Eq. (28) remain within the IST-85 tolerances which are, in this region, clearly smaller than the permissible deviations of ± 0.025 percent (see Section 4.2). It can also be seen that Eq. (28) meets the p_s values at the triple point according to Eqs. (7) and (8), at the normal boiling point according to Eq. (9), and at the critical point according to Eqs. (4) and (5). For comparison, the figure also

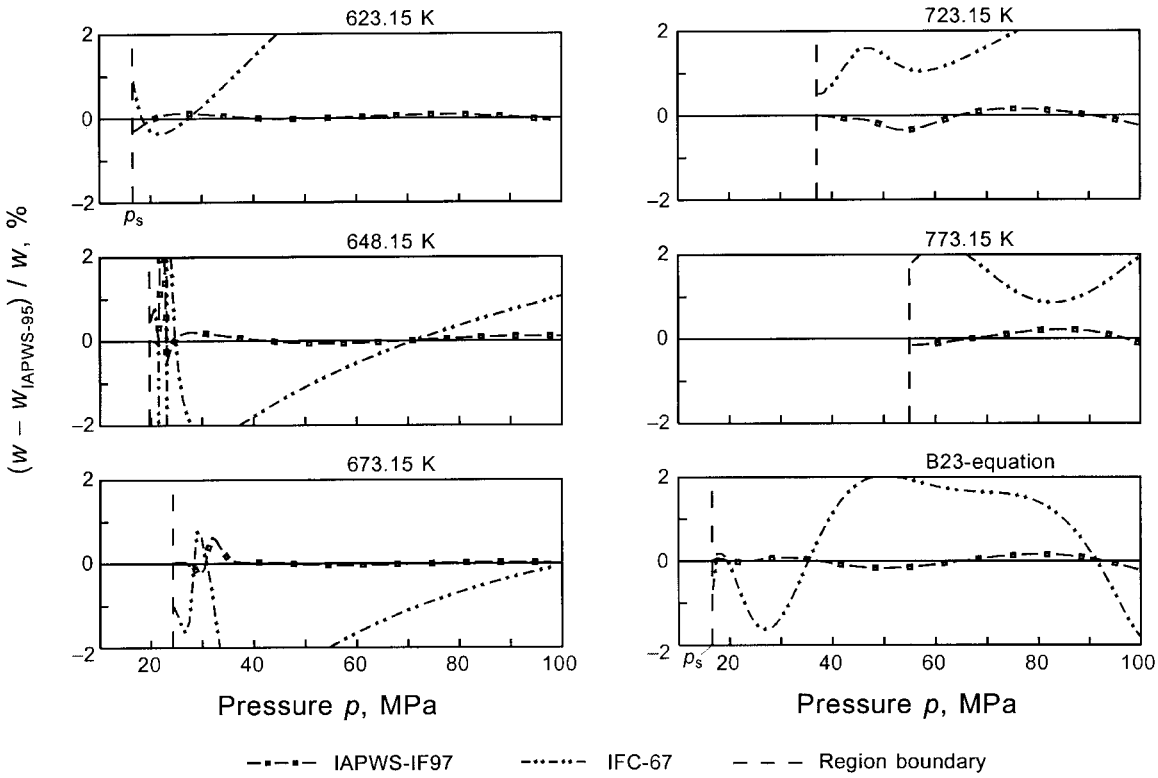

Fig. 17 Percentage deviations of the speeds of sound w calculated from Eq. (25) and IFC-67, respectively, from values $w_{IAPWS-95}$ calculated from IAPWS-95 [7, 8]

contains the corresponding Δp_s line generated from IFC-67; the maximum deviation of the IFC-67 values amounts to 0.12 percent.

5.5.5 The Gibbs Free Energy Equation for Region 5. The basic equation for this high-temperature region is a fundamental equation for the specific Gibbs free energy g in its dimensionless form, $\gamma = g/(RT)$, which is again separated into an ideal-gas part γ^o and a residual part γ^r, so that

$$\frac{g(p, T)}{RT} = \gamma(\pi, \tau) = \gamma^o(\pi, \tau) + \gamma^r(\pi, \tau), \tag{29}$$

where $\pi = p/p^*$ and $\tau = T^*/T$ with R given by Eq. (1).

The equation for the ideal-gas part γ^o of the dimensionless Gibbs free energy reads

$$\gamma^o = \ln \pi + \sum_{i=1}^{6} n_i^o \tau^{J_i^o}, \tag{30}$$

where $\pi = p/p^*$ and $\tau = T^*/T$ with $p^* = 1$ MPa and $T^* = 1000$ K. The coefficients n_1^o and n_2^o were adjusted in such a way that for

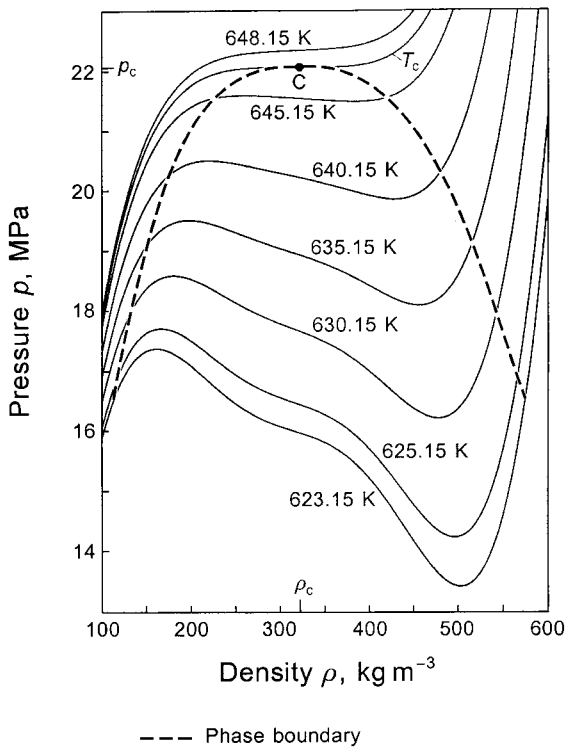

Fig. 18 Behavior of Eq. (25) in the vapor-liquid two-phase region of region 3

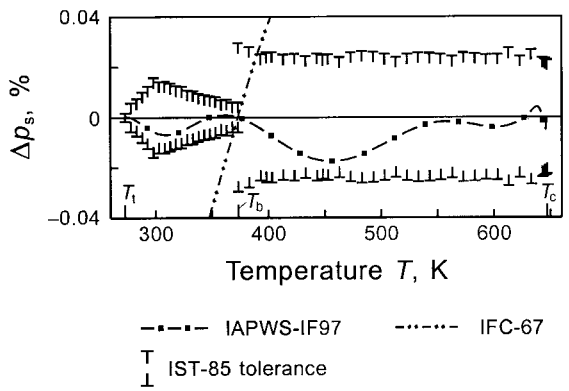

Fig. 19 Percentage deviations of the saturation pressure p_s calculated from Eq. (28) and IFC-67, respectively, from values $p_{s,IAPWS-95}$ calculated from IAPWS-95 [7, 8]

$T = 1073.15$ K the values for the specific internal energy and specific entropy, calculated from Eq. (29), relate to the corresponding values calculated from Eq. (19). Table A13 contains the coefficients n_i^o and exponents J_i^o of Eq. (30).

The form of the residual part γ^r of the dimensionless Gibbs free energy is as follows:

$$\gamma^r = \sum_{i=1}^{5} n_i \pi^{I_i} \tau^{J_i}, \tag{31}$$

where $\pi = p/p^*$ and $\tau = T^*/T$ with $p^* = 1$ MPa and $T^* = 1000$ K. The coefficients n_i and exponents I_i and J_i of Eq. (31) are listed in Table A14.

All thermodynamic properties can be derived from Eq. (29) by using the appropriate combinations of the ideal-gas part γ^o, Eq. (30), and the residual part γ^r, Eq. (31), of the dimensionless Gibbs free energy and their derivatives. Relations between the relevant thermodynamic properties and γ^o and γ^r and their derivatives are summarized in Table 4. All required derivatives of the ideal-gas part and of the residual part of the dimensionless Gibbs free energy are explicitly given in Table 11 and Table 12, respectively.

Equation (29) covers region 5 of IAPWS-IF97 defined by the following temperature and pressure range, see Fig. 2:

$$1073.15 \text{ K} \le T \le 2273.15 \text{ K} \quad 0 < p \le 10 \text{ MPa}.$$

In this range Eq. (29) is only valid for pure undissociated water, dissociation has not been considered.

To assist the user in computer-program verification of Eq. (29), Table A15 contains test values of the most relevant properties.

Development and Accuracy of Eq. (29). For high-temperature applications of the thermodynamic properties of steam such as in gas turbines it was requested to have a simple equation of state for temperatures above 1073.15 K and pressures up to 10 MPa. According to this demand a fundamental equation for the specific Gibbs free energy in its absolute form was developed by Mareš and Šifner [25]. Equation (29) is a simplified version (shortened in residual part) of this equation.

The coefficients n_3^o to n_6^o of Eq. (30) were fitted to values of the dimensionless isobaric heat capacity in the ideal-gas state, (c_p^o/R), calculated from the ideal-gas part ϕ^o of IAPWS-95 [7, 8]. Since this ϕ^o equation of IAPWS-95 is based on the (c_p^o/R) equation of Cooper [26] which was fitted to data in the temperature range from 130 K to 2000 K, the calculation of (c_p^o/R) values from IAPWS-95 for temperatures from 1073.15 K to 2273.15 K corresponds only to a marginal extrapolation. The values of the coefficients n_1^o and n_2^o of Eq. (30) were determined as described in connection with Eq. (30). The coefficients n_i of Eq. (31) were determined by fitting Eq. (29) to values of the specific volume v calculated from IAPWS-95 [7, 8] for given values of p and T at selected grid points distributed over region 5 for $1073.15 \text{ K} < T \le 2273.15$ K and from Eq. (19) for $T = 1073.15$ K. For $T > 1273.15$ K the corresponding IAPWS-95 values were obtained by extrapolating this formulation.

Table 11 The ideal-gas part γ^o of the dimensionless Gibbs free energy, Eq. (30), and its derivatives

$\gamma^o = \ln \pi + \sum_{i=1}^{6} n_i^o \tau^{J_i^o}$	$\gamma_\tau^o = \sum_{i=1}^{6} n_i^o J_i^o \tau^{J_i^o - 1}$
$\gamma_\pi^o = \pi^{-1}$	$\gamma_{\tau\tau}^o = \sum_{i=1}^{6} n_i^o J_i^o (J_i^o - 1) \tau^{J_i^o - 2}$
$\gamma_{\pi\pi}^o = -\pi^{-2}$	$\gamma_{\pi\tau}^o = 0$
$\gamma_\pi^o = \left(\frac{\partial \gamma^o}{\partial \pi}\right)_\tau, \gamma_{\pi\pi}^o = \left(\frac{\partial^2 \gamma^o}{\partial \pi^2}\right)_\tau, \gamma_\tau^o = \left(\frac{\partial \gamma^o}{\partial \tau}\right)_\pi, \gamma_{\tau\tau}^o = \left(\frac{\partial^2 \gamma^o}{\partial \tau^2}\right)_\pi, \gamma_{\pi\tau}^o = \left(\frac{\partial^2 \gamma^o}{\partial \pi \partial \tau}\right)$	

Table 12 The residual part γ^r of the dimensionless Gibbs free energy, Eq. (31), and its derivatives

$\gamma^r = \sum_{i=1}^{5} n_i \pi^{I_i} \tau^{J_i}$	$\gamma_\tau^r = \sum_{i=1}^{5} n_i \pi^{I_i} J_i \tau^{J_i - 1}$
$\gamma_\pi^r = \sum_{i=1}^{5} n_i I_i \pi^{I_i - 1} \tau^{J_i}$	$\gamma_{\tau\tau}^r = \sum_{i=1}^{5} n_i \pi^{I_i} J_i (J_i - 1) \tau^{J_i - 2}$
$\gamma_{\pi\pi}^r = \sum_{i=1}^{5} n_i I_i (I_i - 1) \pi^{I_i - 2} \tau^{J_i}$	$\gamma_{\pi\tau}^r = \sum_{i=1}^{5} n_i I_i \pi^{I_i - 1} J_i \tau^{J_i - 1}$
$\gamma_\pi^r = \left(\frac{\partial \gamma^r}{\partial \pi}\right)_\tau, \gamma_{\pi\pi}^r = \left(\frac{\partial^2 \gamma^r}{\partial \pi^2}\right)_\tau, \gamma_\tau^r = \left(\frac{\partial \gamma^r}{\partial \tau}\right)_\pi, \gamma_{\tau\tau}^r = \left(\frac{\partial^2 \gamma^r}{\partial \tau^2}\right)_\pi, \gamma_{\pi\tau}^r = \left(\frac{\partial^2 \gamma^r}{\partial \pi \partial \tau}\right)$	

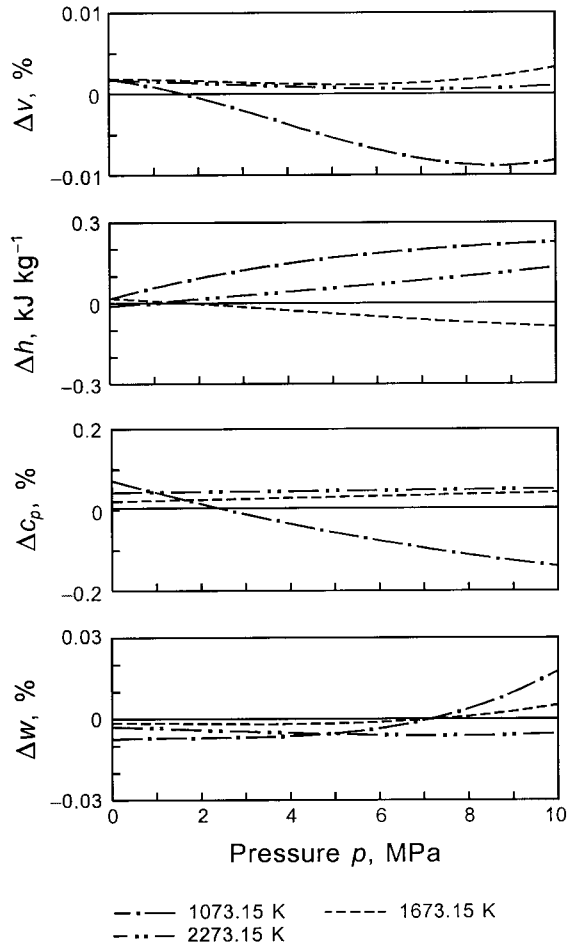

Fig. 20 Percentage deviations of the values of v, c_p, and w and absolute deviations of h values calculated from Eq. (29) from the corresponding values calculated from IAPWS-95 [7, 8]: $\Delta v = (v - v_{\text{IAPWS-95}})/v$; $\Delta c_p = (c_p - c_{p,\text{IAPWS-95}})/c_p$; $\Delta h = h - h_{\text{IAPWS-95}}$; $\Delta w = (w - w_{\text{IAPWS-95}})/w$.

Figure 20 illustrates for three characteristic isotherms that Eq. (29) represents the values of the properties v, h, c_p, and w from IAPWS-95 to within very small deviations. In the entire region, the maximum deviations occur at 10 MPa and amount to 0.009 percent in v at about 1073.15 K, 0.34 kJ kg^{-1} in h near 1373 K, 0.14 percent in c_p at 1073.15 K, and 0.023 percent in w near 1173 K.

5.5.6 Consistency at Region Boundaries. For any calculation of thermodynamic properties of water and steam across the region boundaries of IAPWS-IF97, the basic equations have to be sufficiently consistent at the corresponding boundary, see Section 4.3. For the properties considered in this respect, this section presents the achieved consistencies in comparison with the permitted inconsistencies according to the so-called Prague values [10].

5.5.6.1 Consistency at Boundaries Between Single-Phase Regions. For the boundaries between single-phase regions the consistency investigations were performed for the following basic equations and region boundaries; see Fig. 2:

Table 13 Inconsistencies between basic equations for single-phase regions at the corresponding region boundaries given as maximum and root-mean square (RMS) values

Inconsistency	Prague value [10]	Regions 1/3 Eqs. (15)/(25) Maximum value[a]	RMS value	Regions 2/3 Eqs. (19)/(25) Maximum value[a]	RMS value	Regions 2/5 Eqs. (19)/(29) Maximum value[a]	RMS value
Δv, %	0.05	0.004	0.002	0.018	0.007	0.002	0.001
Δh, kJ kg^{-1}	0.2	0.031	0.014	0.134	0.073	0.020	0.012
Δc_p, %	1	0.195	0.058	0.353	0.169	0.081	0.048
Δs, J kg^{-1}K^{-1}	0.2	0.042	0.022	0.177	0.094	0.042	0.025
Δg, kJ kg^{-1}	0.2	0.005	0.005	0.005	0.003	0.026	0.021
Δw, %	1[b]	0.299	0.087	0.403	0.073	0.021	0.009

[a] Absolute value

[b] The permitted inconsistency value for w is not included in the Prague values

- Equations (15) and (25) along the 623.15 K isotherm for pressures from 16.53 MPa (p_s from Eq. (28) for 623.15 K) to 100 MPa corresponding to the boundary between regions 1 and 3.
- Equations (19) and (25) with respect to the boundary between regions 2 and 3 defined by the B23-equation, Eq. (10), for temperatures between 623.15 K and 863.15 K.
- Equations (19) and (29) with respect to the 1073.15 K isotherm for $p \leq 10$ MPa corresponding to the boundary between regions 2 and 5.

The results of the consistency investigations for these three region boundaries are summarized in Table 13. In addition to the permitted inconsistencies corresponding to the Prague values [10], the actual inconsistencies characterized by their maximum and root-mean-square values at the three boundaries are given for the properties v, h, c_p, s, g, and w. It can be seen that the inconsistencies between the basic equations at the corresponding region boundaries are very small and the consistency requirements given in Section 4.3 are clearly exceeded.

Figure 21 presents the results of these consistency investigations in form of percentage deviations for v, c_p, and w and in form of absolute deviations for s, h, and g for IAPWS-IF97 and for IFC-67 as well; for the permitted inconsistencies according to the Prague values [10] see Table 13.

The diagrams on the left-hand side of Fig. 21 show the results for the 623.15 K isotherm that is the boundary between regions 1 and 3 of IAPWS-IF97 and between regions 1 and 4 of IFC-67, see Figs. 1 and 2. For IAPWS-IF97 the deviations correspond to the inconsistencies between Eq. (15) and Eq. (25), and for IFC-67 between its corresponding g and f equation. The diagrams show how small the inconsistencies between the basic equations of IAPWS-IF97 are along this region boundary. When comparing these inconsistencies with the permitted values it can be seen that the consistency requirement regarding this boundary was exceeded by a large margin. In contrast to this, the corresponding IFC-67 inconsistencies are clearly larger. With regard to v, c_p, and s there are ranges where IFC-67 is slightly outside the permitted inconsistencies; with respect to g IFC-67 is outside the permitted inconsistency value ($\Delta g = 0.2$ kJ kg^{-1}) along the entire boundary.

The diagrams on the right-hand side of Fig. 21 present the result for the boundary between regions 2 and 3 defined by the B23-equation for IAPWS-IF97 and by the so-called L-function for IFC-67, see Figs. 1 and 2. For IAPWS-IF97 the deviations correspond to the inconsistencies between Eqs. (19) and (25) and for IFC-67 between its corresponding g and f equation. In comparison with the diagrams on the left of Fig. 21, here the inconsistencies are on average larger which is a sign of the problems along this boundary. Particularly, for v, h, and s there are greater inconsistencies which are, however, still well within the Prague values. It is very positive that the inconsistencies in c_p remain within 0.35 percent along the entire boundary whereas the corresponding IFC-67 inconsistencies increase up to ± 6 percent. The fulfillment of the consistency requirements regarding c_p along the B23-equation was one of the decisive points during the development of the basic equations for regions 2 and 3 and influenced substantially the structure of these equations. The consistency in w is similarly good as for c_p. For IFC-67 the following consistency statements along this boundary can be made: for g the requirement was completely met, for c_p it was not met at all (see above) and for the other properties considered the inconsistencies are slightly outside the permitted values in a few places.

5.5.6.2 Consistency at the Saturation Curve. The vapor-liquid saturation curve forms the boundary between the following regions of IAPWS-IF97, see Fig. 2: For 273.15 K $\leq T \leq$ 623.15 K it is the boundary between region 4 and regions 1 and 2, respectively, and for 623.15 K $\leq T \leq T_c$ between region 3 and region 4. Thus, the calculations concern the basic equations and ranges of the saturation curve listed below. According to the Prague values the consistency investigations at the saturation curve are performed for the properties p_s, T_s, and g; the way of calculating the inconsistencies Δp_s, ΔT_s, and Δg is given in the following:

- Equations (15), (19) and (28) on the saturation curve for temperatures from 273.15 K to 623.15 K:

$$\Delta p_s = p_{s,\text{Eq.(15)},\text{Eq.(19)}} - p_{s,\text{Eq.(28)}} \tag{32a}$$

$$\Delta T_s = T_{s,\text{Eq.(15)},\text{Eq.(19)}} - T_{s,\text{Eq.(55)}} \tag{32b}$$

$$\Delta g = g_{\text{Eq.(15)}} - g_{\text{Eq.(19)}} \tag{32c}$$

  The calculation of p_s and of T_s from Eqs. (15) and (19) was made via the Maxwell criterion (phase-equilibrium condition) for given values of T or p. The g values are determined for given T values and corresponding p_s values from Eq. (28).
- Equations (25) and (28) on the saturation curve for temperatures from 623.15 K to $T_c = 647.096$ K:

$$\Delta p_s = p_{s,\text{Eq.(25)}} - p_{s,\text{Eq.(28)}} \tag{33a}$$

$$\Delta T_s = T_{s,\text{Eq.(25)}} - T_{s,\text{Eq.(55)}} \tag{33b}$$

$$\Delta g = g'_{\text{Eq.(25)},\text{Eq.(28)}} - g''_{\text{Eq.(25)},\text{Eq.(28)}} \tag{33c}$$

  The calculation of p_s and T_s from Eq. (25) was made via the Maxwell criterion for given temperatures or pressures, respectively. The inconsistency Δg corresponds to the difference $g'(\rho', T) - g''(\rho'', T)$ which was calculated from Eq. (25) after ρ' and ρ'' had been determined from Eq. (25) by iteration for given T values and corresponding p_s values from Eq. (28).
- Equations (15), (19) and (25) on the saturation curve at 623.15 K. This is the only point on the saturation curve where the validity ranges of the fundamental equations of regions 1 to 3 meet each other:

$$\Delta p_s = p_{s,\text{Eq.(15)},\text{Eq.(19)}} - p_{s,\text{Eq.(25)}} \tag{34a}$$

$$\Delta T_s = T_{s,\text{Eq.(15)},\text{Eq.(19)}} - T_{s,\text{Eq.(25)}} \tag{34b}$$

$$\Delta g = g_{\text{Eq.(15)},\text{Eq.(19)}} - g_{\text{Eq.(25)}} \tag{34c}$$

  All three properties p_s, T_s, and g were calculated via the Maxwell criterion from the corresponding equations.

The results of these consistency investigations along the saturation curve are summarized in Table 14. In addition to the permitted inconsistencies corresponding to the Prague values [10], the actual inconsistencies characterized by their maximum and root-mean-square values are given for the two sections of the saturation curve and for the special point at 623.15 K. It can be seen that the inconsistencies between the basic equations for the corresponding single-phase regions and the saturation-pressure equation are very small; except for the Δp_s values for $T \leq 623$ K they are less than one tenth of the permitted value. This statement also holds for the fundamental equations in relation to each other and not just in relation to the saturation-pressure equation, Eq. (28), see Eqs. (34*a*) to (34*c*) and the last column in Table 14.

Along the entire saturation curve, Fig. 22 shows the inconsistencies with regard to the saturation pressure p_s, which is the most important and most sensitive property in this respect. The maxi-

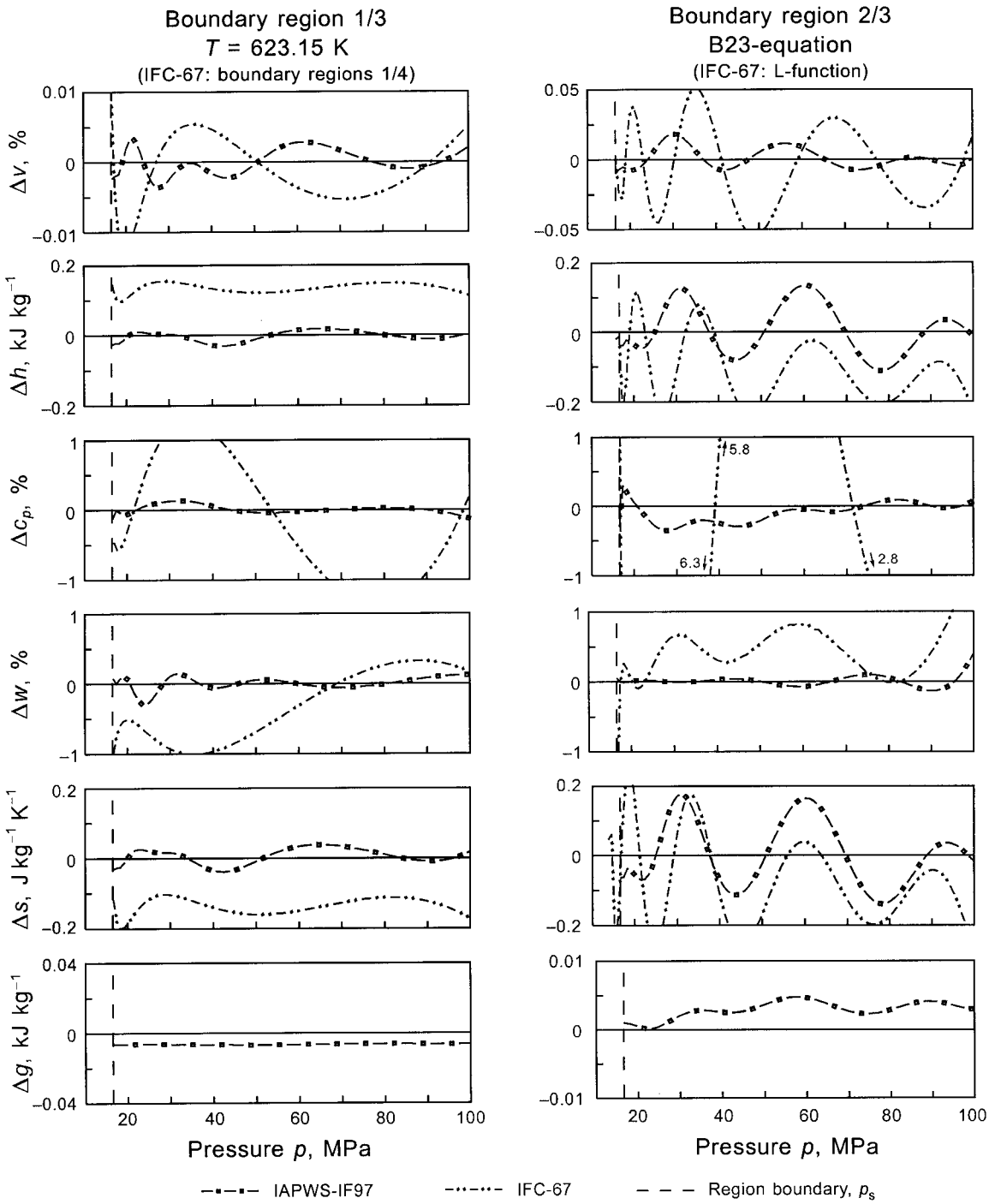

Fig. 21 Inconsistencies Δv, Δh, Δc_p, Δw, Δs, and Δg along the boundary between regions 1 and 3 (left column) and the boundary between regions 2 and 3 (right column) when calculating the properties without an index from the corresponding g equation (Eq. (15) for region 1 and Eq. (19) for region 2) and the properties with the index f from the f equation for region 3, Eq. (25). For the calculations with IFC-67 its corresponding g and f equations were used, see text: $\Delta v = (v - v_f)/v$; $\Delta c_p = (c_p - c_{p,f})/c_p$; $\Delta s = s - s_f$; $\Delta h = h - h_f$; $\Delta w = (w - w_f)/w$; $\Delta g = g - g_f$.

mum difference Δp_s when p_s is calculated once from the basic equations for regions 1 to 3 and the other time from the saturation-pressure equation remains less than 0.007 percent and the (unavoidable) step at 623.15 K when switching from the g equations to the f equation amounts only to 0.005 percent. For IFC-67 the corresponding inconsistency in p_s is on average more than one order of magnitude larger; the maximum inconsistency amounts to 0.12 percent and the step at 623.15 K when switching to the f equations for regions 3 and 4 of IFC-67 (see Fig. 1) is even 0.22 percent.

Table 14 Inconsistencies between the basic equations valid at the saturation curve given as maximum and root-mean square (RMS) values

Inconsistency	Prague value [10]	$T_t \le T \le 623.15$ K Eqs. (15),(19)/(28) Maximum value[a]	RMS value	$623.15 \text{ K} \le T \le T_c$ Eqs. (25)/(28) Maximum value[a]	RMS value	$T = 623.15$ K Eqs. (15),(19)/(25)
Δp_s, %	0.05	0.0069	0.0033	0.0026	0.0015	0.0041
ΔT_s, %	0.02	0.0006	0.0003	0.0003	0.0002	0.0006
Δg, kJ kg^{-1}	0.2	0.012	0.006	0.002	0.001	0.005

[a] Absolute value

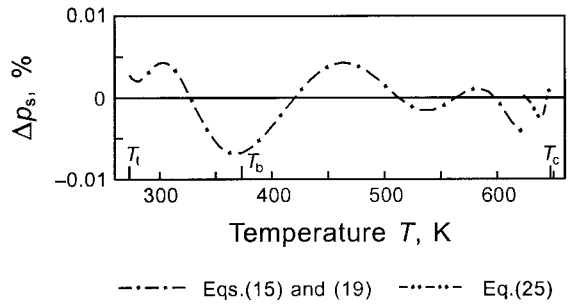

Fig. 22 Inconsistencies Δp_s along region 4 (saturation curve) when calculating the saturation pressures as p_s values from Eq. (15) together with Eq. (19) and from Eq. (25), respectively, and as values $p_{s,\mathrm{Eq.(28)}}$ directly from the saturation-pressure equation, Eq. (28): $\Delta p_s = (p_s - p_{s,\mathrm{Eq.(28)}})/p_s$.

In addition to the inconsistencies in Δp_s shown in Fig. 22, it might be helpful for practical calculations to have an idea of the differences in v, h, s, c_p, and w along the saturated vapor and saturated liquid line when, for given temperatures, these values were calculated one time directly from the corresponding g and f equations by applying the phase-equilibrium condition and the other time from the basic equations after p_s had been calculated from Eq. (28). The second method for these calculations is clearly easier to carry out but the results would not be in full consistency with the results from the fundamental equations. Figure 23 illustrates the corresponding inconsistencies along the saturated vapor line for v'', s'', and c_p''. It can be seen that the inconsistencies $\Delta v''$, $\Delta s''$, and $\Delta c_p''$ are very small (smaller than the Prague values for the region boundaries between single-phases) and increase only when approaching the critical point; however, for temperatures up to (T_c − 2 K) the inconsistencies remain within the corresponding Prague values [10] listed in Table 13. Compared with these three properties the corresponding inconsistencies in h'', w'', v', h', s', c_p', and w' are clearly smaller and thus negligible except for the range 1 K to 2 K below T_c. When approaching the critical point it is not surprising that the inconsistency in c_p' and c_p'' increases to 60 percent and to 75 percent, respectively, at 1 mK below T_c, see also the discussion of Fig. 16(*b*) in Section 5.5.3.2 regarding the c_p behavior in region 3.

5.6 The Backward Equations for Regions 1, 2, and 4. In order to meet the computation-speed requirement for IAPWS-IF97 "three times faster than IFC-67" (see Section 4.4) the concept of so-called backward equations $T(p, h)$ and $T(p, s)$ for regions 1 and 2 and $T_s(p)$ for region 4 has been developed, see Section 5.1 and Fig. 2.

Proceeding from Eq. (13) with $z = T/T^*$, $x = p$, $a = p^*$, $y = h$, and $c = h^*$ or $y = s$ and $c = s^*$ the following general form of a combined polynomial for the $T(p, h)$ and $T(p, s)$ equations is obtained [18, 29]:

$$\frac{T(p, h)}{T^*} = \sum_i n_i \left(\frac{p}{p^*} + b\right)^{I_i} \left(\frac{h}{h^*} + d\right)^{J_i}, \tag{35}$$

$$\frac{T(p, s)}{T^*} = \sum_i n_i \left(\frac{p}{p^*} + b\right)^{I_i} \left(\frac{s}{s^*} + d\right)^{J_i}, \tag{36}$$

where T^*, p^*, h^*, and s^* are again reducing parameters. These two equations form the basis of the backward equations for regions 1 and 2.

In the following sections first the final form of the corresponding backward equation is given including all numerical information for its use, then details of its development are summarized and finally its numerical consistency with the corresponding basic equation is discussed; all table numbers starting with an "A" are listed in the appendix.

5.6.1 The Backward Equations for Region 1. According to the considerations in section 5.1 (item 2*a*, *b*) the two backward equations $T(p, h)$ and $T(p, s)$ have to be numerically consistent with the basic equation of this region, Eq. (15), within $\Delta T = \pm 25$ mK for the same p-h values and p-s values, respectively.

5.6.1.1 The Backward Equation T(p, h). The backward equation $T(p, h)$ for region 1 has the following dimensionless form:

$$\frac{T(p, h)}{T^*} = \theta(\pi, \eta) = \sum_{i=1}^{20} n_i \pi^{I_i} (\eta + 1)^{J_i}, \tag{37}$$

where $\theta = T/T^*$, $\pi = p/p^*$, and $\eta = h/h^*$ with $T^* = 1$ K, $p^* = 1$ MPa, and $h^* = 2500$ kJ kg^{-1}. The coefficients n_i and exponents I_i and J_i of Eq. (37) are listed in Table A16.

Equation (37) covers the same range of validity as the basic equation, Eq. (15), except for the metastable superheated-liquid region, where Eq. (37) is not valid. For the actual numerical inconsistencies between Eqs. (37) and (15) see below.

To assist the user in computer-program verification of Eq. (37), Table A17 contains the corresponding test values.

Development of Eq. (37). Based on test calculations with Eq. (35) for the maximum ranges of the exponents I_i and J_i, the values of the reducing parameters T^*, p^*, and h^* and the shifting parameters b and d, the following dimensionless comprehensive expression of 233 terms (bank of terms) was used as starting point for the development of the backward equation $T(p, h)$ for region 1:

$$\theta = \sum_{i=0}^{6} \sum_{j=0}^{32} n_{ij} \pi^i (\eta + 1)^j, \tag{38}$$

where $\theta = T/T^*$, $\pi = p/p^*$, and $\eta = h/h^*$ with $T^* = 1$ K, $p^* = 1$ MPa, and $h^* = 2500$ kJ kg^{-1}.

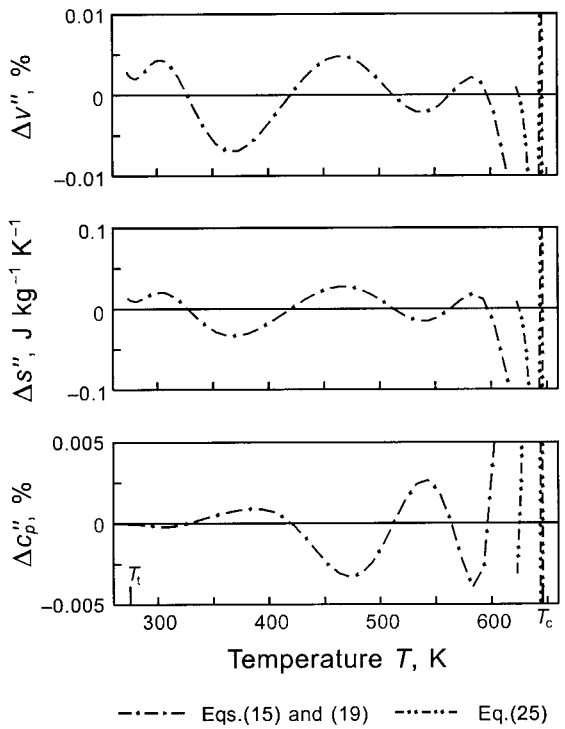

Fig. 23 Inconsistencies $\Delta v''$, $\Delta s''$, and $\Delta c_p''$ caused by two different ways of determining the needed saturation pressures p_s. For $v''_{\mathrm{Eq.(28)}}$, $s''_{\mathrm{Eq.(28)}}$, and $c''_{p,\mathrm{Eq.(28)}}$ the p_s values were directly calculated from Eq. (28) and for v'', s'', and c_p'' the p_s values were determined from Eqs. (15) and (19) and from Eq. (19), respectively, via the phase-equilibrium condition: $\Delta v'' = (v''_{\mathrm{Eq.(28)}} - v'')/v''$, $\Delta s'' = s''_{\mathrm{Eq.(28)}} - s''$, $\Delta c_p'' = (c''_{p,\mathrm{Eq.(28)}} - c_p'')/c_p''$.

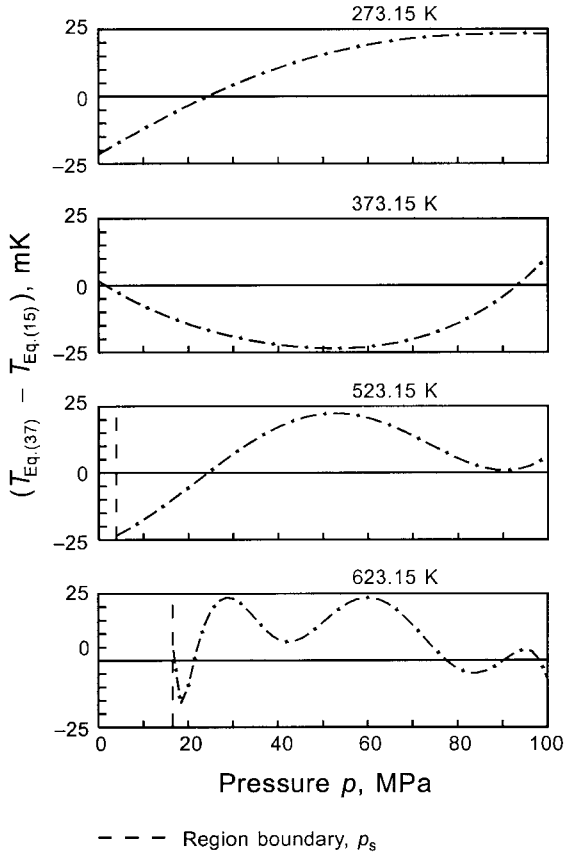

Fig. 24 Absolute deviations of temperatures $T_{Eq.(37)}$ calculated from Eq. (37) from values $T_{Eq.(15)}$ calculated from Eq. (15) for given values of p and h

The structure of the final $T(p, h)$ equation, Eq. (37), was found from Eq. (38) by using the approximation algorithm of Willkommen et al. [23, 27] which combines a special modification of the structure-optimization method of Wagner [19] with the elements automatic data weighting and data-grid condensation. In this entire optimization process Eq. (37) was fitted to T-p-h values, where h had been calculated from the basic equation for region 1, Eq. (15), for given values of p and T distributed as selected grid points over region 1; the final coefficients were determined with the simultaneous steady approximation of Zschunke et al. [24]. Details of such fitting processes are given by Willkommen [27].

Numerical Consistency Between Eqs. (37) and (15). Figure 24 illustrates the numerical consistency achieved between the $T(p, h)$ equation for region 1, Eq. (37), and the corresponding basic equation, Eq. (15), along four isotherms considered to be characteristic for the behavior of Eq. (37). Over the entire region the numerical inconsistency between Eqs. (37) and (15) has a maximum of 23.6 mK and a root-mean-square average of 13.4 mK.

5.6.1.2 The Backward Equation T(p, s). The backward equation $T(p, s)$ for region 1 has the following dimensionless form:

$$\frac{T(p, s)}{T^*} = \theta(\pi, \sigma) = \sum_{i=1}^{20} n_i \pi^{I_i} (\sigma + 2)^{J_i}, \tag{39}$$

where $\theta = T/T^*$, $\pi = p/p^*$, and $\sigma = s/s^*$ with $T^* = 1$ K, $p^* = 1$ MPa, and $s^* = 1$ kJ kg^{-1} K^{-1}. The coefficients n_i and exponents I_i and J_i of Eq. (39) are listed in Table A18.

Equation (39) covers the same range of validity as the basic equation, Eq. (15), except for the metastable superheated-liquid region, where Eq. (39) is not valid.

To assist the user in computer-program verification of Eq. (39), Table A19 contains the corresponding test values.

Development of Eq. (39). Based on test calculations with Eq. (36) for the maximum ranges of the exponents I_i and J_i, the values of the reducing parameters T^*, p^*, and s^* and the shifting parameters b and d, the following dimensionless comprehensive expression of 165 terms (bank of terms) was used as starting point for the development of the backward equation $T(p, s)$ for region 1 [18]:

$$\theta = \sum_{i=0}^{4} \sum_{j=0}^{32} n_{ij} \pi^i (\sigma + 2)^j, \tag{40}$$

where $\theta = T/T^*$, $\pi = p/p^*$, and $\sigma = s/s^*$ with $T^* = 1$ K, $p^* = 1$ MPa, and $s^* = 1$ kJ kg^{-1} K^{-1}.

The structure of the final $T(p, s)$ equation, Eq. (39), was found from Eq. (40) with the structure-optimization method of Setzmann and Wagner [5]. When using this method alone it can happen (as for all procedures based on the least square method) that in relatively small ranges the deviations from the input data are significantly larger than in the rest of the fitting range. Thus, in order to reduce these larger deviations in small ranges at the expense of smaller deviations over larger ranges, a special fitting procedure was tandem-arranged to the application of the structure-optimization method [5]. This special fitting procedure [18, 28] performs a recursive fitting process in which an amplification function increases the weighting factors of such data having the largest deviations in the preceding fitting step. When applying these two methods Eq. (39) was fitted to T-p-s values, where s had been calculated from the basic equation for region 1, Eq. (15), for given values of p and T distributed as selected grid points over region 1. Details of this entire fitting process are given by Kruse and Wagner [18].

Numerical Consistency Between Eqs. (39) and (15). Figure 25 illustrates the numerical consistency achieved between the $T(p, s)$ equation for region 1, Eq. (39), and the corresponding basic equation, Eq. (15), along four isotherms considered to be characteristic for the behavior of Eq. (39). Over the entire region the numerical inconsistency between Eqs. (39) and (15) has a maximum of 21.8 mK and a root-mean-square average of 5.8 mK. It can be seen that the maximum inconsistencies occur only in a small part of region 1, namely at higher temperatures around 600 K.

5.6.2 The Backward Equations for Region 2. According to the considerations in Section 5.1 (item 2*a*,*b*) the two backward equations $T(p, h)$ and $T(p, s)$ have to be numerically consistent with the basic equation of this region, Eq. (19), within $\Delta T = \pm 25$ mK for $s \leq 5.85$ kJ kg^{-1} K^{-1} and within $\Delta T = \pm 10$ mK for $s > 5.85$ kJ kg^{-1} K^{-1}, for the same p-h values and p-s values, respectively.

Due to this very high consistency demand region 2 is covered by three $T(p, h)$ and three $T(p, s)$ equations. Figure 26 shows how region 2 is divided into the three subregions for the backward equations. The boundary between subregions 2(*a*) and 2(*b*) is the isobar $p = 4$ MPa; the boundary between subregions 2(*b*) and 2(*c*) corresponds to the entropy line $s = 5.85$ kJ kg^{-1} K^{-1}.

In order to know whether the $T(p, h)$ equation for subregion 2(*b*) or for subregion 2(*c*) has to be used for given values of p and h, a special correlation equation for the boundary between subregions 2(*b*) and 2(*c*) (which approximates $s = 5.85$ kJ kg^{-1} K^{-1}) is needed, see Fig. 26. This boundary equation, called B2bc-equation, is a simple quadratic pressure-enthalpy relation which reads

$$\pi = n_1 + n_2 \eta + n_3 \eta^2, \tag{41}$$

where $\pi = p/p^*$ and $\eta = h/h^*$ with $p^* = 1$ MPa and $h^* = 1$ kJ kg^{-1}. The coefficients n_1 to n_3 of Eq. (41) are listed in Table A20. Based on its simple form, Eq. (41) does not describe exactly

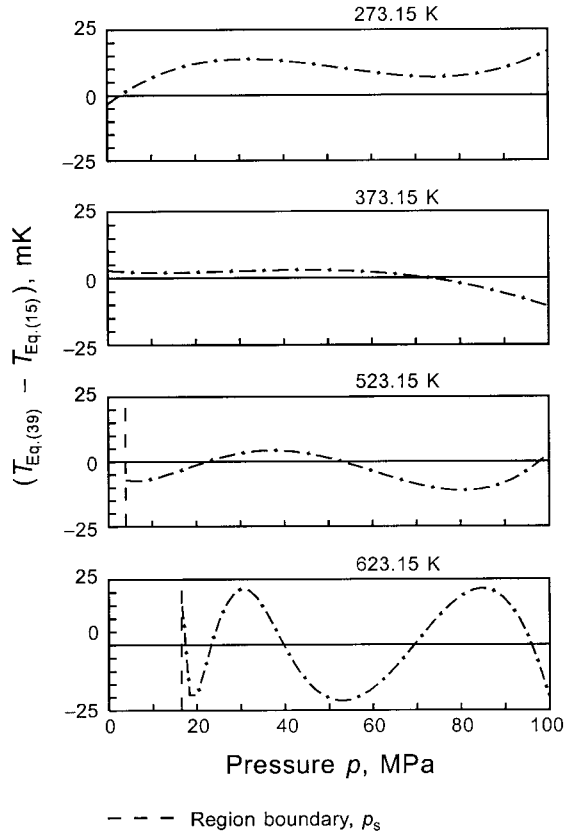

Fig. 25 Absolute deviations of temperatures $T_{Eq.(39)}$ calculated from Eq. (39) from values $T_{Eq.(15)}$ calculated from Eq. (15) for given values of p and s

the isentropic line $s = 5.85$ kJ kg^{-1} K^{-1}; the entropy values corresponding to this p-h relation are between $s = 5.81$ kJ kg^{-1} K^{-1} and $s = 5.85$ kJ kg^{-1} K^{-1}. The enthalpy-explicit form of Eq. (41) is as follows:

$$\eta = n_4 + [(\pi - n_5)/n_3]^{0.5} \tag{42}$$

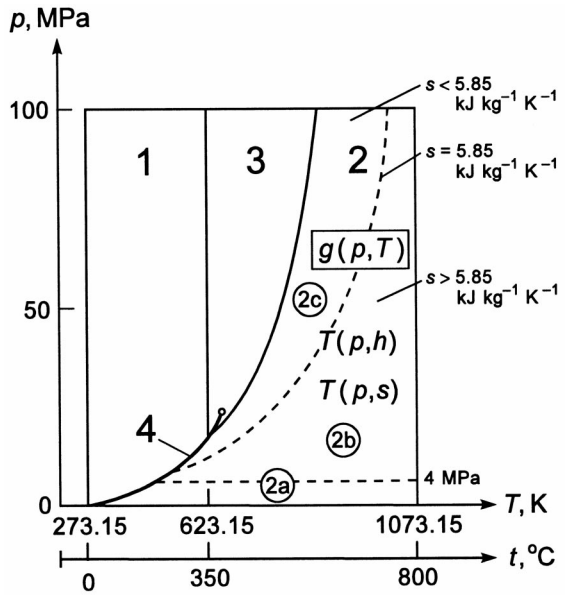

Fig. 26 Division of region 2 of IAPWS-IF97 into the three subregions 2(*a*), 2(*b*), and 2(*c*) for the backward equations $T(p, h)$ and $T(p, s)$

with η and π according to Eq. (41) and the coefficients n_3 to n_5 listed in Table A20. Equations (41) and (42) define the boundary line between subregions 2(*b*) and 2(*c*) from the saturation state at $p_s = 6.546\,669\,967\,8$ MPa (corresponding to about $T = 554.5$ K) up to $p = 100$ MPa (corresponding to about $T = 1019.3$ K).

For the backward equations $T(p, s)$ the boundary between subregions 2(*b*) and 2(*c*) corresponds directly to the isentropic line $s = 5.85$ kJ kg^{-1} K^{-1} and is therefore automatically defined for given values of p and s.

5.6.2.1 The Backward Equations T(p, h) for Subregions 2(a), 2(b), and 2(c). The backward equation $T(p, h)$ for subregion 2(*a*) in its dimensionless form reads

$$\frac{T_{2a}(p, h)}{T^*} = \theta_{2a}(\pi, \eta) = \sum_{i=1}^{34} n_i \pi^{I_i} (\eta - 2.1)^{J_i}, \tag{43}$$

where $\theta = T/T^*$, $\pi = p/p^*$, and $\eta = h/h^*$ with $T^* = 1$ K, $p^* = 1$ MPa, and $h^* = 2000$ kJ kg^{-1}. The coefficients n_i and exponents I_i and J_i of Eq. (43) are listed in Table A21.

The backward equation $T(p, h)$ for subregion 2(*b*) in its dimensionless form reads

$$\frac{T_{2b}(p, h)}{T^*} = \theta_{2b}(\pi, \eta) = \sum_{i=1}^{38} n_i (\pi - 2)^{I_i} (\eta - 2.6)^{J_i}, \tag{44}$$

where $\theta = T/T^*$, $\pi = p/p^*$, and $\eta = h/h^*$ with $T^* = 1$ K, $p^* = 1$ MPa, and $h^* = 2000$ kJ kg^{-1}. The coefficients n_i and exponents I_i and J_i of Eq. (44) are listed in Table A22.

The backward equation $T(p, h)$ for subregion 2(*c*) in its dimensionless form reads

$$\frac{T_{2c}(p, h)}{T^*} = \theta_{2c}(\pi, \eta) = \sum_{i=1}^{23} n_i (\pi + 25)^{I_i} (\eta - 1.8)^{J_i}, \tag{45}$$

where $\theta = T/T^*$, $\pi = p/p^*$, and $\eta = h/h^*$ with $T^* = 1$ K, $p^* = 1$ MPa, and $h^* = 2000$ kJ kg^{-1}. The coefficients n_i and exponents I_i and J_i of Eq. (45) are listed in Table A23.

Equations (43), (44), and (45) are only valid in the respective subregion 2(*a*), 2(*b*), and 2(*c*) that do not include the metastable-vapor region. The boundaries between these subregions are defined at the beginning of Section 5.6.2; the lowest pressure for which Eq. (43) is valid amounts to 611.153 Pa corresponding to the sublimation pressure [20] at 273.15 K.

To assist the user in computer-program verification of Eqs. (43) to (45), Table A24 contains the corresponding test values.

Development of Eqs. (43) to (45). Based on test calculations with Eq. (35) for the maximum ranges of the exponents I_i and J_i, the values of the reducing parameters T^*, p^*, and h^* and the shifting parameters b and d, the following dimensionless comprehensive expressions (bank of terms)[12] were formulated as starting points for the development of the backward equations $T(p, h)$ for subregions 2(*a*), 2(*b*), and 2(*c*):

$$\theta_{2a} = \sum_{i=1}^{10} \sum_{j=1}^{20} n_{ij} \pi^{I_i} (\eta - 2.1)^{J_j} \tag{46}$$

$$\text{with} \quad I_i = 0 \ldots (1) \ldots 9,$$

$$J_j = 0 \ldots (1) \ldots 6, 8 \ldots (2) \ldots 20, 24 \ldots (4) \ldots 44,$$

where $\theta = T/T^*$, $\pi = p/p^*$, and $\eta = h/h^*$ with $T^* = 1$ K, $p^* = 1$ MPa, and $h^* = 2000$ kJ kg^{-1},

[12] The figures given in brackets in the series of the exponents I_i and J_j in Eqs. (46) to (48) correspond to the step size.

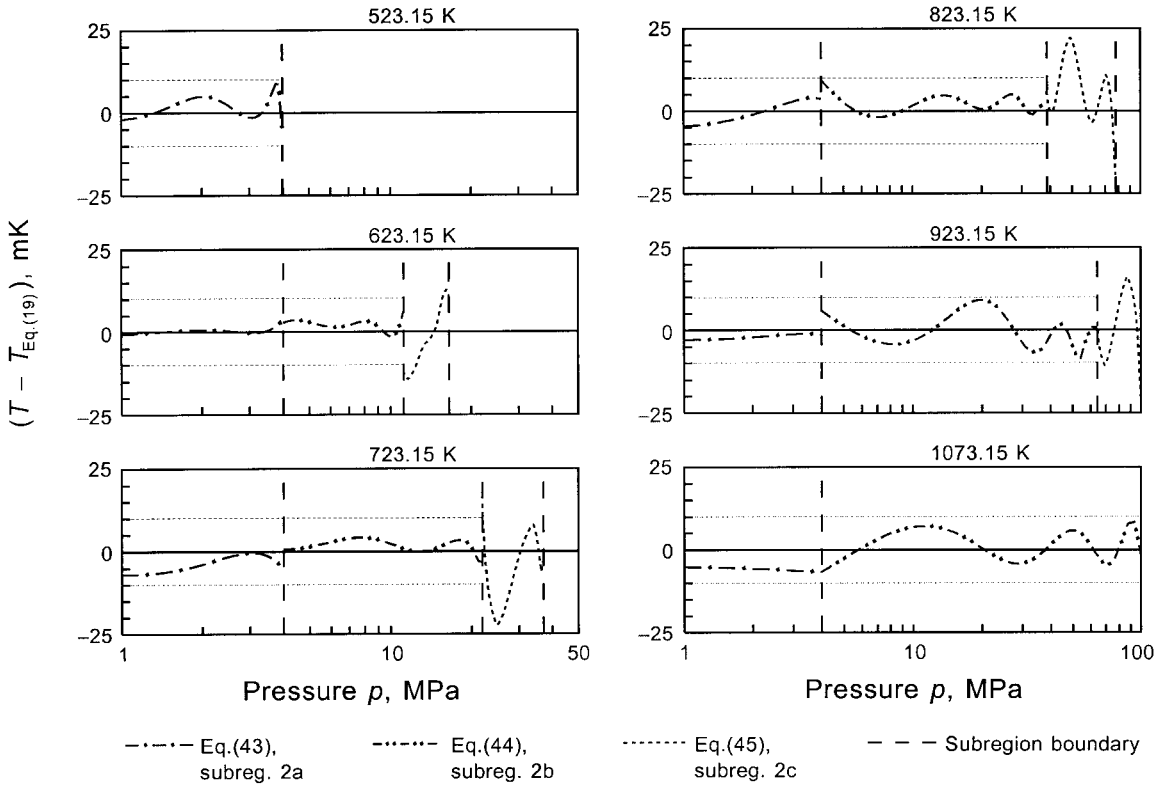

Fig. 27 Absolute deviations of temperatures *T* calculated from Eq. (43) for subregion 2(*a*), Eq. (44) for subregion 2(*b*), and Eq. (45) for subregion 2(*c*) from values $T_{Eq.(19)}$ calculated from Eq. (19) for given values of *p* and *h*

$$\theta_{2b} = \sum_{i=1}^{10} \sum_{j=1}^{30} n_{ij} (\pi - 2)^{I_i} (\eta - 2.6)^{J_j} \tag{47}$$

$$\text{with} \quad I_i = 0 \ldots (1) \ldots 9,$$

$$J_j = 0 \ldots (1) \ldots 17,\ 18 \ldots (2) \ldots 40,$$

where $\theta = T/T^*$, $\pi = p/p^*$, and $\eta = h/h^*$ with $T^* = 1$ K, $p^* = 1$ MPa, and $h^* = 2000$ kJ kg^{-1},

$$\theta_{2c} = \sum_{i=1}^{15} \sum_{j=1}^{20} n_{ij} (\pi + 25)^{I_i} (\eta - 1.8)^{J_j} \tag{48}$$

$$\text{with} \quad I_i = -7 \ldots (1) \ldots 7,$$

$$J_j = 0 \ldots (1) \ldots 6,\ 8 \ldots (2) \ldots 32,$$

where $\theta = T/T^*$, $\pi = p/p^*$, and $\eta = h/h^*$ with $T^* = 1$ K, $p^* = 1$ MPa, and $h^* = 2000$ kJ kg^{-1}.

Equations (43), (44), and (45) were determined from the respective Eqs. (46), (47), and (48) by using the approximation algorithm of Willkommen et al. [23, 27] in which a modified form of the structure-optimization method of Wagner [19] is incorporated. In addition, the algorithm of Trübenbach [29] for setting up equations optimized regarding their computing-time consumption was used. In this entire optimization process Eqs. (43) to (45) were fitted to *T*-*p*-*h* values, where *h* had been calculated from the basic equation for region 1, Eq. (19), for given values of *p* and *T* distributed as selected grid points over subregions 2(*a*), 2(*b*), and 2(*c*). Details of such fitting processes are given by Trübenbach [29].

Numerical Consistency Between Eqs. (43) to (45) and Eq. (19). Figure 27 illustrates the achieved numerical consistency between the three $T(p, h)$ equations for region 2, Eqs. (43) to (45), and the corresponding basic equation, Eq. (19), along six isotherms considered to be characteristic for the behavior of these backward equations. In the diagrams the smaller tolerated inconsistency of ±10 mK for subregions 2(*a*) and 2(*b*) is marked whereas the tolerated inconsistency value of ±25 mK for subregion 2(*c*) corresponds to the maximum value of the deviation scale.

It can be seen that the ΔT values between the two backward equations of adjacent subregions are smaller than the tolerated ΔT values between the backward and basic equation. At the boundaries between subregions 2(*a*) and 2(*b*) and between subregions 2(*b*) and 2(*c*) the maximum temperature differences between the corresponding backward equations amount to 8.7 mK and 21.6 mK, respectively. The tolerated and actual numerical inconsistencies between Eqs. (43) to (45) and Eq. (19), given as maximum and root-mean-square (RMS) temperature differences over the entire region 2, are listed in Table 15.

5.6.2.2 The Backward Equations T(p, s) for Subregions 2(a), 2(b), and 2(c). The backward equation $T(p, s)$ for subregion 2(*a*) in its dimensionless form reads

$$\frac{T_{2a}(p, s)}{T^*} = \theta_{2a}(\pi, \sigma) = \sum_{i=1}^{46} n_i \pi^{I_i} (\sigma - 2)^{J_i}, \tag{49}$$

where $\theta = T/T^*$, $\pi = p/p^*$, and $\sigma = s/s^*$ with $T^* = 1$ K, $p^* = 1$ MPa, and $s^* = 2$ kJ kg^{-1} K^{-1}. The coefficients n_i and exponents I_i and J_i of Eq. (49) are listed in Table A25.

Table 15 Tolerated and actual temperature differences between Eqs. (43) to (45) and Eq. (19)

Subregion	Equation	Temperature differences ΔT, mK		
		Tolerated	Maximum	RMS
2a	43	10	9.3	2.9
2b	44	10	9.6	3.9
2c	45	25	23.7	10.4

The backward equation $T(p, s)$ for subregion 2(b) in its dimensionless form reads

$$\frac{T_{2b}(p, s)}{T^*} = \theta_{2b}(\pi, \sigma) = \sum_{i=1}^{44} n_i \pi^{I_i} (10 - \sigma)^{J_i}, \qquad (50)$$

where $\theta = T/T^*$, $\pi = p/p^*$, and $\sigma = s/s^*$ with $T^* = 1$ K, $p^* = 1$ MPa, and $s^* = 0.7853$ kJ kg^{-1} K^{-1}. The coefficients n_i and exponents I_i and J_i of Eq. (50) are listed in Table A26.

The backward equation $T(p, s)$ for subregion 2(c) in its dimensionless form reads

$$\frac{T_{2c}(p, s)}{T^*} = \theta_{2c}(\pi, \sigma) = \sum_{i=1}^{30} n_i \pi^{I_i} (2 - \sigma)^{J_i}, \qquad (51)$$

where $\theta = T/T^*$, $\pi = p/p^*$, and $\sigma = s/s^*$ with $T^* = 1$ K, $p^* = 1$ MPa, and $s^* = 2.9251$ kJ kg^{-1} K^{-1}. The coefficients n_i and exponents I_i and J_i of Eq. (51) are listed in Table A27.

Equations (49), (50), and (51) are only valid in the respective subregion 2(a), 2(b), and 2(c) which do not include the metastable-vapor region. The boundaries between these subregions are defined at the beginning of Section 5.6.2; the lowest pressure for which Eq. (49) is valid amounts to 611.153 Pa corresponding to the sublimation pressure [20] at 273.15 K.

To assist the user in computer-program verification of Eqs. (49) to (51), Table A28 contains the corresponding test values.

Development of Eqs. (49) to (51). Based on test calculations with Eq. (36) for the maximum ranges of the exponents I_i and J_i, the values of the reducing parameters T^*, p^*, and s^* and the shifting parameters b and d, comprehensive expressions (bank of terms) were formulated as starting points for the development of the backward equations $T(p, s)$ for regions 2(a), 2(b), and 2(c).

For subregion 2(a) this expression in its dimensionless form, consisting of 315 terms [18], was used:

$$\theta_{2a} = \sum_{i=-6}^{-1} \sum_{j=-27}^{0} n_{ij} \pi^{i/4} (\sigma - 2)^j + \sum_{i=0}^{6} \sum_{j=0}^{20} n_{ij} \pi^{i/4} (\sigma - 2)^j, \qquad (52)$$

where $\theta = T/T^*$, $\pi = p/p^*$, and $\sigma = s/s^*$ with $T^* = 1$ K, $p^* = 1$ MPa, and $s^* = 2$ kJ kg^{-1} K^{-1}.

Except for the saturation equation, Eq. (27), this is the only expression which needs noninteger exponents. This fact takes into account that region 2(a) is, when an equation is considered with entropy and pressure as independent variables, a "difficult" region because for $p \to 0$ (ideal-gas behavior) the relation between entropy and pressure is given by $s - s_0 \approx R \ln (p/p_0)$. This means that an logarithmic function in pressure would normally have been necessary. However, due to the long computing times for such functions, as a compromise a power function with noninteger exponents and step sizes of $\frac{1}{4}$ was used.

For subregion 2(b) the bank of terms consisted of 156 terms and had the form [18]:

$$\theta_{2b} = \sum_{i=-6}^{5} \sum_{j=0}^{12} n_{ij} \pi^i (10 - \sigma)^j, \qquad (53)$$

where $\theta = T/T^*$, $\pi = p/p^*$, and $\sigma = s/s^*$ with $T^* = 1$ K, $p^* = 1$ MPa, and $s^* = 0.7853$ kJ kg^{-1} K^{-1}.

For subregion 2(c) the bank of 72 terms read [18]:

$$\theta_{2c} = \sum_{i=-4}^{7} \sum_{j=0}^{5} n_{ij} \pi^i (2 - \sigma)^j, \qquad (54)$$

where $\theta = T/T^*$, $\pi = p/p^*$, and $\sigma = s/s^*$ with $T^* = 1$ K, $p^* = 1$ MPa, and $s^* = 2.9251$ kJ kg^{-1} K^{-1}.

Based on the bank of terms, Eqs. (52) to (54), for the corresponding subregion, the structure of the final $T(p, s)$ equations was determined with the structure-optimization procedure of Setzmann and Wagner [5] supplemented by the recursive fitting procedure [18, 28] to distribute the deviations from the input data more proportionated over the entire region, see the corresponding description in Section 5.6.1.2. When applying these methods Eqs. (49) to (51) were fitted to T-p-s values, where s had been calculated from the basic equation for region 2, Eq. (19), for given values of p and T distributed as selected grid points over regions 2(a), 2(b), and 2(c). Details of these comprehensive fitting processes are given by Kruse and Wagner [18].

Numerical Consistency Between Eqs. (49) to (51) and Eq. (19). Figure 28 illustrates the achieved numerical consistencies between the three $T(p, s)$ equations for region 2, Eqs. (49) to (51), and the corresponding basic equation, Eq. (19), along six isotherms considered to be typical for the behavior of these backward equations. In the diagrams the smaller tolerated inconsistency of ± 10 mK for subregions 2(a) and 2(b) is marked whereas the tolerated inconsistency value of ± 25 mK for subregion 2(c) corresponds to the maximum value of the deviation scale.

It can be seen that the ΔT values between the two backward equations of adjacent subregions are smaller than the tolerated ΔT values between the backward and basic equation. At the boundaries between subregions 2(a) and 2(b) and between subregions 2(b) and 2(c) the maximum temperature differences between the corresponding backward equations amount to 4.1 mK and 9.1 mK, respectively. The tolerated and actual numerical inconsistencies between Eqs. (49) to (51) and Eq. (19), given as maximum and root-mean-square (RMS) temperature differences over the entire region 2, are listed in Table 16.

5.6.3 Typical Effects When Using the Backward Equations for Regions 1 and 2. As described in section 5.1, IAPWS-IF97 is essentially based on the concept of combining the basic equations $g(p, T)$ of regions 1 and 2 with the two types of backward equations $T(p, h)$ and $T(p, s)$. With these three types of equations, properties as function of (p, h) and (p, s) can be calculated without any iteration and for properties as function of (h, s) it is only necessary to perform one-dimensional iterations (instead of two-dimensional iterations when using only $g(p, T)$ equations). This special concept is the basis for achieving high computation speeds with IAPWS-IF97 even for rather complex property functions. However, as the most important precondition for a successful realization of this concept the basic and backward equations had to be numerically extremely consistent with each other. Based on test calculations with characteristic power cycles via iterations with IFC-67, the permitted inconsistencies were set by IAPWS to 10 mK and 25 mK, respectively, depending on the range of state (for details see Section 5.1).

Although all the backward equations $T(p, h)$ and $T(p, s)$ presented in Sections 5.6.1 and 5.6.2 clearly meet these numerical consistency requirements, the inconsistencies are, as a matter of course, not zero. This fact has several consequences of which the user should be aware, for example:

- When calculating a property as function of (p, h) and (p, s), respectively, two different results can be obtained depending on using the $T(p, h)$ and $T(p, s)$ equations or calculating the property directly from the $g(p, T)$ equation by iteration.
- When calculating a property as function of (h, s) three different results can be obtained depending on whether the $T(p, h)$ or the $T(p, s)$ equation is used for a one-dimensional iteration in combination with the basic equation $g(p, T)$ or whether the property is determined directly from the $g(p, T)$ equation by a two-dimensional iteration.
- When calculating properties extremely close to the region boundaries and particularly to the vapor-liquid phase boundary, the user should be aware of the small inconsistencies between the backward and basic equations. For example, in region 2 very close to the saturated vapor line ($|T - T_s| < 25$ mK for

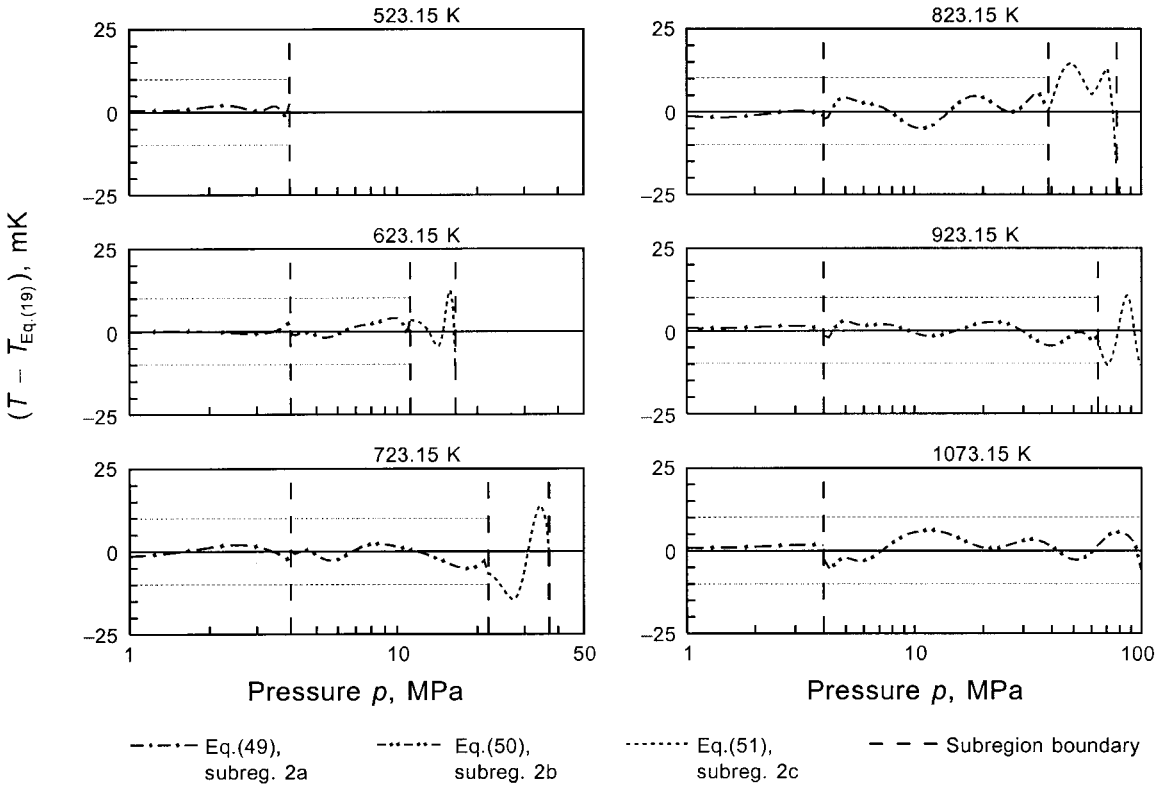

Fig. 28 Absolute deviations of temperatures *T* calculated from Eq. (49) for subregion 2(*a*), Eq. (50) for subregion 2(*b*), and Eq. (51) for subregion 2(*c*) from values $T_{Eq.(19)}$ calculated from Eq. (19) for given values of *p* and *s*

region 1 and subregion 2(*c*) and $|T - T_s| < 10$ mK for subregions 2(*a*) and 2(*b*)), the $T(p, h)$ and the $T(p, s)$ equation, respectively, might yield temperatures $T(p, h) < T_s(p)$ and $T(p, s) < T_s(p)$. Such results would indicate a state in region 1 instead of the correct region 2. The opposite case can occur when the calculations are carried out in region 1 correspondingly close to the saturated liquid line. The user should be aware of such effects in order to avoid possible problems by taking suitable measures in the program code.

The described inconsistencies are unavoidable when using backward equations and are therefore an agreed upon feature of IAPWS-IF97. Due to the insignificance of these inconsistencies they do not have any practical relevance for nearly all technical applications. Thus, because of the great advantage with regard to short computing times, the backward equations should be used whenever possible. For such applications, however, where these small inconsistencies are indeed not acceptable, the calculations must be performed with the basic equations $g(p, T)$ only by iterations. Even in this case the inconsistency is not zero, but depends on the selected convergence criterion of the iteration. The convergence criterion has to be less than 10^{-4} to 10^{-5} in $\Delta T/T$ (depending on region) to achieve a smaller inconsistency than with the backward equations.

5.6.4 The Backward Equation for Region 4. According to the concept of IAPWS-IF97 there is also a backward equation for region 4, the saturation curve, see Section 5.1 and Fig. 2. This backward equation is the saturation-temperature equation, which follows directly from the implicit saturation equation, Eq. (27), by solving it with respect to the saturation temperature T_s.

The saturation-temperature equation reads

$$\frac{T_s}{T^*} = \frac{n_{10} + D - [(n_{10} + D)^2 - 4(n_9 + n_{10}D)]^{0.5}}{2}, \quad (55)$$

where $T^* = 1$ K and

$$D = \frac{2G}{-F - (F^2 - 4EG)^{0.5}}$$

with

$$E = \beta^2 + n_3\beta + n_6$$

$$F = n_1\beta^2 + n_4\beta + n_7$$

$$G = n_2\beta^2 + n_5\beta + n_8$$

$$\text{and} \quad \beta = (p_s/p^*)^{0.25} \quad (55a)$$

with $p^* = 1$ MPa; Eq. (55*a*) is identical with Eq. (27*a*). The coefficients n_i of Eq. (55) are listed in Table A11.

Equation (55) has the same range of validity as the saturation-pressure equation, Eq. (28), which means that it covers the vapor-liquid saturation curve according to the pressure range

$$611.213 \text{ Pa} \le p \le 22.064 \text{ MPa}.$$

The value of 611.213 Pa corresponds to the pressure when Eq. (55) is extrapolated to 273.15 K. Since the saturation-pressure equation, Eq. (28), and the saturation-temperature equation, Eq. (55), have been derived from the same implicit equation, Eq. (27), for de-

Table 16 Tolerated and actual temperature differences between Eqs. (49) to (51) and Eq. (19)

Subregion	Equation	Temperature differences ΔT, mK		
		Tolerated	Maximum	RMS
2a	49	10	8.8	1.2
2b	50	10	6.5	2.8
2c	51	25	19.0	8.3

Table 17 Results of the computing-time investigations of IAPWS-IF97 in relation to IFC-67 for regions 1, 2, and 4

Region[a]	Function	Frequency of use %	Computing-time ratio (CTR value) IFC-67/IAPWS-IF97
1	$v(p,T)$	2.9	2.7
	$h(p,T)$	9.7	2.9
	$T(p,h)$	3.5	24.8
	$h(p,s)$	1.2	10.0
		Σ region 1:	5.6[b]
2	$v(p,T)$	6.1	2.1
	$h(p,T)$	12.1	2.9
	$s(p,T)$	1.4	1.4
	$T(p,h)$	8.5	12.4
	$v(p,h)$	3.1	6.4
	$s(p,h)$	1.7	4.2
	$T(p,s)$	1.7	8.1
	$h(p,s)$	4.9	5.6
		Σ region 2:	5.0[b]
4	$p_s(T)$	8.0	1.7
	$T_s(p)$	30.7	5.6
	$h'(p)$	2.25	4.4
	$h''(p)$	2.25	4.2
		Σ region 4:	4.9[b]
		Σ regions 1, 2 and 4:	**5.1**[b]

[a] For the definition of the regions see Fig. 2

[b] This CTR value is based on the computing times for the single functions weighted by the frequency-of-use values, see text

Table 18 Results of the computing-time investigations of IAPWS-IF97 in relation to IFC-67 for regions 3 and 5

Region[a]	Function	Computing-time ratio (CTR value) IFC-67/IAPWS-IF97
3	$p(v,T)$	3.8
	$h(v,T)$	4.3
	$c_p(v,T)$	2.9
	$s(v,T)$	3.2
5	$v(p,T)$	8.9[b]
	$h(p,T)$	11.9[b]
	$c_p(p,T)$	15.8[b]

[a] For the definition of the regions see Fig. 2

[b] Determined for the 1073.15 K isotherm for which IFC-67 was valid

scribing the saturation curve both Eq. (28) and Eq. (55) are completely consistent with each other. Thus, the basic and backward equation for region 4 meet the numerical consistency requirements, see Section 5.1 (item 2(*c*)).

To assist the user in computer-program verification of Eq. (55), Table A29 contains corresponding test values.

5.7 Computing Time of IAPWS-IF97 in Relation to IFC-67. A very important requirement on IAPWS-IF97 was that its computation speed in relation to IFC-67 should be significantly faster, see Section 4.4. The computation-speed investigations of IAPWS-IF97 in comparison with IFC-67 were based on a special procedure agreed within IAPWS.

The computing times were measured with a benchmark program developed by IAPWS; this program calculates the corresponding functions at a large number of state points well distributed proportionately over each region. The test configuration agreed on was a PC Intel 486 DX 33 processor and the MS Fortran 5.1 compiler.[13] The relevant functions of IAPWS-IF97 were programmed with regard to short computing times. The calculations with IFC-67 were carried out with the ASME program package [30] speeded up by excluding all parts which were not needed for these special benchmark tests.

The measured computing times were used to calculate computing-time ratios IFC-67/IAPWS-IF97, called CTR values in the following. These CTR values, determined in a different way for regions 1, 2, and 4 and for regions 3 and 5 (see Section 4.4), are the characteristic quantities for the judgment of how much faster the calculations with IAPWS-IF97 are in comparison with IFC-67. Metastable states were not included in these investigations.

5.7.1 Computing-Time Investigations for Regions 1, 2, and 4. The computing-time investigations for regions 1, 2, and 4 of IAPWS-IF97, which are particularly relevant to computing time for industrial calculations, were performed for the functions listed in Table 17. Each function is associated with a frequency-of-use value. Both the selection of the functions and the values for the corresponding frequency of use are based on a worldwide survey made among the power plant companies and related industries, see also Section 4.4.

For the computing-time comparison between IAPWS-IF97 and IFC-67 for regions 1, 2, and 4, the total CTR value of these three regions together was the decisive criterion, where the frequencies of use have to be taken into account. The total CTR value was calculated as follows: As has been described before, the computing times for each function were determined for IFC-67 and for IAPWS-IF97. Then, these values were weighted by the corresponding frequencies of use and added up for the 16 functions of the three regions. The total CTR value is obtained from the sum of the weighted computing times for IFC-67 divided by the corresponding value for IAPWS-IF97. The total CTR value for regions 1, 2, and 4 amounts to

$$\mathrm{CTR}_{\mathrm{regions1,2,4}} = 5.1. \tag{56}$$

This means that for regions 1, 2, and 4 together the property calculations with IAPWS-IF97 are more than five times faster than with IFC-67.

Table 17 also contains total CTR values separately for each of regions 1, 2, and 4. In addition, CTR values for each single function are given. When using IAPWS-IF97 the functions depending on p, h and p, s for regions 1 and 2 and on p for region 4 were calculated from the backward equations alone (functions explicit in T) or from the basic equations in combination with the corresponding backward equation.

5.7.2 Computing-Time Investigations for Regions 3 and 5. For regions 3 and 5 of IAPWS-IF97 the CTR values only relate to the single functions listed in Table 18 and are given by the quotient of the computing time needed for IFC-67 calculation and the computing time when using IAPWS-IF97; there were no frequency-of-use values for functions relevant to these two regions.

For region 3 of IAPWS-IF97, corresponding to regions 3 and 4 of IFC-67, 10 percent of the test points were in region 4 of IFC-67. For region 5 of IAPWS-IF97, the CTR values were determined for 1073.15 K, the maximum temperature for which IFC-67 was valid. Table 18 lists the CTR values obtained for the relevant functions of regions 3 and 5. Roughly speaking, IAPWS-IF97 is more than three times faster than IFC-67 for region 3 and more than nine times faster for region 5 measured for the 1073.15 K isotherm where region 5 overlaps IFC-67.

5.8 Uncertainties of IAPWS-IF97. In this section uncertainties are given for the properties specific volume, specific isobaric heat capacity, speed of sound, and saturation pressure when calculated from the corresponding equations of IAPWS-IF97. Uncertainties cannot be derived for the specific enthalpy, since there is no reasonable basis for their estimation; the values of the specific enthalpy depend on the selection of the zero point. For enthalpy differences, and here only these are of interest, one can conclude that the uncertainty of isobaric enthalpy differences is always smaller than the uncertainty of the isobaric heat capacity.

[13] This test configuration was established at the IAPWS meeting in 1992. If a faster processor and/or an other compiler than specified above are used for the described benchmark tests, similar results are obtained for the computation-speed comparisons between IAPWS-IF97 and IFC-67; this statement is based on recent test calculations using more recent processors and compilers.

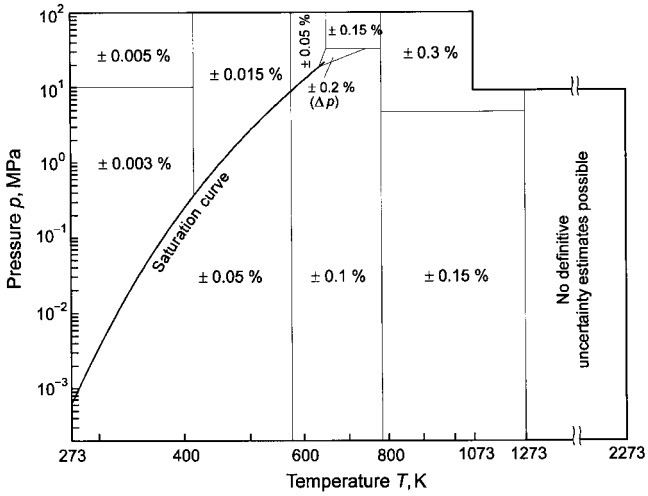

Fig. 29 Uncertainties in specific volume, Δv, estimated for the corresponding equations of IAPWS-IF97. In the enlarged critical region (triangle), the uncertainty is given as percentage uncertainty in pressure, Δp. This region is bordered by the two isochores 0.0019 m^3 kg^{-1} and 0.0069 m^3 kg^{-1} and by the 30 MPa isobar. The positions of the lines separating the uncertainty regions are approximate.

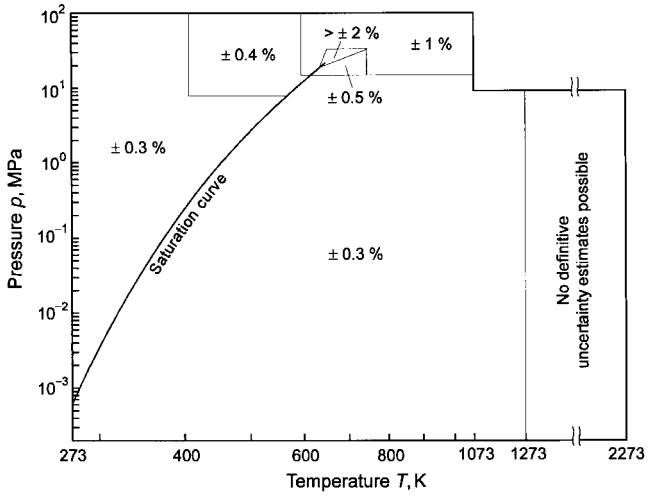

Fig. 31 Uncertainties in speed of sound, Δw, estimated for the corresponding equations of IAPWS-IF97. For the definition of the triangle around the critical point, see Fig. 29. The positions of the lines separating the uncertainty regions are approximate.

The estimated uncertainties for the above mentioned properties result from two contributions:

- Uncertainty of the scientific standard for the thermodynamic properties of water and steam, the IAPWS-95 formulation [7, 8], from which the values of the properties were calculated to fit the equations of the industrial formulation IAPWS-IF97. The uncertainty of IAPWS-95 is mainly based on the estimated uncertainties of the selected experimental data of the properties [8], which had been used for the development of the scientific standard.
- Deviations of IAPWS-IF97 from IAPWS-95 regarding the properties considered.

The uncertainties of the properties v, c_p, and w calculated from IAPWS-IF97 for the single-phase region are indicated in Figs. 29 to 31 as tolerance values. As used here "tolerance" means the range of possible values as judged by IAPWS, and no statistical significance can be attached to it. With regard to the uncertainty for the specific isobaric heat capacity and the speed of sound, see Figs. 30 and 31, it should be noted that the uncertainties for these properties increase drastically when approaching the critical point. The statement "no definitive uncertainty estimates possible" for temperatures above 1273 K is based on the fact that this range is beyond the range of validity of IAPWS-95 and the corresponding input values for IAPWS-IF97 were extrapolated from IAPWS-95.

The estimated uncertainties of the saturation pressure calculated from the IAPWS-IF97 are given in Fig. 32.

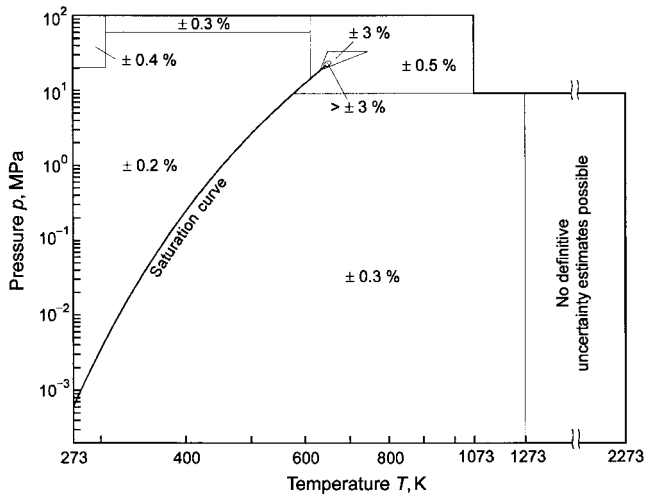

Fig. 30 Uncertainties in specific isobaric heat capacity, Δc_p, estimated for the corresponding equations of IAPWS-IF97. For the definition of the triangle around the critical point, see Fig. 29. The positions of the lines separating the uncertainty regions are approximate.

6 Concluding Remarks

The decisive factor for the development of a new industrial formulation was the explicit desire for a significant increase of the computation speed in comparison with the previous industrial standard IFC-67. For the technically most important regions of state the calculations with IAPWS-IF97 are more than five times faster than with IFC-67 and hence the new formulation clearly exceeds the requirement of a three times faster calculation of the thermodynamic properties of water and steam. Moreover, in the meantime, from many test calculations it has become evident that the enormous improvement of the consistency along region boundaries is of great advantage particularly for common use. Concerning accuracy, IAPWS-IF97 is clearly better than IFC-67, namely on average 7.5 times more accurate in the specific volume, 18 times in the specific enthalpy, 12 times in the isobaric heat capacity, 32 times in the speed of sound, and 8.5 times in the saturation pressure, where the improvement in both the isobaric heat capacity and the speed of sound is to be particularly emphasized. A further important advantage is that IAPWS-IF97 does not only yield reasonable results for the main properties v, h, s, c_p, and w but

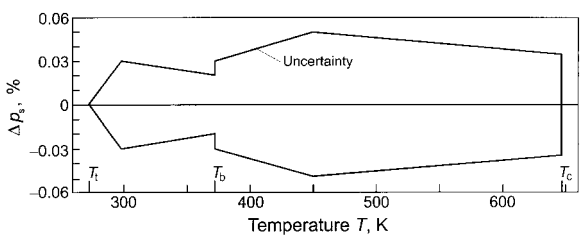

Fig. 32 Uncertainties in saturation pressure, Δp_s, estimated for the saturation-pressure equation, Eq. (28)

for any property which can be calculated from any combination of the first and second derivatives of the fundamental equations $g(p, T)$ and $f(\rho, T)$, respectively, with respect to their independent variables. All in all it can be concluded that with regard to all three items, computation speed, consistency along region boundaries, and accuracy, a new quality standard has been achieved with the IAPWS Industrial Formulation 1997.

The new formulation IAPWS-IF97 is valid for immediate general use. Thus, there is need to modify the corresponding design and application codes.

In addition to this comprehensive article, there are also new steam tables based on IAPWS-IF97, as examples see references [3, 4, 4*a*]. Moreover, computer codes based on IAPWS-IF97 are available from several institutions; information about such software can be obtained from the IAPWS national committees, see the IAPWS Web site http://www.iapws.org.

Acknowledgments

The authors are indebted to the members of the following IAPWS groups (so far as we are not members ourselves): Task Group "New Industrial Formulation," Working Group "Industrial Calculations," Working Group "Thermophysical Properties of Water and Steam," and Task Group "New Industrial Formulation-Evaluation." In particular we are grateful to the chairman and vice chairman of the Working Group "Industrial Calculations," B. Rukes and W. T. Parry, for their continuous support of this comprehensive project over the years. We are also indebted to the chairman of the Task Group "New Industrial Formulation-Evaluation," K. Miyagawa, and his colleagues R. Spencer, R. B. McClintock, and H. W. Bradly for their exceptional efforts when testing IAPWS-IF97 regarding the fulfillment of requirements and checking the influence on real power-cycle calculations. Moreover, we are grateful to all IAPWS colleagues who contributed to the entire project of the development of the new industrial formulation IAPWS-IF97. On behalf of all of them we would like to thank the presidents of IAPWS who held office during the development period of IAPWS-IF97, namely J. R. Cooper, J. M. H. Levelt Sengers, K. Watanabe, and R. Fernández-Prini.

One of us (W.W.) wishes to express his warmest thanks to Mr. C. Bonsen for his help in handling the computer programs for plotting the most part of the figures. Two of us (W.W. and A.D.) are particularly grateful to the Deutsche Forschungsgemeinschaft (German Research Association) for their financial support of that part of the development of IAPWS-IF97 which was carried out at the Ruhr-University Bochum and the Technical University Dresden.

Finally, we are very grateful to the members of the US Steam Properties subcommittee and to the US National Representative to IAPWS, J. M. H. Levelt Sengers, for their help to get published this comprehensive article in the ASME journal. Our special thank is due to the Secretary of the US subcommittee, A. H. Harvey, for his very effective help in this matter.

References

1 International Formulation Committee of the 6th International Conference on the Properties of Steam, 1967, "The 1967 IFC Formulation for Industrial Use," Verein Deutscher Ingenieure, Düsseldorf.

2 International Association for the Properties of Water and Steam, 1997, "IAPWS Industrial Formulation 1997 for the Thermodynamic Properties of Water and Steam," IAPWS Release, IAPWS Secretariat.[14]

3 Wagner, W., and Kruse, A., 1998, "Properties of Water and Steam/ Zustandsgrößen von Wasser und Wasserdampf/IAPWS-IF97," Springer-Verlag, Berlin, Heidelberg.

4 1999 JSME Steam Tables Based on IAPWS-IF97, 1999, The Japan Society of Mechanical Engineers, Tokyo.

4*a* Parry, W. T., Bellows, J. C., Gallagher, J. S., and Harvey, A. H., 2000, "ASME International Steam Tables for Industrial Use," ASME Press, New York.

5 Setzmann, U., and Wagner, W., 1989, "A New Method for Optimizing the Structure of Thermodynamic Correlation Equations," *Int. J. Thermophysics*, Vol. 10, pp. 1103–1126.

6 Preston–Thomas, H., 1990, "The International Temperature Scale of 1990 (ITS-90)," *Metrologia*, Vol. 27, pp. 3–10.

7 International Association for the Properties of Water and Steam, 1996, "IAPWS Formulation 1995 for the Thermodynamic Properties of Ordinary Water Substance for General and Scientific Use," *IAPWS Release*, IAPWS Secretariat.[14]

8 Wagner, W., and Pruß, A., 1999, "The IAPWS Formulation 1995 for the Thermodynamic Properties of Ordinary Water Substance for General and Scientific Use," to be submitted to J. Phys. Chem. Ref. Data.

9 International Association for the Properties of Water and Steam, 1994, "Skeleton Tables 1985 for the Thermodynamic Properties of Ordinary Water Substance," *IAPWS Release*, IAPWS Secretariat; also in: White, Jr., H. J., Sengers, J. V., Neumann, D. B., and Bellows, J. C., eds., 1995, "Physical Chemistry of Aqueous Systems: Meeting the Needs of Industry," Proceedings of the 12th International Conference on the Properties of Water and Steam, Begell House, New York, pp. A13–A32.

10 International Formulation Committee of ICPS, 1965, "Minutes of the Meeting of the International Formulation Committee of ICPS," Prague.

11 Cohen, E. R., and Taylor, B. N., 1986, "The 1986 Adjustment of the Fundamental Physical Constants," *CODATA Bulletin*, No. 63, Committee on Data for Science and Technology, Int. Council of Scientific Unions, Pergamon Press, Oxford.

12 Audi, G., and Wapstra, A. H., 1993, "The 1993 Atomic Mass Evaluation, (I) Atomic Mass Table," *Nuclear Physics*, Vol. A 565, pp. 1–65.

13 IUPAC, 1991, "Isotopic Compositions of the Elements 1989," Commission on Atomic Weights and Isotopic Abundances, Subcommittee for Isotopic Abundance Measurements, *Pure and Appl. Chem.*, Vol. 63, pp. 991–1002.

14 International Association for the Properties of Water and Steam, 1995, "Release on The Values of Temperature, Pressure and Density of Ordinary and Heavy Water Substances at Their Respective Critical Points," IAPWS Secretariat; also in: White, Jr., H. J., Sengers, J. V., Neumann, D. B., and Bellows, J. C., eds., 1995, "Physical Chemistry of Aqueous Systems: Meeting the Needs of Industry," Proceedings of the 12th International Conference on the Properties of Water and Steam, Begell House, New York, pp. A101–A102.

15 Guildner, L. A., Johnson, D. P., and Jones, F. E., 1976, "Vapor Pressure of Water at Its Triple Point," *J. Res. Natl. Bur. Stand.*, Vol. 80A, pp. 505–521.

16 Setzmann, U., and Wagner, W., 1991, "A New Equation of State and Tables of Thermodynamic Properties for Methane Covering the Range from the Melting Line to 625 K at Pressures up to 1000 MPa," *J. Phys. Chem. Ref. Data*, Vol. 20, pp. 1061–1155.

17 Span, R., and Wagner, W., 1996, "A New Equation of State for Carbon Dioxide Covering the Fluid Region from the Triple-Point Temperature to 1100 K at Pressures up to 800 MPa," *J. Phys. Chem. Ref. Data*, Vol. 25, pp. 1509–1596.

18 Kruse, A., and Wagner, W., 1998, "Neue Zustandsgleichungen für industrielle Anwendungen im technisch relevanten Zustandsgebiet von Wasser," *Fortschr.-Ber. VDI*, Reihe 6, Nr. 393, VDI-Verlag, Düsseldorf.

19 Wagner, W., 1974, "Eine mathematisch statistische Methode zum Aufstellen thermodynamischer Gleichungen—gezeigt am Beispiel der Dampfdruckkurve reiner fluider Stoffe," *Fortschr.-Ber. VDI-Z.*, Reihe 3, Nr. 39, VDI-Verlag, Düsseldorf.

19*a* Kretzschmar, H.-J., Stöcker, I., Klinger, J., and Dittmann, A., 2000, "Calculation of Thermodynamic Derivatives of Water and Steam Using the New Industrial Formulation IAPWS-IF97," Proceedings of the 13th International Conference on the Properties of Water and Steam, P. Tremaine, P. G. Hill, D. Irish, and P. V. Balakrishnan, eds., NRC Press, Ottawa.

20 International Association for the Properties of Water and Steam, 1994, "Release on the Pressure along the Melting and the Sublimation Curves of Ordinary Water Substance," in Wagner, W., Saul, A., and Pruß, A., 1994, *J. Phys. Chem. Ref. Data*, Vol. 23, pp. 515–527; also in White, Jr., H. J., Sengers, J. V., Neumann, D. B., and Bellows, J. C., eds., 1995, "Physical Chemistry of Aqueous Systems: Meeting the Needs of Industry," Proceedings of the 12th International Conference on the Properties of Water and Steam, Begell House, New York, pp. A9–A12.

21 Miyagawa, K., Spencer, R. C., McClintock, R. B., Bradly, H. W., Kodl, I., Perstrup, C., Parry, W. T., Rukes, B., Scala, M., and Smith, P. F., 1997, "Acceptance Test Report of Proposal of a New Industrial Formulation of IAPWS," report, IAPWS Task Group NIF Evaluation.[14]

22 Kretzschmar, H.-J., Oguchi, K., and Willkommen, Th., 2000, "Numerically Consistent Equations for Vapor Pressure $p_s(T)$ and Saturation Temperature $T_s(p)$ of Ordinary Water Substance," to be submitted to *Int. J. Thermophysics.*

23 Willkommen, Th., Kretzschmar, H.-J., and Dittmann, A., 1995, "An Algorithm for Setting Up Numerically Consistent Forward and Backward Equations for Process Modelling," in White, Jr., H. J., Sengers, J. V., Neumann, D. B., Bellows, J. C., eds., "Physical Chemistry of Aqueous Systems: Meeting the Needs of Industry," Proceedings of the 12th International Conference on the Properties of Water and Steam, Begell House, New York, pp. 194–201.

24 Zschunke, T., Kretzschmar, H.-J., and Dittmann, A., 1991, "Erstellung von konsistenten Zustandsgleichungen mit simultaner gleichmäßiger Approximation," *Brennstoff-Wärme-Kraft*, Vol. 43, pp. 567–570.

25 Mareš, R., and Šifner, O., 1996, "Equation of state for Superheated Steam in the Range from 800 to 2000°C and Pressures up to 10 MPa," *Acta Techn. CSAV*, Vol. 41, pp. 647–652.

26 Cooper, J. R., 1982, "Representation of the Ideal-Gas Thermodynamic Properties of Water," *Int. J. Thermophysics*, Vol. 3, pp. 35–43.

27 Willkommen, Th., 1996, "Ein Algorithmus zur Aufstellung numerisch kon-

[14] Mailing address: Executive Secretary of IAPWS, Dr. R. B. Dooley, EPRI, 3412 Hillview Avenue, Palo Alto, California 94304, USA

sistenter Gleichungen für die in Prozeßmodellierungen benötigten thermodynamihen Umkehrfunktionen," dissertation, Technische Universität Dresden, Fakultät Maschinenwesen, Dresden.

28 Smukala, J., 1995, "Entwicklung eines Verfahrens zur Berücksichtigung der numerischen Konsistenz bei der Aufstellung von Zustandsgleichungen in Form von Vorwärts- und Rückwärtsgleichungen," Diplomarbeit, Lehrstuhl für Thermodyamik, Ruhr-Universität Bochum, Bochum.

29 Trübenbach, J., 1999, "Ein Algorithmus zur Aufstellung rechenzeitoptimierter Gleichungen für thermodynamische Zustandsgrößen," *Fortschr.-Ber. VDI*, Reihe 6, Nr. 417, VDI-Verlag, Düsseldorf.

30 McClintock, R. B., and Silvestri, G. J., 1968, *Formulations and Iterative Procedures for the Calculation of Properties of Steam*, ASME, New York.

APPENDIX

This appendix contains Tables A1 to A29 in which the coefficients, exponents, and test values for computer-program verification are listed.

Table A1 Coefficients of Eqs. (10) and (11)[a]

i	n_i	i	n_i
1	$0.348\,051\,856\,289\,69 \times 10^{3}$	4	$0.572\,544\,598\,627\,46 \times 10^{3}$
2	$-0.116\,718\,598\,799\,75 \times 10^{1}$	5	$0.139\,188\,397\,788\,70 \times 10^{2}$
3	$0.101\,929\,700\,393\,26 \times 10^{-2}$		

[a] For computer-program verification, Eqs.(10) and (11) must meet the following T-p point: $T = 0.623\,150\,000 \times 10^{3}$ K, $p = 0.165\,291\,643 \times 10^{2}$ MPa

Table A2 Coefficients and exponents of Eq. (15)

i	I_i	J_i	n_i	i	I_i	J_i	n_i
1	0	−2	$0.146\,329\,712\,131\,67$	18	2	3	$-0.441\,418\,453\,308\,46 \times 10^{-5}$
2	0	−1	$-0.845\,481\,871\,691\,14$	19	2	17	$-0.726\,949\,962\,975\,94 \times 10^{-15}$
3	0	0	$-0.375\,636\,036\,720\,40 \times 10^{1}$	20	3	−4	$-0.316\,796\,448\,450\,54 \times 10^{-4}$
4	0	1	$0.338\,551\,691\,683\,85 \times 10^{1}$	21	3	0	$-0.282\,707\,979\,853\,12 \times 10^{-5}$
5	0	2	$-0.957\,919\,633\,878\,72$	22	3	6	$-0.852\,051\,281\,201\,03 \times 10^{-9}$
6	0	3	$0.157\,720\,385\,132\,28$	23	4	−5	$-0.224\,252\,819\,080\,00 \times 10^{-5}$
7	0	4	$-0.166\,164\,171\,995\,01 \times 10^{-1}$	24	4	−2	$-0.651\,712\,228\,956\,01 \times 10^{-6}$
8	0	5	$0.812\,146\,299\,835\,68 \times 10^{-3}$	25	4	10	$-0.143\,417\,299\,379\,24 \times 10^{-12}$
9	1	−9	$0.283\,190\,801\,238\,04 \times 10^{-3}$	26	5	−8	$-0.405\,169\,968\,601\,17 \times 10^{-6}$
10	1	−7	$-0.607\,063\,015\,658\,74 \times 10^{-3}$	27	8	−11	$-0.127\,343\,017\,416\,41 \times 10^{-8}$
11	1	−1	$-0.189\,900\,682\,184\,19 \times 10^{-1}$	28	8	−6	$-0.174\,248\,712\,306\,34 \times 10^{-9}$
12	1	0	$-0.325\,297\,487\,705\,05 \times 10^{-1}$	29	21	−29	$-0.687\,621\,312\,955\,31 \times 10^{-18}$
13	1	1	$-0.218\,417\,171\,754\,14 \times 10^{-1}$	30	23	−31	$0.144\,783\,078\,285\,21 \times 10^{-19}$
14	1	3	$-0.528\,383\,579\,699\,30 \times 10^{-4}$	31	29	−38	$0.263\,357\,816\,627\,95 \times 10^{-22}$
15	2	−3	$-0.471\,843\,210\,732\,67 \times 10^{-3}$	32	30	−39	$-0.119\,476\,226\,400\,71 \times 10^{-22}$
16	2	0	$-0.300\,017\,807\,930\,26 \times 10^{-3}$	33	31	−40	$0.182\,280\,945\,814\,04 \times 10^{-23}$
17	2	1	$0.476\,613\,939\,069\,87 \times 10^{-4}$	34	32	−41	$-0.935\,370\,872\,924\,58 \times 10^{-25}$

Table A3 Thermodynamic property values calculated from Eq. (15) for selected temperatures and pressures

Property	$T = 300$ K $p = 3$ MPa	$T = 300$ K $p = 80$ MPa	$T = 500$ K $p = 3$ MPa
v, m^3 kg^{-1}	$0.100\,215\,168 \times 10^{-2}$	$0.971\,180\,894 \times 10^{-3}$	$0.120\,241\,800 \times 10^{-2}$
h, kJ kg^{-1}	$0.115\,331\,273 \times 10^{3}$	$0.184\,142\,828 \times 10^{3}$	$0.975\,542\,239 \times 10^{3}$
u, kJ kg^{-1}	$0.112\,324\,818 \times 10^{3}$	$0.106\,448\,356 \times 10^{3}$	$0.971\,934\,985 \times 10^{3}$
s, kJ kg^{-1} K^{-1}	0.392 294 792	0.368 563 852	$0.258\,041\,912 \times 10^{1}$
c_p, kJ kg^{-1} K^{-1}	$0.417\,301\,218 \times 10^{1}$	$0.401\,008\,987 \times 10^{1}$	$0.465\,580\,682 \times 10^{1}$
w, m s^{-1}	$0.150\,773\,921 \times 10^{4}$	$0.163\,469\,054 \times 10^{4}$	$0.124\,071\,337 \times 10^{4}$

Table A4 Coefficients and exponents of Eq. (20)[a]

i	J_i^o	n_i^o	i	J_i^o	n_i^o
1[a]	0	$-0.969\,276\,865\,002\,17 \times 10^{1}$	6	−2	$0.142\,408\,191\,714\,44 \times 10^{1}$
2[a]	1	$0.100\,866\,559\,680\,18 \times 10^{2}$	7	−1	$-0.438\,395\,113\,194\,50 \times 10^{1}$
3	−5	$-0.560\,879\,112\,830\,20 \times 10^{-2}$	8	2	$-0.284\,086\,324\,607\,72$
4	−4	$0.714\,527\,380\,814\,55 \times 10^{-1}$	9	3	$0.212\,684\,637\,533\,07 \times 10^{-1}$
5	−3	$-0.407\,104\,982\,239\,28$			

[a] If Eq. (20) is incorporated into Eq. (23), instead of the values for n_1^o and n_2^o given above, the following values for these two coefficients must be used:
$n_1^o = -0.969\,372\,683\,930\,49 \times 10^{1}$, $n_2^o = 0.100\,872\,759\,700\,06 \times 10^{2}$

Table A5 Coefficients and exponents of Eq. (21)

i	I_i	J_i	n_i	i	I_i	J_i	n_i
1	1	0	$-0.177\,317\,424\,732\,13 \times 10^{-2}$	23	7	0	$-0.590\,595\,643\,242\,70 \times 10^{-17}$
2	1	1	$-0.178\,348\,622\,923\,58 \times 10^{-1}$	24	7	11	$-0.126\,218\,088\,991\,01 \times 10^{-5}$
3	1	2	$-0.459\,960\,136\,963\,65 \times 10^{-1}$	25	7	25	$-0.389\,468\,424\,357\,39 \times 10^{-1}$
4	1	3	$-0.575\,812\,590\,834\,32 \times 10^{-1}$	26	8	8	$0.112\,562\,113\,604\,59 \times 10^{-10}$
5	1	6	$-0.503\,252\,787\,279\,30 \times 10^{-1}$	27	8	36	$-0.823\,113\,408\,979\,98 \times 10^{1}$
6	2	1	$-0.330\,326\,416\,702\,03 \times 10^{-4}$	28	9	13	$0.198\,097\,128\,020\,88 \times 10^{-7}$
7	2	2	$-0.189\,489\,875\,163\,15 \times 10^{-3}$	29	10	4	$0.104\,069\,652\,101\,74 \times 10^{-18}$
8	2	4	$-0.393\,927\,772\,433\,55 \times 10^{-2}$	30	10	10	$-0.102\,347\,470\,959\,29 \times 10^{-12}$
9	2	7	$-0.437\,972\,956\,505\,73 \times 10^{-1}$	31	10	14	$-0.100\,181\,793\,795\,11 \times 10^{-8}$
10	2	36	$-0.266\,745\,479\,140\,87 \times 10^{-4}$	32	16	29	$-0.808\,829\,086\,469\,85 \times 10^{-10}$
11	3	0	$0.204\,817\,376\,923\,09 \times 10^{-7}$	33	16	50	$0.106\,930\,318\,794\,09$
12	3	1	$0.438\,706\,672\,844\,35 \times 10^{-6}$	34	18	57	$-0.336\,622\,505\,741\,71$
13	3	3	$-0.322\,776\,772\,385\,70 \times 10^{-4}$	35	20	20	$0.891\,858\,453\,554\,21 \times 10^{-24}$
14	3	6	$-0.150\,339\,245\,421\,48 \times 10^{-2}$	36	20	35	$0.306\,293\,168\,762\,32 \times 10^{-12}$
15	3	35	$-0.406\,682\,535\,626\,49 \times 10^{-1}$	37	20	48	$-0.420\,024\,676\,982\,08 \times 10^{-5}$
16	4	1	$-0.788\,473\,095\,593\,67 \times 10^{-9}$	38	21	21	$-0.590\,560\,296\,856\,39 \times 10^{-25}$
17	4	2	$0.127\,907\,178\,522\,85 \times 10^{-7}$	39	22	53	$0.378\,269\,476\,134\,57 \times 10^{-5}$
18	4	3	$0.482\,253\,727\,185\,07 \times 10^{-6}$	40	23	39	$-0.127\,686\,089\,346\,81 \times 10^{-14}$
19	5	7	$0.229\,220\,763\,376\,61 \times 10^{-5}$	41	24	26	$0.730\,876\,105\,950\,61 \times 10^{-28}$
20	6	3	$-0.167\,147\,664\,510\,61 \times 10^{-10}$	42	24	40	$0.554\,147\,153\,507\,78 \times 10^{-16}$
21	6	16	$-0.211\,714\,723\,213\,55 \times 10^{-2}$	43	24	58	$-0.943\,697\,072\,412\,10 \times 10^{-6}$
22	6	35	$-0.238\,957\,419\,341\,04 \times 10^{2}$				

Table A6 Thermodynamic property values calculated from Eq. (19) for selected temperatures and pressures

Property	$T = 300$ K $p = 0.0035$ MPa	$T = 700$ K $p = 0.0035$ MPa	$T = 700$ K $p = 30$ MPa
v, m^3 kg^{-1}	$0.394\,913\,866 \times 10^{2}$	$0.923\,015\,898 \times 10^{2}$	$0.542\,946\,619 \times 10^{-2}$
h, kJ kg^{-1}	$0.254\,991\,145 \times 10^{4}$	$0.333\,568\,375 \times 10^{4}$	$0.263\,149\,474 \times 10^{4}$
u, kJ kg^{-1}	$0.241\,169\,160 \times 10^{4}$	$0.301\,262\,819 \times 10^{4}$	$0.246\,861\,076 \times 10^{4}$
s, kJ kg^{-1} K^{-1}	$0.852\,238\,967 \times 10^{1}$	$0.101\,749\,996 \times 10^{2}$	$0.517\,540\,298 \times 10^{1}$
c_p, kJ kg^{-1} K^{-1}	$0.191\,300\,162 \times 10^{1}$	$0.208\,141\,274 \times 10^{1}$	$0.103\,505\,092 \times 10^{2}$
w, m s^{-1}	$0.427\,920\,172 \times 10^{3}$	$0.644\,289\,068 \times 10^{3}$	$0.480\,386\,523 \times 10^{3}$

Table A7 Coefficients and exponents of Eq. (24)

i	I_i	J_i	n_i	i	I_i	J_i	n_i
1	1	0	$-0.733\,622\,601\,865\,06 \times 10^{-2}$	8	3	4	$-0.634\,980\,376\,573\,13 \times 10^{-2}$
2	1	2	$-0.882\,238\,319\,431\,46 \times 10^{-1}$	9	3	16	$-0.860\,430\,930\,285\,88 \times 10^{-1}$
3	1	5	$-0.723\,345\,552\,132\,45 \times 10^{-1}$	10	4	7	$0.753\,215\,815\,227\,70 \times 10^{-2}$
4	1	11	$-0.408\,131\,785\,344\,55 \times 10^{-2}$	11	4	10	$-0.792\,383\,754\,461\,39 \times 10^{-2}$
5	2	1	$0.200\,978\,033\,802\,07 \times 10^{-2}$	12	5	9	$-0.228\,881\,607\,784\,47 \times 10^{-3}$
6	2	7	$-0.530\,459\,218\,986\,42 \times 10^{-1}$	13	5	10	$-0.264\,565\,014\,828\,10 \times 10^{-2}$
7	2	16	$-0.761\,904\,090\,869\,70 \times 10^{-2}$				

Table A8 Thermodynamic property values calculated from Eq. (23) for selected values of temperature and pressure

Property	$T = 450$ K $p = 1$ MPa	$T = 440$ K $p = 1$ MPa	$T = 450$ K $p = 1.5$ MPa
v, m^3 kg^{-1}	$0.192\,516\,540$	$0.186\,212\,297$	$0.121\,685\,206$
h, kJ kg^{-1}	$0.276\,881\,115 \times 10^{4}$	$0.274\,015\,123 \times 10^{4}$	$0.272\,134\,539 \times 10^{4}$
u, kJ kg^{-1}	$0.257\,629\,461 \times 10^{4}$	$0.255\,393\,894 \times 10^{4}$	$0.253\,881\,758 \times 10^{4}$
s, kJ kg^{-1} K^{-1}	$0.656\,660\,377 \times 10^{1}$	$0.650\,218\,759 \times 10^{1}$	$0.629\,170\,440 \times 10^{1}$
c_p, kJ kg^{-1} K^{-1}	$0.276\,349\,265 \times 10^{1}$	$0.298\,166\,443 \times 10^{1}$	$0.362\,795\,578 \times 10^{1}$
w, m s^{-1}	$0.498\,408\,101 \times 10^{3}$	$0.489\,363\,295 \times 10^{3}$	$0.481\,941\,819 \times 10^{3}$

Table A9 Coefficients and exponents of Eq. (25)

i	I_i	J_i	n_i	i	I_i	J_i	n_i
1	0	0	$0.106\,580\,700\,285\,13 \times 10^{1}$	21	3	4	$-0.201\,899\,150\,235\,70 \times 10^{1}$
2	0	0	$-0.157\,328\,452\,902\,39 \times 10^{2}$	22	3	16	$-0.821\,476\,371\,739\,63 \times 10^{-2}$
3	0	1	$0.209\,443\,969\,743\,07 \times 10^{2}$	23	3	26	$-0.475\,960\,357\,349\,23$
4	0	2	$-0.768\,677\,078\,787\,16 \times 10^{1}$	24	4	0	$0.439\,840\,744\,735\,00 \times 10^{-1}$
5	0	7	$0.261\,859\,477\,879\,54 \times 10^{1}$	25	4	2	$-0.444\,764\,354\,287\,39$
6	0	10	$-0.280\,807\,811\,486\,20 \times 10^{1}$	26	4	4	$0.905\,720\,707\,197\,33$
7	0	12	$0.120\,533\,696\,965\,17 \times 10^{1}$	27	4	26	$0.705\,224\,500\,879\,67$
8	0	23	$-0.845\,668\,128\,125\,02 \times 10^{-2}$	28	5	1	$0.107\,705\,126\,263\,32$
9	1	2	$-0.126\,543\,154\,777\,14 \times 10^{1}$	29	5	3	$-0.329\,136\,232\,589\,54$
10	1	6	$-0.115\,244\,078\,066\,81 \times 10^{1}$	30	5	26	$-0.508\,710\,620\,411\,58$
11	1	15	$0.885\,210\,439\,843\,18$	31	6	0	$-0.221\,754\,008\,730\,96 \times 10^{-1}$
12	1	17	$-0.642\,077\,651\,816\,07$	32	6	2	$0.942\,607\,516\,650\,92 \times 10^{-1}$
13	2	0	$0.384\,934\,601\,866\,71$	33	6	26	$0.164\,362\,784\,479\,61$
14	2	2	$-0.852\,147\,088\,242\,06$	34	7	2	$-0.135\,033\,722\,413\,48 \times 10^{-1}$
15	2	6	$0.489\,722\,815\,418\,77 \times 10^{1}$	35	8	26	$-0.148\,343\,453\,524\,72 \times 10^{-1}$
16	2	7	$-0.305\,026\,172\,569\,65 \times 10^{1}$	36	9	2	$0.579\,229\,536\,280\,84 \times 10^{-3}$
17	2	22	$0.394\,205\,368\,791\,54 \times 10^{-1}$	37	9	26	$0.323\,089\,047\,037\,11 \times 10^{-2}$
18	2	26	$0.125\,584\,084\,243\,08$	38	10	0	$0.809\,648\,029\,962\,15 \times 10^{-4}$
19	3	0	$-0.279\,993\,296\,987\,10$	39	10	1	$-0.165\,576\,797\,950\,37 \times 10^{-3}$
20	3	2	$0.138\,997\,995\,694\,60 \times 10^{1}$	40	11	26	$-0.449\,238\,990\,618\,15 \times 10^{-4}$

Table A10 Thermodynamic property values calculated from Eq. (25) for selected temperatures and densities

Property	$T = 650$ K $\rho = 500$ kg m^{-3}	$T = 650$ K $\rho = 200$ kg m^{-3}	$T = 750$ K $\rho = 500$ kg m^{-3}
p, MPa	$0.255\,837\,018 \times 10^{2}$	$0.222\,930\,643 \times 10^{2}$	$0.783\,095\,639 \times 10^{2}$
h, kJ kg^{-1}	$0.186\,343\,019 \times 10^{4}$	$0.237\,512\,401 \times 10^{4}$	$0.225\,868\,845 \times 10^{4}$
u, kJ kg^{-1}	$0.181\,226\,279 \times 10^{4}$	$0.226\,365\,868 \times 10^{4}$	$0.210\,206\,932 \times 10^{4}$
s, kJ kg^{-1} K^{-1}	$0.405\,427\,273 \times 10^{1}$	$0.485\,438\,792 \times 10^{1}$	$0.446\,971\,906 \times 10^{1}$
c_p, kJ kg^{-1} K^{-1}	$0.138\,935\,717 \times 10^{2}$	$0.446\,579\,342 \times 10^{2}$	$0.634\,165\,359 \times 10^{1}$
w, m s^{-1}	$0.502\,005\,554 \times 10^{3}$	$0.383\,444\,594 \times 10^{3}$	$0.760\,696\,041 \times 10^{3}$

Table A11 Coefficients of Eqs. (27), (28), and (55)

i	n_i	i	n_i
1	$0.116\,705\,214\,527\,67 \times 10^{4}$	6	$0.149\,151\,086\,135\,30 \times 10^{2}$
2	$-0.724\,213\,167\,032\,06 \times 10^{6}$	7	$-0.482\,326\,573\,615\,91 \times 10^{4}$
3	$-0.170\,738\,469\,400\,92 \times 10^{2}$	8	$0.405\,113\,405\,420\,57 \times 10^{6}$
4	$0.120\,208\,247\,024\,70 \times 10^{5}$	9	$-0.238\,555\,575\,678\,49$
5	$-0.323\,255\,503\,223\,33 \times 10^{7}$	10	$0.650\,175\,348\,447\,98 \times 10^{3}$

Table A12 Saturation-pressure values calculated from Eq. (28) for selected temperatures

T, K	p_s, MPa
300	$0.353\,658\,941 \times 10^{-2}$
500	$0.263\,889\,776 \times 10^{1}$
600	$0.123\,443\,146 \times 10^{2}$

Table A13 Coefficients and exponents of Eq. (30)

i	J_i^o	n_i^o	i	J_i^o	n_i^o
1	0	$-0.131\,799\,836\,742\,01 \times 10^{2}$	4	−2	0.369 015 349 803 33
2	1	$0.685\,408\,416\,344\,34 \times 10^{1}$	5	−1	$-0.311\,613\,182\,139\,25 \times 10^{1}$
3	−3	$-0.248\,051\,489\,334\,66 \times 10^{-1}$	6	2	−0.329 616 265 389 17

Table A14 Coefficients and exponents of Eq. (31)

i	I_i	J_i	n_i	i	I_i	J_i	n_i
1	1	0	$-0.125\,631\,835\,895\,92 \times 10^{-3}$	4	2	9	$-0.397\,248\,283\,595\,69 \times 10^{-5}$
2	1	1	$0.217\,746\,787\,145\,71 \times 10^{-2}$	5	3	3	$0.129\,192\,282\,897\,84 \times 10^{-6}$
3	1	3	$-0.459\,428\,208\,999\,10 \times 10^{-2}$				

Table A15 Thermodynamic property values calculated from Eq. (29) for selected temperatures and pressures

Property	$T = 1500$ K $p = 0.5$ MPa	$T = 1500$ K $p = 8$ MPa	$T = 2000$ K $p = 8$ MPa
v, m^3 kg^{-1}	$0.138\,455\,354 \times 10^{1}$	$0.865\,156\,616 \times 10^{-1}$	0.115 743 146
h, kJ kg^{-1}	$0.521\,976\,332 \times 10^{4}$	$0.520\,609\,634 \times 10^{4}$	$0.658\,380\,291 \times 10^{4}$
u, kJ kg^{-1}	$0.452\,748\,654 \times 10^{4}$	$0.451\,397\,105 \times 10^{4}$	$0.565\,785\,774 \times 10^{4}$
s, kJ kg^{-1} K^{-1}	$0.965\,408\,431 \times 10^{1}$	$0.836\,546\,724 \times 10^{1}$	$0.915\,671\,044 \times 10^{1}$
c_p, kJ kg^{-1} K^{-1}	$0.261\,610\,228 \times 10^{1}$	$0.264\,453\,866 \times 10^{1}$	$0.285\,306\,750 \times 10^{1}$
w, m s^{-1}	$0.917\,071\,933 \times 10^{3}$	$0.919\,708\,859 \times 10^{3}$	$0.105\,435\,806 \times 10^{4}$

Table A16 Coefficients and exponents of Eq. (37)

i	I_i	J_i	n_i	i	I_i	J_i	n_i
1	0	0	$-0.238\,724\,899\,245\,21 \times 10^{3}$	11	1	4	$-0.659\,647\,494\,236\,38 \times 10^{1}$
2	0	1	$0.404\,211\,886\,379\,45 \times 10^{3}$	12	1	10	$0.939\,654\,008\,783\,63 \times 10^{-2}$
3	0	2	$0.113\,497\,468\,817\,18 \times 10^{3}$	13	1	32	$0.115\,736\,475\,053\,40 \times 10^{-6}$
4	0	6	$-0.584\,576\,160\,480\,39 \times 10^{1}$	14	2	10	$-0.258\,586\,412\,820\,73 \times 10^{-4}$
5	0	22	$-0.152\,854\,824\,131\,40 \times 10^{-3}$	15	2	32	$-0.406\,443\,630\,847\,99 \times 10^{-8}$
6	0	32	$-0.108\,667\,076\,953\,77 \times 10^{-5}$	16	3	10	$0.664\,561\,861\,916\,35 \times 10^{-7}$
7	1	0	$-0.133\,917\,448\,726\,02 \times 10^{2}$	17	3	32	$0.806\,707\,341\,030\,27 \times 10^{-10}$
8	1	1	$0.432\,110\,391\,835\,59 \times 10^{2}$	18	4	32	$-0.934\,777\,712\,139\,47 \times 10^{-12}$
9	1	2	$-0.540\,100\,671\,705\,06 \times 10^{2}$	19	5	32	$0.582\,654\,420\,206\,01 \times 10^{-14}$
10	1	3	$0.305\,358\,922\,039\,16 \times 10^{2}$	20	6	32	$-0.150\,201\,859\,535\,03 \times 10^{-16}$

Table A17 Temperature values calculated from Eq. (37) for selected pressures and enthalpies

p, MPa	h, kJ kg^{-1}	T, K
3	500	$0.391\,798\,509 \times 10^{3}$
80	500	$0.378\,108\,626 \times 10^{3}$
80	1500	$0.611\,041\,229 \times 10^{3}$

Table A18 Coefficients and exponents of Eq. (39)

i	I_i	J_i	n_i	i	I_i	J_i	n_i
1	0	0	$0.174\,782\,680\,583\,07 \times 10^{3}$	11	1	12	$0.356\,721\,106\,073\,66 \times 10^{-9}$
2	0	1	$0.348\,069\,308\,928\,73 \times 10^{2}$	12	1	31	$0.173\,324\,969\,948\,95 \times 10^{-23}$
3	0	2	$0.652\,925\,849\,784\,55 \times 10^{1}$	13	2	0	$0.566\,089\,006\,548\,37 \times 10^{-3}$
4	0	3	0.330 399 817 754 89	14	2	1	$-0.326\,354\,831\,397\,17 \times 10^{-3}$
5	0	11	$-0.192\,813\,829\,231\,96 \times 10^{-6}$	15	2	2	$0.447\,782\,866\,906\,32 \times 10^{-4}$
6	0	31	$-0.249\,091\,972\,445\,73 \times 10^{-22}$	16	2	9	$-0.513\,221\,569\,085\,07 \times 10^{-9}$
7	1	0	$-0.261\,076\,364\,893\,32$	17	2	31	$-0.425\,226\,570\,422\,07 \times 10^{-25}$
8	1	1	0.225 929 659 815 86	18	3	10	$0.264\,004\,413\,606\,89 \times 10^{-12}$
9	1	2	$-0.642\,564\,633\,952\,26 \times 10^{-1}$	19	3	32	$0.781\,246\,004\,597\,23 \times 10^{-28}$
10	1	3	$0.788\,762\,892\,705\,26 \times 10^{-2}$	20	4	32	$-0.307\,321\,999\,036\,68 \times 10^{-30}$

Table A19 Temperature values calculated from Eq. (39) for selected pressures and entropies

p, MPa	s, kJ kg^{-1} K^{-1}	T, K
3	0.5	$0.307\,842\,258 \times 10^{3}$
80	0.5	$0.309\,979\,785 \times 10^{3}$
80	3	$0.565\,899\,909 \times 10^{3}$

Table A20 Coefficients of Eqs. (41) and (42)[a]

i	n_i	i	n_i
1	$0.905\,842\,785\,147\,23 \times 10^{3}$	4	$0.265\,265\,719\,084\,28 \times 10^{4}$
2	−0.679 557 863 992 41	5	$0.452\,575\,789\,059\,48 \times 10^{1}$
3	$0.128\,090\,027\,301\,36 \times 10^{-3}$		

[a] For computer-program verification, Eqs. (41) and (42) must meet the following p-h point: $p = 0.100\,000\,000 \times 10^{3}$ MPa, $h = 0.351\,600\,432\,3 \times 10^{4}$ kJ kg^{-1}

Table A21 Coefficients and exponents of the backward equation $T(p, h)$ for subregion 2(*a*), Eq. (43)

i	I_i	J_i	n_i	i	I_i	J_i	n_i
1	0	0	$0.108\,989\,523\,182\,88 \times 10^{4}$	18	2	7	$0.116\,708\,730\,771\,07 \times 10^{2}$
2	0	1	$0.849\,516\,544\,955\,35 \times 10^{3}$	19	2	36	$0.128\,127\,984\,040\,46 \times 10^{9}$
3	0	2	$-0.107\,817\,480\,918\,26 \times 10^{3}$	20	2	38	$-0.985\,549\,096\,232\,76 \times 10^{9}$
4	0	3	$0.331\,536\,548\,012\,63 \times 10^{2}$	21	2	40	$0.282\,245\,469\,730\,02 \times 10^{10}$
5	0	7	$-0.742\,320\,167\,902\,48 \times 10^{1}$	22	2	42	$-0.359\,489\,714\,107\,03 \times 10^{10}$
6	0	20	$0.117\,650\,487\,243\,56 \times 10^{2}$	23	2	44	$0.172\,273\,499\,131\,97 \times 10^{10}$
7	1	0	$0.184\,457\,493\,557\,90 \times 10^{1}$	24	3	24	$-0.135\,513\,342\,407\,75 \times 10^{5}$
8	1	1	$-0.417\,927\,005\,496\,24 \times 10^{1}$	25	3	44	$0.128\,487\,346\,646\,50 \times 10^{8}$
9	1	2	$0.624\,781\,969\,358\,12 \times 10^{1}$	26	4	12	$0.138\,657\,242\,832\,26 \times 10^{1}$
10	1	3	$-0.173\,445\,631\,081\,14 \times 10^{2}$	27	4	32	$0.235\,988\,325\,565\,14 \times 10^{6}$
11	1	7	$-0.200\,581\,768\,620\,96 \times 10^{3}$	28	4	44	$-0.131\,052\,365\,450\,54 \times 10^{8}$
12	1	9	$0.271\,960\,654\,737\,96 \times 10^{3}$	29	5	32	$0.739\,998\,354\,747\,66 \times 10^{4}$
13	1	11	$-0.455\,113\,182\,858\,18 \times 10^{3}$	30	5	36	$-0.551\,966\,970\,300\,60 \times 10^{6}$
14	1	18	$0.309\,196\,886\,047\,55 \times 10^{4}$	31	5	42	$0.371\,540\,859\,962\,33 \times 10^{7}$
15	1	44	$0.252\,266\,403\,578\,72 \times 10^{6}$	32	6	34	$0.191\,277\,292\,396\,60 \times 10^{5}$
16	2	0	$-0.617\,074\,228\,683\,39 \times 10^{-2}$	33	6	44	$-0.415\,351\,648\,356\,34 \times 10^{6}$
17	2	2	$-0.310\,780\,466\,295\,83$	34	7	28	$-0.624\,598\,551\,925\,07 \times 10^{2}$

Table A22 Coefficients and exponents of the backward equation $T(p, h)$ for subregion 2(*b*), Eq. (44)

i	I_i	J_i	n_i	i	I_i	J_i	n_i
1	0	0	$0.148\,950\,410\,795\,16 \times 10^{4}$	20	2	40	$0.712\,803\,519\,595\,51 \times 10^{-4}$
2	0	1	$0.743\,077\,983\,140\,34 \times 10^{3}$	21	3	1	$0.110\,328\,317\,899\,99 \times 10^{-3}$
3	0	2	$-0.977\,083\,187\,978\,37 \times 10^{2}$	22	3	2	$0.189\,552\,483\,879\,02 \times 10^{-3}$
4	0	12	$0.247\,424\,647\,056\,74 \times 10^{1}$	23	3	12	$0.308\,915\,411\,605\,37 \times 10^{-2}$
5	0	18	$-0.632\,813\,200\,160\,26$	24	3	24	$0.135\,555\,045\,549\,49 \times 10^{-2}$
6	0	24	$0.113\,859\,521\,296\,58 \times 10^{1}$	25	4	2	$0.286\,402\,374\,774\,56 \times 10^{-6}$
7	0	28	$-0.478\,118\,636\,486\,25$	26	4	12	$-0.107\,798\,573\,575\,12 \times 10^{-4}$
8	0	40	$0.852\,081\,234\,315\,44 \times 10^{-2}$	27	4	18	$-0.764\,627\,124\,548\,14 \times 10^{-4}$
9	1	0	$0.937\,471\,473\,779\,32$	28	4	24	$0.140\,523\,928\,183\,16 \times 10^{-4}$
10	1	2	$0.335\,931\,186\,049\,16 \times 10^{1}$	29	4	28	$-0.310\,838\,143\,314\,34 \times 10^{-4}$
11	1	6	$0.338\,093\,556\,014\,54 \times 10^{1}$	30	4	40	$-0.103\,027\,382\,121\,03 \times 10^{-5}$
12	1	12	$0.168\,445\,396\,719\,04$	31	5	18	$0.282\,172\,816\,350\,40 \times 10^{-6}$
13	1	18	$0.738\,757\,452\,366\,95$	32	5	24	$0.127\,049\,022\,719\,45 \times 10^{-5}$
14	1	24	$-0.471\,287\,374\,361\,86$	33	5	40	$0.738\,033\,534\,682\,92 \times 10^{-7}$
15	1	28	$0.150\,202\,731\,397\,07$	34	6	28	$-0.110\,301\,392\,389\,09 \times 10^{-7}$
16	1	40	$-0.217\,641\,142\,197\,50 \times 10^{-2}$	35	7	2	$-0.814\,563\,652\,078\,33 \times 10^{-13}$
17	2	2	$-0.218\,107\,553\,247\,61 \times 10^{-1}$	36	7	28	$-0.251\,805\,456\,829\,62 \times 10^{-10}$
18	2	8	$-0.108\,297\,844\,036\,77$	37	9	1	$-0.175\,652\,339\,694\,07 \times 10^{-17}$
19	2	18	$-0.463\,333\,246\,358\,12 \times 10^{-1}$	38	9	40	$0.869\,341\,563\,441\,63 \times 10^{-14}$

Table A23 Coefficients and exponents of the backward equation $T(p, h)$ for subregion 2(*c*), Eq. (45)

i	I_i	J_i	n_i	i	I_i	J_i	n_i
1	−7	0	$-0.323\,683\,985\,552\,42 \times 10^{13}$	13	1	4	$0.379\,660\,012\,724\,86 \times 10^{1}$
2	−7	4	$0.732\,633\,509\,021\,81 \times 10^{13}$	14	1	8	$-0.108\,429\,848\,800\,77 \times 10^{2}$
3	−6	0	$0.358\,250\,899\,454\,47 \times 10^{12}$	15	2	4	$-0.453\,641\,726\,766\,60 \times 10^{-1}$
4	−6	2	$-0.583\,401\,318\,515\,90 \times 10^{12}$	16	6	0	$0.145\,591\,156\,586\,98 \times 10^{-12}$
5	−5	0	$-0.107\,830\,682\,174\,70 \times 10^{11}$	17	6	1	$0.112\,615\,974\,072\,30 \times 10^{-11}$
6	−5	2	$0.208\,255\,445\,631\,71 \times 10^{11}$	18	6	4	$-0.178\,049\,822\,406\,86 \times 10^{-10}$
7	−2	0	$0.610\,747\,835\,645\,16 \times 10^{6}$	19	6	10	$0.123\,245\,796\,908\,32 \times 10^{-6}$
8	−2	1	$0.859\,777\,225\,355\,80 \times 10^{6}$	20	6	12	$-0.116\,069\,211\,309\,84 \times 10^{-5}$
9	−1	0	$-0.257\,457\,236\,041\,70 \times 10^{5}$	21	6	16	$0.278\,463\,670\,885\,54 \times 10^{-4}$
10	−1	2	$0.310\,810\,884\,227\,14 \times 10^{5}$	22	6	20	$-0.592\,700\,384\,741\,76 \times 10^{-3}$
11	0	0	$0.120\,823\,158\,659\,36 \times 10^{4}$	23	6	22	$0.129\,185\,829\,918\,78 \times 10^{-2}$
12	0	1	$0.482\,197\,551\,092\,55 \times 10^{3}$				

Table A24 Temperature values calculated from Eqs. (43) to (45) for selected pressures and enthalpies

Equation	p, MPa	h, kJ kg^{-1}	T, K
	0.001	3000	$0.534\,433\,241 \times 10^{3}$
43	3	3000	$0.575\,373\,370 \times 10^{3}$
	3	4000	$0.101\,077\,577 \times 10^{4}$
	5	3500	$0.801\,299\,102 \times 10^{3}$
44	5	4000	$0.101\,531\,583 \times 10^{4}$
	25	3500	$0.875\,279\,054 \times 10^{3}$
	40	2700	$0.743\,056\,411 \times 10^{3}$
45	60	2700	$0.791\,137\,067 \times 10^{3}$
	60	3200	$0.882\,756\,860 \times 10^{3}$

Table A25 Coefficients and exponents of the backward equation $T(p, s)$ for subregion 2(*a*), Eq. (49)

i	I_i	J_i	n_i	i	I_i	J_i	n_i
1	−1.5	−24	$-0.392\,359\,838\,619\,84 \times 10^{6}$	24	−0.25	−11	$-0.597\,806\,388\,727\,18 \times 10^{4}$
2	−1.5	−23	$0.515\,265\,738\,272\,70 \times 10^{6}$	25	−0.25	−6	$-0.704\,014\,639\,268\,62 \times 10^{3}$
3	−1.5	−19	$0.404\,824\,431\,610\,48 \times 10^{5}$	26	0.25	1	$0.338\,367\,841\,075\,53 \times 10^{3}$
4	−1.5	−13	$-0.321\,937\,909\,239\,02 \times 10^{3}$	27	0.25	4	$0.208\,627\,866\,351\,87 \times 10^{2}$
5	−1.5	−11	$0.969\,614\,242\,186\,94 \times 10^{2}$	28	0.25	8	$0.338\,341\,726\,561\,96 \times 10^{-1}$
6	−1.5	−10	$-0.228\,678\,463\,717\,73 \times 10^{2}$	29	0.25	11	$-0.431\,244\,284\,148\,93 \times 10^{-4}$
7	−1.25	−19	$-0.449\,429\,141\,243\,57 \times 10^{6}$	30	0.5	0	$0.166\,537\,913\,564\,12 \times 10^{3}$
8	−1.25	−15	$-0.501\,183\,360\,201\,66 \times 10^{4}$	31	0.5	1	$-0.139\,862\,920\,558\,98 \times 10^{3}$
9	−1.25	−6	0.356 844 635 600 15	32	0.5	5	−0.788 495 479 998 72
10	−1.0	−26	$0.442\,353\,358\,481\,90 \times 10^{5}$	33	0.5	6	$0.721\,324\,117\,538\,72 \times 10^{-1}$
11	−1.0	−21	$-0.136\,733\,888\,117\,08 \times 10^{5}$	34	0.5	10	$-0.597\,548\,393\,982\,83 \times 10^{-2}$
12	−1.0	−17	$0.421\,632\,602\,078\,64 \times 10^{6}$	35	0.5	14	$-0.121\,413\,589\,539\,04 \times 10^{-4}$
13	−1.0	−16	$0.225\,169\,258\,374\,75 \times 10^{5}$	36	0.5	16	$0.232\,270\,967\,338\,71 \times 10^{-6}$
14	−1.0	−9	$0.474\,421\,448\,656\,46 \times 10^{3}$	37	0.75	0	$-0.105\,384\,635\,661\,94 \times 10^{2}$
15	−1.0	−8	$-0.149\,311\,307\,976\,47 \times 10^{3}$	38	0.75	4	$0.207\,189\,254\,965\,02 \times 10^{1}$
16	−0.75	−15	$-0.197\,811\,263\,204\,52 \times 10^{6}$	39	0.75	9	$-0.721\,931\,552\,604\,27 \times 10^{-1}$
17	−0.75	−14	$-0.235\,543\,994\,707\,60 \times 10^{5}$	40	0.75	17	$0.207\,498\,870\,811\,20 \times 10^{-6}$
18	−0.5	−26	$-0.190\,706\,163\,020\,76 \times 10^{5}$	41	1.0	7	$-0.183\,406\,579\,113\,79 \times 10^{-1}$
19	−0.5	−13	$0.553\,756\,698\,831\,64 \times 10^{5}$	42	1.0	18	$0.290\,362\,723\,486\,96 \times 10^{-6}$
20	−0.5	−9	$0.382\,936\,914\,373\,63 \times 10^{4}$	43	1.25	3	0.210 375 278 936 19
21	−0.5	−7	$-0.603\,918\,605\,805\,67 \times 10^{3}$	44	1.25	15	$0.256\,812\,397\,299\,99 \times 10^{-3}$
22	−0.25	−27	$0.193\,631\,026\,203\,31 \times 10^{4}$	45	1.5	5	$-0.127\,990\,029\,337\,81 \times 10^{-1}$
23	−0.25	−25	$0.426\,606\,436\,986\,10 \times 10^{4}$	46	1.5	18	$-0.821\,981\,026\,520\,18 \times 10^{-5}$

Table A26 Coefficients and exponents of the backward equation $T(p, s)$ for subregion 2(*b*), Eq. (50)

i	I_i	J_i	n_i	i	I_i	J_i	n_i
1	−6	0	$0.316\,876\,650\,834\,97 \times 10^{6}$	23	0	2	$0.417\,273\,471\,596\,10 \times 10^{2}$
2	−6	11	$0.208\,641\,758\,818\,58 \times 10^{2}$	24	0	4	$0.219\,325\,494\,345\,32 \times 10^{1}$
3	−5	0	$-0.398\,593\,998\,035\,99 \times 10^{6}$	25	0	5	$-0.103\,200\,500\,090\,77 \times 10^{1}$
4	−5	11	$-0.218\,160\,585\,188\,77 \times 10^{2}$	26	0	6	0.358 829 435 167 03
5	−4	0	$0.223\,697\,851\,942\,42 \times 10^{6}$	27	0	9	$0.525\,114\,537\,260\,66 \times 10^{-2}$
6	−4	1	$-0.278\,417\,034\,458\,17 \times 10^{4}$	28	1	0	$0.128\,389\,164\,507\,05 \times 10^{2}$
7	−4	11	$0.992\,074\,360\,714\,80 \times 10^{1}$	29	1	1	$-0.286\,424\,372\,193\,81 \times 10^{1}$
8	−3	0	$-0.751\,975\,122\,991\,57 \times 10^{5}$	30	1	2	0.569 126 836 648 55
9	−3	1	$0.297\,086\,059\,511\,58 \times 10^{4}$	31	1	3	$-0.999\,629\,545\,849\,31 \times 10^{-1}$
10	−3	11	$-0.344\,068\,785\,485\,26 \times 10^{1}$	32	1	7	$-0.326\,320\,377\,784\,59 \times 10^{-2}$
11	−3	12	0.388 155 642 491 15	33	1	8	$0.233\,209\,225\,767\,23 \times 10^{-3}$
12	−2	0	$0.175\,112\,950\,857\,50 \times 10^{5}$	34	2	0	−0.153 348 098 574 50
13	−2	1	$-0.142\,371\,128\,544\,49 \times 10^{4}$	35	2	1	$0.290\,722\,882\,399\,02 \times 10^{-1}$
14	−2	6	$0.109\,438\,033\,641\,67 \times 10^{1}$	36	2	5	$0.375\,347\,027\,411\,67 \times 10^{-3}$
15	−2	10	0.899 716 193 084 95	37	3	0	$0.172\,966\,917\,024\,11 \times 10^{-2}$
16	−1	0	$-0.337\,597\,400\,989\,58 \times 10^{4}$	38	3	1	$-0.385\,560\,508\,445\,04 \times 10^{-3}$
17	−1	1	$0.471\,628\,858\,183\,55 \times 10^{3}$	39	3	3	$-0.350\,177\,122\,926\,08 \times 10^{-4}$
18	−1	5	$-0.191\,882\,419\,936\,79 \times 10^{1}$	40	4	0	$-0.145\,663\,936\,314\,92 \times 10^{-4}$
19	−1	8	0.410 785 804 921 96	41	4	1	$0.564\,208\,572\,672\,69 \times 10^{-5}$
20	−1	9	−0.334 653 781 720 97	42	5	0	$0.412\,861\,500\,746\,05 \times 10^{-7}$
21	0	0	$0.138\,700\,347\,775\,05 \times 10^{4}$	43	5	1	$-0.206\,846\,711\,188\,24 \times 10^{-7}$
22	0	1	$-0.406\,633\,261\,958\,38 \times 10^{3}$	44	5	2	$0.164\,093\,936\,747\,25 \times 10^{-8}$

Table A27 Coefficients and exponents of the backward equation $T(p, s)$ for subregion 2(*c*), Eq. (51)

i	I_i	J_i	n_i	i	I_i	J_i	n_i
1	−2	0	$0.909\,685\,010\,053\,65 \times 10^{3}$	16	3	1	$-0.145\,970\,082\,847\,53 \times 10^{-1}$
2	−2	1	$0.240\,456\,670\,884\,20 \times 10^{4}$	17	3	5	$0.566\,311\,756\,310\,27 \times 10^{-2}$
3	−1	0	$-0.591\,623\,263\,871\,30 \times 10^{3}$	18	4	0	$-0.761\,558\,645\,845\,77 \times 10^{-4}$
4	0	0	$0.541\,454\,041\,280\,74 \times 10^{3}$	19	4	1	$0.224\,403\,429\,193\,32 \times 10^{-3}$
5	0	1	$-0.270\,983\,084\,111\,92 \times 10^{3}$	20	4	4	$-0.125\,610\,950\,134\,13 \times 10^{-4}$
6	0	2	$0.979\,765\,250\,979\,26 \times 10^{3}$	21	5	0	$0.633\,231\,326\,609\,34 \times 10^{-6}$
7	0	3	$-0.469\,667\,729\,594\,35 \times 10^{3}$	22	5	1	$-0.205\,419\,896\,753\,75 \times 10^{-5}$
8	1	0	$0.143\,992\,746\,047\,23 \times 10^{2}$	23	5	2	$0.364\,053\,703\,900\,82 \times 10^{-7}$
9	1	1	$-0.191\,042\,042\,304\,29 \times 10^{2}$	24	6	0	$-0.297\,598\,977\,892\,15 \times 10^{-8}$
10	1	3	$0.532\,991\,671\,119\,71 \times 10^{1}$	25	6	1	$0.101\,366\,185\,297\,63 \times 10^{-7}$
11	1	4	$-0.212\,529\,753\,759\,34 \times 10^{2}$	26	7	0	$0.599\,257\,196\,923\,51 \times 10^{-11}$
12	2	0	−0.311 473 344 137 60	27	7	1	$-0.206\,778\,701\,051\,64 \times 10^{-10}$
13	2	1	0.603 348 408 946 23	28	7	3	$-0.208\,742\,781\,818\,86 \times 10^{-10}$
14	2	2	$-0.427\,648\,397\,025\,09 \times 10^{-1}$	29	7	4	$0.101\,621\,668\,250\,89 \times 10^{-9}$
15	3	0	$0.581\,855\,972\,552\,59 \times 10^{-2}$	30	7	5	$-0.164\,298\,282\,813\,47 \times 10^{-9}$

Table A28 Temperature values calculated from Eqs. (49) to (51) for selected pressures and entropies

Equation	p, MPa	s, kJ kg^{-1}K^{-1}	T, K
49	0.1	7.5	$0.399\,517\,097 \times 10^{3}$
	0.1	8	$0.514\,127\,081 \times 10^{3}$
	2.5	8	$0.103\,984\,917 \times 10^{4}$
50	8	6	$0.600\,484\,040 \times 10^{3}$
	8	7.5	$0.106\,495\,556 \times 10^{4}$
	90	6	$0.103\,801\,126 \times 10^{4}$
51	20	5.75	$0.697\,992\,849 \times 10^{3}$
	80	5.25	$0.854\,011\,484 \times 10^{3}$
	80	5.75	$0.949\,017\,998 \times 10^{3}$

Table A29 Saturation-temperature values calculated from Eq. (55) for selected pressures

p, MPa	T_s, K
0.1	$0.372\,755\,919 \times 10^{3}$
1	$0.453\,035\,632 \times 10^{3}$
10	$0.584\,149\,488 \times 10^{3}$